Environmental Security Technology Certification Program (ESTCP)

Ultra-Wideband, Fully Polarimetric Ground Penetrating Radar for UXO Discrimination

FINAL TECHNICAL REPORT Project 199902

Dr. Kevin O'Neill
US Army Corps of Engineers
Engineer Research and Development Center (ERDC)
Hanover Site - 72 Lyme Rd
Hanover NH 03755
koneill@CRREL.usace.army.mil

30 June 2005

Report Documentation Page

Form Approved
OMB No. 0704-0188

1. REPORT DATE	2. REPORT TYPE	3. DATES COVERED
30 JUN 2005		**00-00-2005 to 00-00-2005**

4. TITLE AND SUBTITLE	5a. CONTRACT NUMBER
Ultra-Wideband, Fully Polarimetric Ground Penetrating Radar for UXO Discrimination	5b. GRANT NUMBER
	5c. PROGRAM ELEMENT NUMBER
6. AUTHOR(S)	5d. PROJECT NUMBER
	5e. TASK NUMBER
	5f. WORK UNIT NUMBER
7. PERFORMING ORGANIZATION NAME(S) AND ADDRESS(ES) **U.S. Army Engineer Research and Development Center (ERDC),Cold Regions Research and Engineering Laboratory (CRREL),72 Lyme Road,hanover,NH,03755**	8. PERFORMING ORGANIZATION REPORT NUMBER
9. SPONSORING/MONITORING AGENCY NAME(S) AND ADDRESS(ES)	10. SPONSOR/MONITOR'S ACRONYM(S)
	11. SPONSOR/MONITOR'S REPORT NUMBER(S)

12. DISTRIBUTION/AVAILABILITY STATEMENT
Approved for public release; distribution unlimited

13. SUPPLEMENTARY NOTES

14. ABSTRACT

In this project, demonstrations were carried out for the purpose of ascertaining the buried UXO discrimination capabilities of UWB, fully polarimetric ground penetrating radar (GPR). Work concentrated on ?cued identification? or ?close interrogation? by GPR of signal anomaly locations that were identified by other means. The unknown buried objects were sorted into UXO and non-UXO classes and the results scored independently against closely held ground truth. The ultimate purpose of the work was to contribute to a knowledge base that decision makers might exploit to determine when GPR application would be beneficial relative to other discrimination alternatives. ?Discrimination? as used here contrasts with ?straight detection,? the latter being simply identification and location of signal anomalies for further attention. The emphasis in straight detection is on finding as many UXO's as possible, with only secondary concern for false alarm rate. The emphasis in discrimination, as the word is used here, is on correct classification maximizing correct "dig" decisions while minimizing false alarms. The demos took place between January of 2000 and November of 2001 at four sites: Tyndall AFB; Blossom Pt, MD; Jefferson Proving Ground, Madison, IN; and the former Ft Ord in Monterey, CA. Time requirements at each site are listed in Section 5 below. The one-of-a-kind GPR operated from about 10 MHz to 810 MHz and was fully polarimetric. The implication of fullpolarimetry is that complete amplitude and phase information is obtained for orthogonal direct and cross-channel reception, for any particular antenna orientation. Given this information for any single orientation, one can synthesize the co-polarization and cross-polarization responses for any other polarizations of transmission and reception. These features allowed operators and analysts to extract basic discrimination parameters from the data, including prominently the estimated target depth, horizontal plane location, orientation, complex (frequency) natural resonance, length linearity factor, and the density of signal about the most prominent polarization orientation, as well as spatial distribution of some of those parameters along survey scans. Estimated linearity factor (ELF), in connection with various of the others, is probably the most crucial of these for the classification processing sequence that was applied. That processing was designed to ascertain when the received signal should be construed as coming from an object with the overall geometry of a UXO or not. Correct sorting of unknown targets into the UXO class counts here as a detection while incorrect sorting into that class counts here as a false alarm.

15. SUBJECT TERMS

16. SECURITY CLASSIFICATION OF:			17. LIMITATION OF ABSTRACT	18. NUMBER OF PAGES	19a. NAME OF RESPONSIBLE PERSON
a. REPORT	b. ABSTRACT	c. THIS PAGE			
unclassified	**unclassified**	**unclassified**	**Same as Report (SAR)**	**99**	

ACKNOWLEDGMENTS

With the support of the Environmental Security Technology Certification Program, Dr. Jeffrey Marqusee, Director, under project 199902, the ground penetrating radar (GPR) work reported herein was carried out by a joint team of personnel from the Ohio State University Electroscience Laboratory (OSU-ESL) and the U.S. Army Corps of Engineers, Engineer Research and Development Center (ERDC), Hanover site (CRREL). The principal investigator was Dr. Kevin O'Neill of ERDC, with the OSU-ESL's Dr. Chi-Chih Chen as Co-PI. Dr. Chen was at the heart of the project at all times, performing essential tasks and giving crucial guidance in all aspects of the work. Dr. Richard Detsch of ERDC-CRREL assisted in planning and executing the initial fieldwork. Dr. Chen's graduate students, Matthew B. Higgins and Hyoung-Sun Youn, were invaluable and extraordinarily assiduous in everything from design and construction of equipment to modeling, execution of fieldwork, and processing and interpretation. All of us benefited from proximity of the deep wisdom as well as the occasional direct guidance of Professor Leon Peters, Jr., now retired from the OSU-ESL and widely acknowledged as one of the Fathers of GPR.

Computational and modeling work in support of the data processing and interpretation was also provided by Professor Robert Lee of the OSU Department of Electrical Engineering and by his students, including Kishore Rama Rao and Kwan-Ho Lee. Dr. Fridon Shubitidze of the Thayer School of Engineering at Dartmouth also performed modeling work, and participated in the execution of some fieldwork as well.

This diverse, talented, and dedicated team merits heartfelt thanks for contributing in such an exemplary manner to the successful execution of the project.

TABLE OF CONTENTS

1 INTRODUCTION 8

1.1 Abstract 8
1.2 Official DoD Requirement Statement 11
1.3 Background 12
1.4 Objectives of the Demonstration Series 15
1.5 Regulatory Issues 15

2 TECHNOLOGY DESCRIPTION 16

2.1 Overview of System Development and Its Implementation in the Demos 16
2.2 Fully Polarimetric GPR for UXO Discrimination 23
2.2.1 RF Transceiver 23
2.2.2 Antenna Unit 24
2.2.3 Heading and Positioning 29

3 DEMONSTRATION DESIGN 30

3.1 Performance Objectives 30
3.2 Survey, Processing, and Interpretation Methods 32
3.2.1 Measurement Approach 33
3.2.2 Pre-processing of GPR Data 35
3.2.2.1 Ensemble Background Subtraction 36
3.2.2.2 Data Calibration 37
3.2.2.3 Adaptive 2-D Spatial Smoothing 39
3.2.3 Feature Extraction 40
3.2.3.1 Electromagnetic Complex Natural Resonance (CNR) Feature Extraction 40
3.2.3.2 Late-Time Polarization Feature Extraction 41
3.2.3.3 Depth Information Extraction 44
3.2.4 Data Processing Summary 45
3.3 UXO CLASSIFICATION RULES 49

4 CLASSIFICATION PERFORMANCE 52

4.1 Baseline Performance 52
4.2 Performance Improvement 55
4.3 Analysis of Performance 62
4.4 Performance Comparisons 64

5 COST ASSESSMENT 67

5.1 Cost of the Demonstrations 67
5.2 Cost Comparisons and Savings 68

6 DISCUSSION, EVALUATION, AND RECOMMENDATIONS 69

7 REFERENCES 75

8 APPENDIX A. POINTS OF CONTACT 79

9 APPENDIX B: AUTOMATION OF GPR CLASSIFICATION PROCESSING 80

9.1.1 Feature Extraction 80
9.1.2 Classification 83

10 APPENDIX C: THE NEW GPR SYSTEM 90

10.1 RF Front End 91
10.2 Digital Down Converter (DDC) 93
10.3 Direct Digital Synthesizer 95
10.4 Small Footprint, Low-RCS GPR Antenna Development 97
10.4.1 Quad-Ridge Horn Antenna with Dielectric Loading 97
10.4.2 Dual-Linear Resistive-Loaded Dipoles on a High Dielectric Constant Layer 98

List of Figures

Figure 1. Local magnetometer survey around flagged spot. 21
Figure 2. The orthogonal nature of radar and EMI/Magnetometer systems. 22
Figure 3. Badger hole beneath clustered targets at Ft Ord 22
Figure 4. Vector Network Analyzer (HP8712ET). 24
Figure 5. Sketch of the bottom (left) and side view (right) of the OSU/ESL UWB full-polarization GPR antenna. 25
Figure 6. The input reflection and input impedance values for the fully polarimetric HFB antenna, calculated with a 3-D FDTD model. 26
Figure 7. Fully polarimetric GPR configuration at Tyndall AFB UXO site. 27
Figure 8. Simulated radiation field distribution in dB, plotted over a horizontal plane near the HFB antenna aperture. (a) co-polarized (b) cross-polarized. 27
Figure 9. Principal planes of the radiating fields. 28
Figure 10. UXO GPR configuration used at BP, JPG, and Ft Ord sites, showing antenna arms aligned with and perpendicular to the travel direction. 28
Figure 11. Marks on the front wheel for incremental positioning during each radar pass. 29
Figure 12. Hypothetical example ROC curves. The black circle markers indicate arbitrary or random Pd/Pfa classifications of 0/0%, 50/50%, and 100/100%. LOND = line of no discrimination. 31
Figure 13. Top: Spatial view, in which the horizontal axis is spatial location of the antenna and the vertical axis shows depth in space. Bottom: Data for same, with antenna position again on horizontal axis but signal travel time ("delay") on the vertical axis. 32
Figure 14. Recorded GPR response, displayed in terms of signal travel time (vertical) vs antenna position (horizontal), for a horizontal steel cylinder buried 75 cm deep at BP. 33
Figure 15. GPR passes for targets in Area 1 at JPG-V. (Red – Pass 1; Green- Pass 2; Blue-Pass 3; Black- Pass 4) 34
Figure 16. Example of clutter caused by underground badger tunnel networks in an empty site at Ft Ord. 36
Figure 17. Antenna transfer functions measured at JPG-V using a long, thin conducting wire on the ground surface, under dry and wet conditions. 38
Figure 18. Comparison of GPR data before (left) and after field calibration (right). The target is an 81 mm mortar buried at 0.35 m depth, visible on the left at about 30 ns delay. 38
Figure 19. Comparison of GPR data before (left) and after (right) adaptive data smoothing, for BP known target G. 40
Figure 20. Measured response of a rebar buried at Tyndall site. 42
Figure 21. Response from a horizontal MK-82 (500 lb bomb) rotated 45^{o} between the antenna arms. 42
Figure 22. Full polarimetric, UWB GPR data processing and feature extraction procedures for UXO classification. 47
Figure 23. Typical time-position data obtained using the whole frequency band (10~410 MHz), for the case of a relatively small, high-frequency target.. 48
Figure 24. Time-position data in Figure 23 after application of a bandpass filter (150~410 MHz), for the same target. 48
Figure 25. Target classification rule structure based on GPR signatures. 51

Figure 26. Classification ROC curves based on TRUE UXO criterion with dashed "line of no discrimination" 53
Figure 27. Classification ROC curves based on the UXO-LIKE criterion. 54
Figure 28. Example 6-inch and 1.5-inch holes in Ft Ord site. 54
Figure 29. Field view of the Ft Ord site, showing the density of the holes and covered openings (bare spots). 55
Figure 30. ROC curves for Ft Ord, showing performance obtained from GPR alone, and improvement from inclusion of Mag dipole presence as a factor. 57
Figure 31. ROC curves for the Ft. Ord data derived from the Mag data alone. 57
Figure 32. "ROC points" from the GPR classification for JPG, all based on same decision criteria except for Round 1 = classification based on GPR only; Round 2 = GPR processing + depth estimations from EMI; Round 3 = GPR processing + ground truth depth information 58
Figure 33. Absolute depth estimation error (left) and length estimation error (right) for correctly classified UXO-like items. Data were compiled from JPG-V and Ft Ord blind-test results based on GPR alone. 59
Figure 34. ROC curve for 105 mm projectile based on usual decision criteria plus estimated target length, for different ETL error tolerances. 60
Figure 35. ROC curves for the Tyndall site for different ordnance types, obtained when LET's are 150% for the 60 mm, 125% for the 105 mm, 67% for the 500 lb bomb, and 50% for the 8 inch shell. 62
Figure 36. From ESTCP-9812 final technical report: Red line to represent MTADS discrimination using Mag data alone; Green line: enhanced results obtainable from MTADS Mag data, including mag dipole orientation information; Blue line: Results including information from "three β" EMI data. 66
Figure 37. Simulated GPR data containing surface clutter. 81
Figure 38. Output from neural network trained to detect target arcs. 81
Figure 39. GPR measurements showing buried drainage pipes in farmland. 82
Figure 40. Neural network detection of the drainage pipes from time vs position GPR data. 82
Figure 41. Top of ANN/ fuzzy logic classification tree 84
Figure 42. Bottom of ANN/ fuzzy logic classification tree. 85
Figure 43. Classification ROC curve based on UXO-like criteria (Ft Ord) 89
Figure 44. New OSU/ESL GPR System Block Diagram. 91
Figure 45 . Hardware of the new dual-channel GPR radar. 92
Figure 46. Conventional Analog Radar Receiver Architecture. 93
Figure 47. OSU/ESL Digital Down Converter (DDC) Radar Receiver Architecture. 94
Figure 48. OSU/ESL Digital Receiver Block Diagram. 94
Figure 49. OSU/ESL Dual Channel Digital Receiver. 95
Figure 50. DDS board as frequency source for new OSU/ESL GPR. 96
Figure 51. Quad-ridge horn antenna under construction without dielectric filler. 97
Figure 52. Small UWB GPR antenna with high dielectric loading being developed for fully polarimetric UXO classification. 98
Figure 53. Calculated gain of the small UWB GPR antenna with high dielectric loading being developed for fully polarimetric UXO classification. 99

Acronyms and Abbreviations

AFB:	U.S. Air Force Base
ANN:	Artificial Neural Network
CNR:	Complex [electromagnetic] natural resonance
CRREL:	U.S. Army Corps of Engineers ERDC Cold Regions Research & Engineering Laboratory
DEMO:	[field] Demonstration of project technology
DEN:	Angular density of response about the ETO
DoD:	U.S. Department of Defense
ELF:	Estimated linearity factor
ERDC:	The U.S. Army Corps of Engineers Engineer Research and Development Center
ESTCP:	Environmental Security Technology Certification Program
ETL:	Estimated target length
ETO:	Estimated target orientation
FELF:	Resonant frequency ELF
GPR:	Ground penetrating radar
HFB:	Horn-fed bowtie (GPR antenna)
IFFT:	Inverse Fast Fourier Transform
JPG:	Jefferson Proving Ground, Madison, IN.
L/D:	Length to diameter ratio
LOND:	Line of no discrimination
Mag:	Magnetometry
OSU-ESL:	Ohio State University Electroscience Laboratory
PEC:	Perfect electrical conductor (perfect reflector)
PI:	Principal Investigator
Pd:	Probability of detection
Pfa:	Probability of false alarm
Q:	Resonance quality factor
RF:	Radio frequency
SCR:	Signal to clutter ratio
SNR:	Signal to noise ratio
SOCS:	Subsurface Ordnance Characterization System
TEM:	Transverse electromagnetic [wave]
UWB:	Ultrawide frequency band

1 INTRODUCTION

1.1 Abstract

In this project, demonstrations were carried out for the purpose of ascertaining the buried UXO discrimination capabilities of UWB, fully polarimetric ground penetrating radar (GPR). Work concentrated on “cued identification” or “close interrogation” by GPR of signal anomaly locations that were identified by other means. The unknown buried objects were sorted into UXO and non-UXO classes and the results scored independently against closely held ground truth. The ultimate purpose of the work was to contribute to a knowledge base that decision makers might exploit to determine when GPR application would be beneficial relative to other discrimination alternatives. “Discrimination” as used here contrasts with “straight detection,” the latter being simply identification and location of signal anomalies for further attention. The emphasis in straight detection is on finding as many UXO's as possible, with only secondary concern for false alarm rate. The emphasis in discrimination, as the word is used here, is on correct classification, maximizing correct "dig" decisions while minimizing false alarms.

The demos took place between January of 2000 and November of 2001 at four sites: Tyndall AFB; Blossom Pt, MD; Jefferson Proving Ground, Madison, IN; and the former Ft Ord in Monterey, CA. Time requirements at each site are listed in Section 5 below. The one-of-a-kind GPR operated from about 10 MHz to 810 MHz and was fully polarimetric. The implication of full-polarimetry is that complete amplitude and phase information is obtained for orthogonal direct and cross-channel reception, for any particular antenna orientation. Given this information for any single orientation, one can synthesize the co-polarization and cross-polarization responses for any other polarizations of transmission and reception. These features allowed operators and analysts to extract basic discrimination parameters from the data, including prominently the estimated target depth, horizontal plane location, orientation, complex (frequency) natural resonance, length, linearity factor, and the density of signal about the most prominent polarization orientation, as well as spatial distribution of some of those parameters along survey scans. Estimated linearity factor (ELF), in connection with various of the others, is probably the most crucial of these for the classification processing sequence that was applied. That processing was designed to ascertain

when the received signal should be construed as coming from an object with the overall geometry of a UXO or not. Correct sorting of unknown targets into the UXO class counts here as a detection, while incorrect sorting into that class counts here as a false alarm.

Performance was quantified and analyzed in terms of (misnamed) receiver operating characteristic (ROC) curves, showing the probability of detection (Pd) on the vertical axis vs the probability of false alarm (Pfa) on the horizontal axis. These are defined as

$$Pd \equiv \frac{Number\ of\ correct\ UXO\ classifications}{Total\ number\ in\ UXO\ class}$$

$$Pfa \equiv \frac{Number\ of\ items\ incorrectly\ classified\ as\ UXO}{Total\ number\ in\ non-UXO\ class} \quad .$$

Curves, or at least sequences of points, are obtained as decision criteria are loosened or tightened. In these terms, a system shows discrimination capability better than would be obtained from completely arbitrary or random guesses when the ROC curve lies above the 45 deg line from (0,0) to (100%,100%) in the Pd-Pfa plane. The GPR system that was demonstrated exhibited definite discrimination capability in the baseline performance analyses. Also, despite considerable variation of relevant environmental e.g. soil factors, the ultimate ROC curve performance pattern was similar for the different sites. Before various improvements were applied, about a 55% Pd of UXO-like targets was obtained with only a 10% Pfa; however, progress along the curve to 90% Pd was achieved slowly, only after an 80% Pfa was reached. Thus the primary limitation of the system could be viewed as difficulty achieving high or 100% Pd. If one discards the ground truth classification in terms of whether or not objects are UXO-like in geometry but sorts them instead according to true UXO identity, regardless of object geometry (i.e. using "TRUE UXO" criterion), then performance in terms of ROC curves is distinctly worse. Under this TRUE UXO criterion the system shows definite discrimination capability, but not very much, with a peak Pd/Pfa ratio at 50%/30%.

Various processing improvements were tested by which additional external or "prior" information was worked into the GPR classification system. This produced "collaborative" processing such as would be achieved by pooling results or parameters extracted from another sensing mode's data in addition to those from GPR. In the cases considered, use of prior depth

estimates decreased the Pfa by about 15% to 30% without significantly affecting the Pd, provided that the depth information was accurate. In another test, as a handheld magnetometer preceded the GPR in the survey, the operator made crude determinations of obvious presence or absence of a magnetic dipole in the presumed target locale. When this information was pooled with the GPR parameters, it, too, improved performance, particularly in the resistant upper portion of the ROC curve (~ 90% Pd obtained at ~ 55% Pfa). Presumably the inclusion of more complete and sophisticated use of magnetometry or EMI information would reinforce this result or amplify this trend.

It is difficult to make cost comparisons between the GPR system here and other discrimination technologies. This is because 1) it is difficult to identify a "baseline" discrimination (as opposed to detection) technology; 2) the GPR technology and consequent application techniques have developed rapidly during the course of the demos and thereafter during this report's preparation; and 3) other, e.g. emerging discrimination systems often use different approaches to analyze tests that were different from those described here, sometimes quantifying results in other terms. Be this as it may, one can say that the initial capital cost for the GPR equipment as it existed at the time of the ultimate demos is not great, as survey equipment goes (~ $37k). The primary cost did and will reside in man-hours in the field and during processing. The average number of man-hours per target, for all activities over all demos, was about 0.7. During the demos, highly trained personnel often performed the simplest tasks, given the prototype nature of the system and the importance of oversight during these tests. This translates into the equivalent of an upper limit of ~ $100 labor cost/target. At the same time, much less skilled and trained personnel could be (and were also) used for these tasks, and some of the tasks have now been automated. Thus a reasonable low estimate for future work with essentially the same technology is about $50/target.

Emerging GPR systems (Section 10) should be able to cover a grid of points around a presumed target location in less time than the demo GPR required to do its few linear scans over a target. Given this faster surveying and the more complete information it can provide, it is a reasonable estimation that the emerging GPR survey and processing systems, including collaborative Mag/EMI data, should be capable of achieving the best of the "improved" performance examples shown below, at a cost less than the $50/target low estimate for the existing technology.

Lastly, there is no *a priori* reason to suppose that GPR discrimination should supplement Mag or EMI discrimination, as opposed to the other way around, or as opposed to some flexible mix. What precedence to give to which aspects or parameters from which system will be case dependent. In any event, it is unlikely that GPR will gain a prominent position for the straight detection part of surveying, except in distinct circumstances, such as magnetic but relatively non-conductive soil/rock or small, shallow, widely dispersed metallic clutter items.

1.2 Official DoD Requirement Statement

Particularly over about the last 100 years, the problem of clearing buried UXO has been an important task from the point of view of public safety, environmental protection, and land usage worldwide. The U.S. government specifically has spent a great deal of money and effort on clearing UXO's in recent years and yet the bulk of the task remains before us. Therefore this project addresses the Tri-Service Environmental Quality Research, Development, Test, and Evaluation Strategic Plan, UXO requirements, which state in part [1]

> *There are more than twenty million acres of bombing and target ranges under DOD control.... Each year a significant fraction (200,000-500,000 acres) of these spaces are returned to civilian (Private or Commercial) use. All these areas must be surveyed for buried ordnance and other hazardous materials, rendered certified and safe for the intended end use. This is an extremely labor intensive and expensive process, with costs often far exceeding the value of the land.... Improved technologies for locating, identifying and marking ordnance items must be developed to address all types of terrain, such as open fields, wooded areas, rugged inaccessible areas, and underwater sites.*

Similar requirements are reflected in the U.S. Army Requirement A(1.6a), titled Unexploded Ordnance (UXO) Screening, Detection, and Discrimination [2] and described in the FY99 Army Environmental Requirements and Technology Assessments (AERTA). This Army requirement has been ranked as the highest priority user need in the Environmental Cleanup Pillar. This project also addresses the UXO detection and discrimination requirements and recommendations described in the Defense Science Board Task Force Final Report on UXO Clearance and Remediation published in 1998 [3]. In response to all of these mandates, the work in this project concentrated on the assessment of GPR capabilities for UXO discrimination.

1.3 Background

As the need for systematic remediation of UXO sites has taken shape, safety, efficiency, and cost have been the main issues in clearance operations. Various sensor technologies have been under development worldwide in an effort to produce an effective and non-destructive means for locating potential UXO sites, and for distinguishing UXO from widespread scrap prior to the excavation. Among the sensors being used, magnetometry (Mag) detects a perturbation of the earth's magnetic field due to the presence of ferrous metal. As most (but not all) UXO contain ferrous steel, this has grown to be perhaps the most reliable sensing approach for detection *per se*, i.e. identification of a significant signal anomaly that could correspond to a UXO. However, non-ferrous targets will be missed; the smallest UXO's may be lost against the Mag background; and in any case some studies have found that large numbers of targets are missed in typical “mag and flag” surveys [4]. Overall, aside from detection of significant magnetic anomalies, Mag signals offer only very limited opportunity for discrimination of UXO from widespread clutter. Typically the target is assumed to behave like a simple infinitesimal magnetic dipole. On the basis of this model its ground surface location and perhaps depth, size, and orientation are roughly estimated, e.g. [5].

Electromagnetic induction (EMI) sensors induce transient magnetic fields and currents within a metallic body, and then detect the consequent secondary magnetic fields that these produce. The patterns of the induced responses depend significantly on the material and geometrical character of the object. For this reason as well as its ability to penetrate earth materials easily, EMI has looked particularly promising for discrimination. Ground penetrating radar (GPR) transmits radio energy into the ground, which reflects from the metallic body of a UXO. The beam transmitted by a GPR does not penetrate the target’s metal and is therefore insensitive to material type. However, as explained below, geometrical characteristics of the object still affect the signal content very significantly. Thus GPR has both the advantage and disadvantage that its signals are not complicated/informed by material heterogeneity in the target. Unfortunately, reflections from dielectric heterogeneity in the environment and signal losses in conductive soil challenge GPR and frequently compromise its usefulness. Altogether, given that remote sensing of the encased explosive itself is not possible, these three sensor technologies represent the alternative routes for UXO detection and classification. All three sensors collect data as a function of sensor position and thus produce signal maps that may be subject to interpretation. In particular, the magnetometry and EMI systems have been found to be most effective and accurate in detecting the presence of most UXO’s within a meter depth. The presence of vast amounts of metallic clutter such as shrapnel in

many sites reduces the effectiveness of these two sensors by causing significant numbers of false alarms. This is because there is no *a priori* way of distinguishing signals produced by UXO from those produced by similarly sized pieces of clutter. Indications from other project work suggest that GPR may have very significant advantages relative to Mag and EMI in the face of widespread metallic (as opposed to dielectric) clutter [6]. However this project focused only on circumstances in which dielectric environmental properties and their distributions are the main source of clutter and performance limitation.

Commercial GPR systems are available and have been widely used on a daily basis by geologists, archeologists, engineers, and industrial enterprises. In UXO/landmine applications, the Ohio State University ElectroScience Laboratory (OSU-ESL) developed an impulse GPR system for the U.S. Army in the 1970s, ultimately leading to designs for detection and classification of anti-tank mines [7-11]. The technology was later adopted by the UK and was used successfully to locate landmines during the Falklands war. The OSU-ESL became involved in GPR UXO detection/classification development in 1993 under the support of NAVEODTECHDIV. From 1994 to 1995, the first autonomous multi-sensor UXO platform, the Subsurface Ordnance Characterization System (SOCS) [12] was assembled under the collaboration of OSU-ESL, Battelle (Columbus), and the Tyndall Air Force Base Robotics Group. SOCS was capable of surveying a wide area at a speed of 10 mph and collecting impulse GPR data and magnetometer array data in real time. The OSU-ESL was responsible for the GPR system and AETC, Inc., was responsible for the magnetometer array system.

A special cross-polarized antenna was developed for the SOCS system, operating from 50 to 300 MHz. The cross-polarized configuration is well known for its lower antenna mutual coupling between channels and its relative insensitivity to surface or layer scattering. The impulse GPR data collected from two-dimensional surveying was used to generate 3-D images using the inverse synthetic aperture array imaging method [13]. For each detected target, the electromagnetic signature was extracted for further discrimination based on resonance quality and implied target length [12]. The SOCS platform later collected data at various Jefferson Proving Ground (JPG) Demonstrations and at Yuma Proving Ground in 1998, where an additional EMI (EM-61) array was added. All the measurement results clearly indicated the superior detection capability of the magnetometry and EMI compared to GPR. GPR suffered from a higher clutter level compared to its counterparts. During the Yuma effort, the idea arose to use GPR signatures as discriminators rather than primary detection tools [14]. This has been the guiding notion in the project described

in this report. In particular, the GPR survey system is designed to dwell in an area located as a "hot spot" (signal anomaly) by other means (EMI, Mag, optical examination, historical records...), in order to perform more intensive measurement and processing for discrimination. That is, having been cued, the GPR systems seeks to determine which or what kind of object is present, and to classify it in terms that help enable a dig/no-dig decision. As shown below, information from Mag or EMI surveying may also be used to enhance the interpretation of the GPR data.

Based on the experiences described above, a new type of GPR antenna was designed and developed for the demos reported here. Its features were selected to address the sensitivity and stability issues associated with commonly used dipole antennas when they are operating close to the ground. This new design exploited the dielectric-loaded horn-fed bowtie (HFB) antenna design first introduced in 1997 [15]. Two single-polarization HFB prototypes were built to replace the previous cross-polarized antenna. The new antenna also measured co-polarized data and was much lighter and smaller compared to previous SOCS antenna. Better stability and broader bandwidth was achieved with this new HFB design. During the JPG IV field tests, use of the polarization signature was introduced for UXO classification using a newly constructed fully polarimetric version of HFB antenna [16]. Fully polarimetric GPR data were collected directly above a “hot spot” using a step-frequency system while the antenna was physically rotated. “Fully polarimetric” means that reflections are recorded having both the same polarization and the orthogonal polarization relative to that transmitted. Further, two transmitted fields are produced with orthogonal polarizations. As explained below, the resulting matrix of fully polarimetric signals may be rotated mathematically to obtain principal directions of the scattered response.

The polarization signature from a UXO relies in large part on the fact that the scattered field from an elongated object tends to be linearly polarized. Thus one may examine the angular spectrum of each individual polarization channel (two co-polarized and one cross polarized), obtaining the response as the orientation of each transmission is rotated horizontally. It was possible to use this for classification because a linearly polarized field results in peaks of energy in the angular spectrum. The JPG-IV classification results were inconclusive because of (1) excessive dielectric clutter caused by surface depressions that created a variable and distorting air gap beneath the HFB; (2) limitations on physical dimensions of the rotating device so that the new fully polarimetric HFB was not optimized to reduce antenna ringing. In a later version of the antenna system, as used in this project, a fixed orientation of the antenna was used and the scattering matrix was rotated mathematically, which also reduced recording time.

1.4 Objectives of the Demonstration Series

The overall objectives of the demonstration series were

- To show what, if any, the UXO discrimination capabilities of the UWB full-polarimetric GPR are;
- To quantify the discrimination capability as a function of environmental conditions, UXO and clutter types, and processing approaches;
- Where possible, to compare the GPR's discrimination performance with that of other, baseline technologies; and
- To estimate cost and cost savings from using GPR for UXO discrimination.

Showing some discrimination capability means producing a more successful UXO/non-UXO classification than random or arbitrary classification of anomalies. In terms of ROC curves, material in the sections below explains what corresponds to “random or arbitrary” classification and how departure from that is quantified.

1.5 Regulatory Issues

All the demos were carried out at DoD or former DoD government-managed facilities. All activities and aspects of the technologies necessarily complied with applicable regulations as enforced by the site institutions. To the authors’ knowledge, there are currently no regulations elsewhere that would prohibit use of the GPR survey technology. The primary regulatory issue facing this and other UXO discrimination technology is gaining confidence and approval of Federal, state, and local regulators and stakeholders. Hopefully the publication of findings in reports such as this, dissemination through ESTCP and other publication, and tech transfer as outlined below will all contribute to this. Further, government entities such as the U.S. Army Corps of Engineers and the Naval Facilities and Engineering Command must be induced to design requests for cleanup proposals so that newer technologies and approaches may be considered. Contract specifications in terms of performance standards instead of approach used is a desirable

option. This would place greater burden on quality assurance and quality control measures, which would then logically have a prominent place in contractual arrangements.

2 Technology Description

2.1 Overview of System Development and Its Implementation in the Demos

To demonstrate the UXO classification capability of GPR and to establish its performance baseline, the OSU and the Cold Regions Research and Engineering Laboratory (CRREL) of the U.S Army Corps of Engineers Engineer Research and Development Center (ERDC) teamed up for a three-year project supported by the DoD Environmental Security Technology Certification Program (ESTCP). Dr. Kevin O'Neill of ERDC-CRREL was the PI with Dr. Chi-Chih Chen Co-PI and leader of the OSU-ESL team. First, a broadband fully polarimetric GPR prototype was set up by the OSU-ESL with improved dual-polarization HFB antennas. Although the network analyzer based prototype has the disadvantage of slow data rate compared to most commercial units, its ultrawide bandwidth and fully polarimetric features could not be matched by any of the commercial GPR systems. Also, pending successful demonstration, the data rate could readily be improved. This prototype was taken for blind classification demonstrations (demos) at four test sites, the details of which are contained in reports on the individual demos [17-21] and in the references therein. At each site, the CRREL-OSU team collected GPR data locally around each flagged "hot spot," not knowing whether the spot contained a UXO. The flagging and decision as to what locations to flag were executed at each demonstration site by a field crew associated with the particular site, usually in consultation with ESTCP, without divulging this information to the OSU-ESL/CRREL survey team. In the last two demos, the flag locations and their uncertainties were chosen to resemble the locations that would be obtained from magnetometer or EMI surveys at live sites. All ground truth was closely held until after the CRREL/OSU crew reported results of processing.

Data were collected between 20 MHz and 810 MHz in typically well drained sandy soil or between 10 MHz ands 410 MHz in lossy soil (soil with a strong tendency to absorb the radar signal, e.g. wet soil). UXO classification was done during post processing, after the team returned from the field. The first processing pass was generally completed overnight. Processing refinements for the

more inobvious cases were pursued later at a home base. In the ultimate form of the system, targets were sorted according to target types (UXO-like or non-UXO) and confidence level (high, medium, or low). This information was then delivered to the ESTCP office, along with other estimated target features such as depth, length, and azimuthal orientation, for each measurement cell. In detailed reports submitted for each demo, after the ground truth had been provided, other summarizations of results were also included, such as ROC curves. The initial (blind) reporting usually took approximately from two to four weeks after the field measurements. Sometimes the ESTCP staff and/or site crew released the ground truth in stages, for further performance assessment of processing in which some partial prior knowledge is available (see below).

As the project evolved, system configuration, measurement approaches, data pre-processing techniques, feature extraction methods, classification rules, and performance assessment methods were refined and the improvements implemented. For instance, after the first field test conducted at Tyndall AFB, Florida, January 2000, it was apparent that collecting data at a single position directly above a “hot spot” had undesirable limitations. In practice, the antenna was swept along lines over each supposed target location, in a variety of line orientations. However, at Tyndall this was done primarily to ascertain the best (single) location from which to select data for processing, and there were only seven measurement positions on each line. The frequency and angular spectra were examined for target linearity, meaning here evidence that an object was elongated, with a dominant axis. In this context, the opposite of "linear" is "compact" (for lack of a better term), meaning "having no strongly dominant orientation." While a flat plate has a distinctly elongated profile when viewed from the edge, the response is weak from that orientation; further, when viewed by GPR from the side, a plate produces strong responses for any horizontal rotation about an axis normal to the side. For this reason, it is not considered to show high linearity in the sense used here, such as would apply to an elongated body of revolution. Establishing this, however, requires diverse enough views to delineate the relevant signal patterns. Also, initially the position directly above a UXO, usually more or less coinciding with the flagged location, was considered the "logical" position for which to process measurements. Actually, this antenna position produces weaker response and reduced resonance excitation whenever a UXO is tilted more than 30 degrees from the horizontal. This accounted for several UXO’s missed during the Tyndall test [17, 18, 22]. In subsequent demos, a more general system was implemented. Data were examined for many more closely spaced positions along each antenna pass. Spatial and frequency patterns along each pass were also exploited. This is explained further below.

In order to assess the GPR classification performance appropriately at Tyndall and the subsequent sites, two systems were employed. In the first, default system, any object in the target list with a length-to-diameter (L/D) ratio greater than three was designated as UXO-like. That is, this was the criterion applied to sort items within the ground truth list into UXO-like or non-UXO-like classes. Its use was based on the notion that such items would have to be dug if *any* sensing system produced comparable shape/size information. As explained more specifically below, virtually all other available classification systems are based in effect on equivalent inferences. The radar signal processing does not directly produce an estimate of L/D. Rather, other parameters are obtained and used to estimate likeness to a UXO response. When the GPR parameters indicated that a particular target was UXO-like and the corresponding object in the ground truth list had an L/D greater than or equal to 3, this was viewed as a successful detection. If the GPR parameters indicated that an object was UXO-like by these criteria but in fact its L/D was less than 3, then this constituted a false alarm. In isolated instances, when some actual UXO at site were in fact not very elongated, a criterion of L/D $\geq$ 2 was implemented to distinguish UXO-like from non-UXO in the ground truth. Sorting criteria used in all results displayed are specified below along with the results, usually including both the TRUE UXO and UXO-like criteria.

In the course of the project, this use of "UXO-like" as a basis for sorting the ground truth became a source of some controversy. The CRREL/OSU team felt that this was a logical criterion, particularly in view of information that might be produced by alternative sensor systems. GPR reacts to the overall shape of an object, not its details. Similarly, Mag or EMI data, while also (possibly) registering some aspects of an object's composition or detailed geometry, ultimately are interpreted in terms of evidence of an elongated shape. For example, distinct Mag dipole/depolarization or particular ranges in the ratio of inferred axial to transverse response may be used [4, 5]. As here, in those treatments classification may sometimes be enhanced by further gross indications of object depth and overall size.

To pursue this, consider a key GPR signal feature in our classification system, namely the estimated linearity factor (ELF). This is calculated from the eigenvalues obtained from the scattering matrix in the late-time response region. The ELF can have a value from zero to one, depending on the degree of linear polarization in the scattered field. A value of zero indicates complete rotational symmetry, i.e. L/D ~ 1 in all orientations, as for a sphere or other compact object. A value of unity indicates a long thin object. The resonant frequency also implies the length of the target (greatest linear extent in a dominant direction), and this is determined as an

adjunct parameter. While EMI and magnetometer systems respond to additional target features besides L/D or linearity, in practice (to our knowledge) there are only very limited examples of successful "fingerprinting" of UXO signals for discrimination. That is, the other technologies typically try instead 1) to estimate the overall size of the object and 2) to examine (in effect) dipole moments along different target axes, to ascertain the presence of a dominant direction and any evidence of cylindrical symmetry. Such processing rarely indicates that an object is a specific UXO, or in fact that it is necessarily a UXO at all. Rather, at best, it indicates that an unseen target has generic features associated with a UXO, *i.e. that it is UXO-like*. If such Mag/EMI processing indicates a target of UXO size and shape in terms of directional response, then such a target will unquestionably be placed on the "dig list." Clearly, the approach here using ELF and estimated target length is not sufficient to separate a UXO-like piece of clutter from a true UXO item of similar dimensions. However, the same can be said of Mag/EMI systems that consider ratios of eigenvalues (directional dipole moments). Thus the UXO-like/non-UXO criterion seemed like a logical means of comparison. That said, the GPR classification performance was evaluated according to *both* "true UXO" and "UXO-like" sorting criteria, allowing readers to pursue their own notions in this regard, and to see the difference. These criteria are discussed further below.

The second field test was conducted at the NRL Blossom Point UXO site [23], in January 2001. The soil type at Blossom Point (BP) had a much higher electromagnetic energy absorption rate than that at the Tyndall site, because it was fine grained and also very wet at the time of the test. All the UXO-like items at the Blossom Point site were less than three feet in length. There were also many vertical UXO-like items since the site was designed primarily with magnetic sensor evaluation in mind. This orientation is least favorable for GPR because the targets present the smallest cross section to the sensor. To deal with this and the previously noted issues at Tyndall, a multi-position, multi-pass scheme was implemented at BP. This approach produced additional spatial variation information and provided a diversity of look angles at the target. Examination of the spatial variations in ELF and in resonance patterns reduced the false alarms caused by shallow, horizontally offset non-UXO items. It also increased the detection rate of UXO-like items that approach a vertical orientation. Most of the vertical UXO-like items were correctly classified. A few of the vertical UXO-like items were missed because their relatively great depths caused weak response and limited observation angle [19]. Processing experiments were performed to see the influence of improved prior information on target depths, in various degrees of accuracy. Also, additional data patterns were examined and classification rules added to avoid false alarms associated with such items as vertical plates, horseshoes, and barbwire bundles [20].

The revised classification rules were adopted in the subsequent blind tests conducted at JPG-V (Madison, Indiana), June 2001 and at the former Ft Ord (Monterey, CA), October 2001. Two new measurement approaches were also implemented to better simulate the real-world scenarios and to improve the scan efficiency. First, a position error of size and direction unknown to the CRREL/OSU team was added to the actual GPS location of the target. This was to reflect a more realistic situation in which each hot spot is most likely determined from magnetometer/EMI survey data. At real cleanup sites, the offset is probably not random but related to the depth, size, and orientation of the UXO, given the sensor systems used to locate "hot spots." Additional location errors may also be introduced by the positioning system used on the EMI/magnetometer surveying unit.

The second change in procedure consisted of manually surveying each flagged location prior to the GPR measurements, using a Schonstedt Model GA-72Cd handheld magnetometer (Figure 1). This is the type of instrument commonly used by EOD personnel during a “mag and flag” survey. Because the Mag surveyor could easily progress from flag to flag faster than the GPR, this did not influence the execution time during any of the demos. Further, one person was usually required to precede and direct the GPR rig, and adding Mag duties therefore did not increase personnel time. As a kind of "reality check," this provided a confirmation of the hot spot and also detected small near-surface clutter here and there.

An important side benefit of the Mag measurements was that signal sign change during the magnetometer sweep was sometimes clear enough to indicate the presence of a magnetic dipole pattern, as is associated with elongated targets. If a magnetic dipole was observed, the approximate dipole orientation was then used as the orientation of the initial radar pass. Other uses of this information for possible improvement of the GPR processing are described below. Those performing the Mag work had no special skills or training. Typically someone did this who had never previously operated a magnetometer, after about 10 minutes of training. Of course, if a more accurate magnetometer survey map could be provided by a previous e.g. vehicular survey, this would supersede the handheld measurements. Although realistic, using the “mag and flag” position did introduce an additional challenge to the GPR survey because the optimal observation angle for a GPR system is usually orthogonal to that for an EMI/Mag system. This is illustrated in Figure 2. Whether an offset from the ideal GPR survey position was introduced purposely by the site management crew or by real-time interpretation of our magnetometer readings, it placed a greater

burden on accurate inference of azimuthal (horizontal angle) target orientation. Whenever the estimated target orientation (ETO) from GPR processing was clear enough to warrant it, at least one subsequent GPR pass was made in the ETO. This meant that a pass would still likely pass directly over the target (and through the optimal GPR view), despite the initial offset. However, poor initial ETO information combined with an offset of deeper targets could degrade performance.

It is striking that classification performances were quite similar in the JPG-V and Ft Ord tests despite the very different environmental, UXO, and clutter characteristics. The soil at the Ft Ord site was mainly dry sand, which is generally very favorable for GPR. Overall, this site "should" have produced the best discrimination performance in the series of demos. However, extensive tunnel networks created by small animals resulted in high clutter level. These burrows and also the clustering of flags (Figure 3) and presumably targets near one another reduced the signal-to-clutter ratio significantly. Because of the randomized offsets of the flags from target locations, the targets may often have been even closer than the clustered flags. The effect of all this on the data was that, while essential resonances frequently still showed through, ambiguities appeared in ETO's. From this consideration, it is not surprising to see classification performance similar to that obtained at the JPG site, where low signal-to-clutter ratio has repeatedly been observed in GPR studies. Notably, the crude handheld magnetic dipole detection at Ft Ord actually improved classification accuracy significantly, strengthening the case for a multi-sensor system.

Figure 1. Local magnetometer survey around flagged spot.

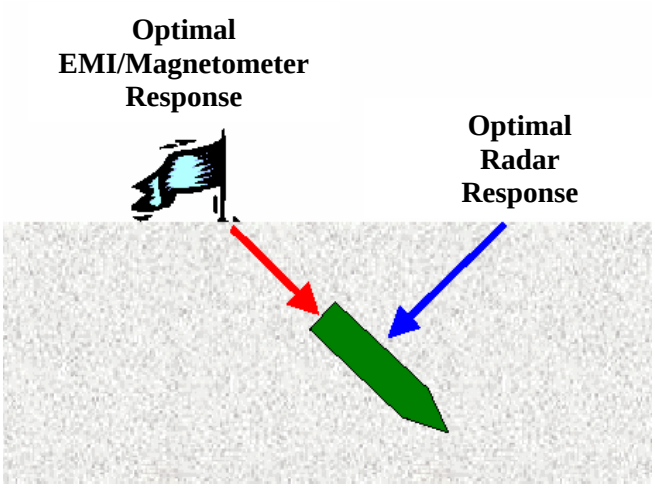

Figure 2. The orthogonal nature of radar and EMI/Magnetometer systems.

Figure 3. Badger hole beneath clustered targets at Ft Ord.

Overall, valuable lessons and experience were obtained from four UXO test sites covering contrasting environmental conditions, UXO types, and clutter issues. During the course of study, many improvements in the system configuration, the measurement approach, data processing method, and classification rules resulted in a need for fewer test sites than originally foreseen. Classification performance at other sites with characteristics in the range encountered would likely be similar to that seen here, until a new generation of GPR development and survey technique is fielded. The ultimate system applied in this study still has significant limitations in terms of missed detections and inability to distinguish true UXO items from those that are UXO-like. However, this ESTCP effort has established a performance baseline and provided understanding of GPR potential and limitations, based on rigorous tests employing about the limit of what could be achieved in both bandwidth and polarimetric information.

2.2 Fully Polarimetric GPR for UXO Discrimination

The demos in this project were executed using the fully polarimetric GPR prototype developed by the OSU-ESL. The following sections provide brief descriptions of the RF components, antenna unit, positioning and orientation instruments, and operation software. More detailed information can also be found in the references, some of which are in the open literature, with the greatest detail available in ESTCP project reports on the individual demos [17-22].

2.2.1 RF Transceiver

The heart of the GPR system is a commercial Vector Network Analyzer (VNA) model HP8712ET by Agilent, as shown in Figure 4. This device performs reflection and transmission measurements between chosen frequencies in steps of variable i.e. specifiable size. The frequency range was chosen to be from 20 MHz to 810 MHz in sandy soil and from 10 MHz to 410 MHz in lossy soil. The frequency increment was as little as 2 MHz and as great as 10 MHz. The particular VNA model used could perform two kinds of reflection measurements in any single shot: 1) direct reflection measurement in the same polarization as was transmitted (S_{11}); and 2) measurement of cross-polarized transmission (S_{21}), i.e. measurement of reflection in polarization (E field orientation) #2 due to transmission in the orthogonal polarization direction #1. (See next section for

explanation of antenna orientation and principal antenna directions). The VNA could not measure S_{22} data (transmission and reflection polarization both in the orientation perpendicular to the antenna orientation, which was also ultimately the direction of travel). Therefore, a special RF switch box was built so the system could collect the fully polarimetric data. Some newer models of VNA come with this capability built in. By reciprocity, $S_{12} = S_{21}$, so it was not necessary to measure more than the three components, S_{11}, S_{21}, and S_{22} to infer complete polarimetric data. Because both amplitude and phase were recorded for each of these three components, the scattering matrix can be rotated mathematically to obtain full polarimetric information for any other set of principal antenna axis directions 1 and 2, without physically rotating the antenna itself about an axis normal to the ground.

Figure 4. Vector Network Analyzer (HP8712ET).

2.2.2 Antenna Unit

An ultra-wideband fully polarimetric HFB antenna is the key component of the whole system. Such an antenna element needs to be able to operate over a wide frequency range (10~810 MHz) to cover the resonant features of the majority of UXO sizes in most soil types. A HFB antenna is composed of a dielectric loaded TEM horn section and a resistively terminated bowtie dipole section, as illustrated in Figure 5. This horn section is detachable such that different horn sections with different dielectric constants can be used. This can produce a better match with the dielectric constant of the ground, in turn providing better sensitivity. Two linearly polarized HFB elements are arranged perpendicular to one another, as shown in the figure, to provide the two

necessary send and receive channels. Each element can be configured to operate in the transmitting or receiving mode. The complete polarimetric information can be used to infer the UXO orientation projected onto the plane of antenna aperture.

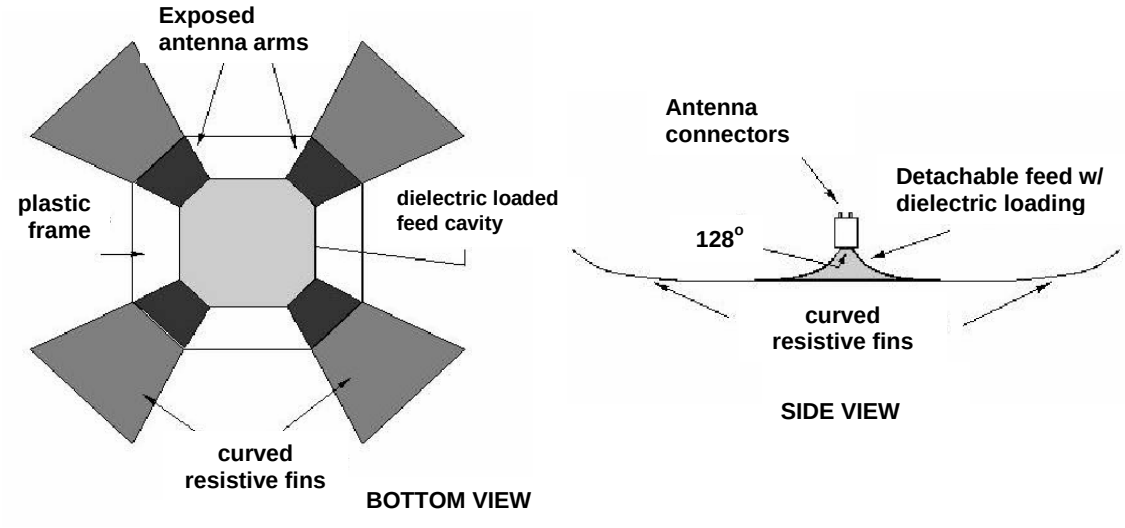

Figure 5. Sketch of the bottom (left) and side view (right) of the OSU/ESL UWB full-polarization GPR antenna.

The surge impedance of the antenna was designed to be 100 ohms so that it matched the impedance of the feed cable. Figure 6 shows the surge reflection coefficient and impedance, clearly indicating the broadband nature of this antenna. These values were calculated using a 3-D FDTD model developed to characterize the HFB antenna [24].

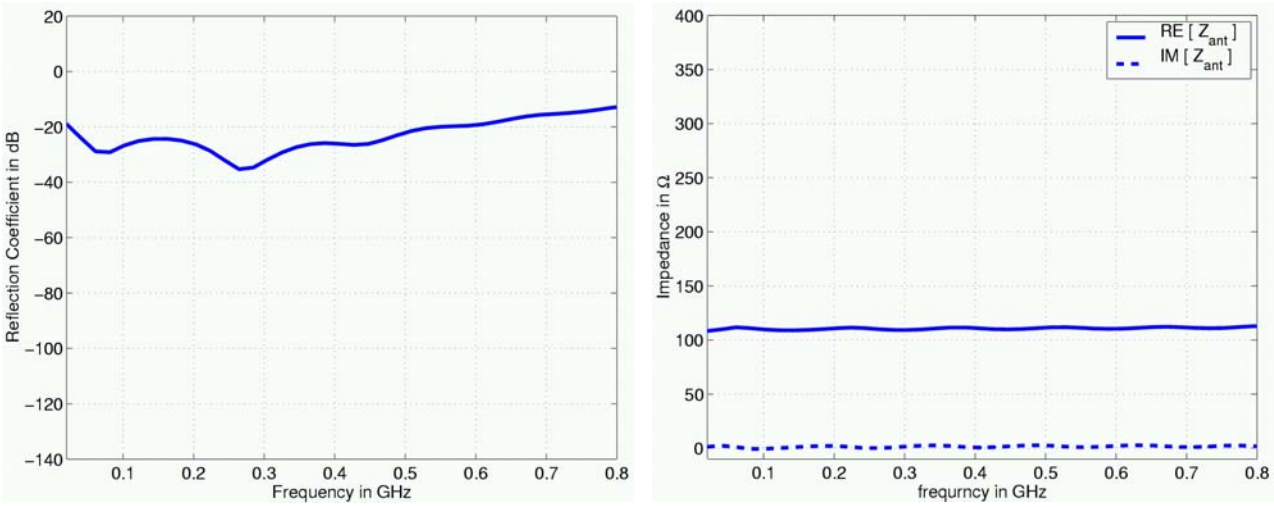

Figure 6. The input reflection and input impedance values for the fully polarimetric HFB antenna, calculated with a 3-D FDTD model.

During the first test at Tyndall AFB, the antenna was mounted in front of an ATV and was oriented at 45 degrees with respect to the direction of progress, as shown in Figure 7. This initially seemed like a good design because it provided maximum diversity in polarization in the illumination, not constrained by the orientation of the vehicle. However, if there is lateral offset in the target position from the travel path or if one wishes to perform a linear scan by moving the antenna along a straight line passing through a hot spot, this 45-degree configuration is not desirable. This is because the target passes through the maximum intrinsic depolarization of the radiated fields. Calculated distributions of the radiated fields in a plane beneath the antenna clearly demonstrate this. Figure 8 plots the magnitude of the co-polarized and cross-polarized field distributions over a horizontal plane beneath the antenna. As one can see, when the observation point moves away from the principal axes (see Figure 9), the magnitude of the cross-polarized field increases. After the Tyndall demo, the 45-degree antenna orientation was reconfigured into parallel and transverse orientations as shown in Figure 10. This also better suited the needs of the scan scheme and data processing adopted later on, in addition to providing a minimal depolarization in the scan plane. Notice that the front-mount configuration was also changed into back-tow configuration, to avoid mechanical problems in antenna-ground contacts (plowing with the antenna).

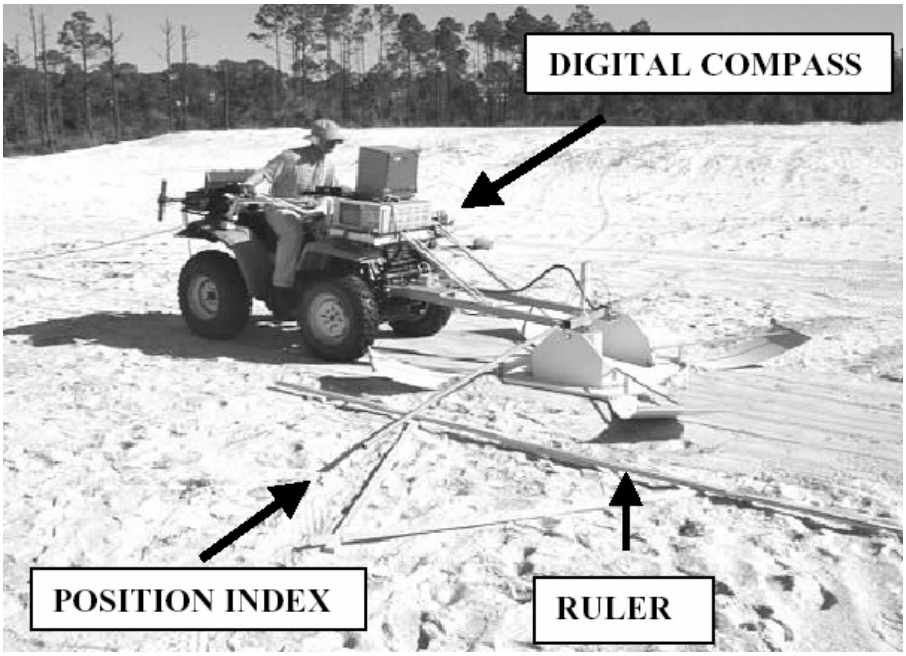

Figure 7. Fully polarimetric GPR configuration at Tyndall AFB UXO site.

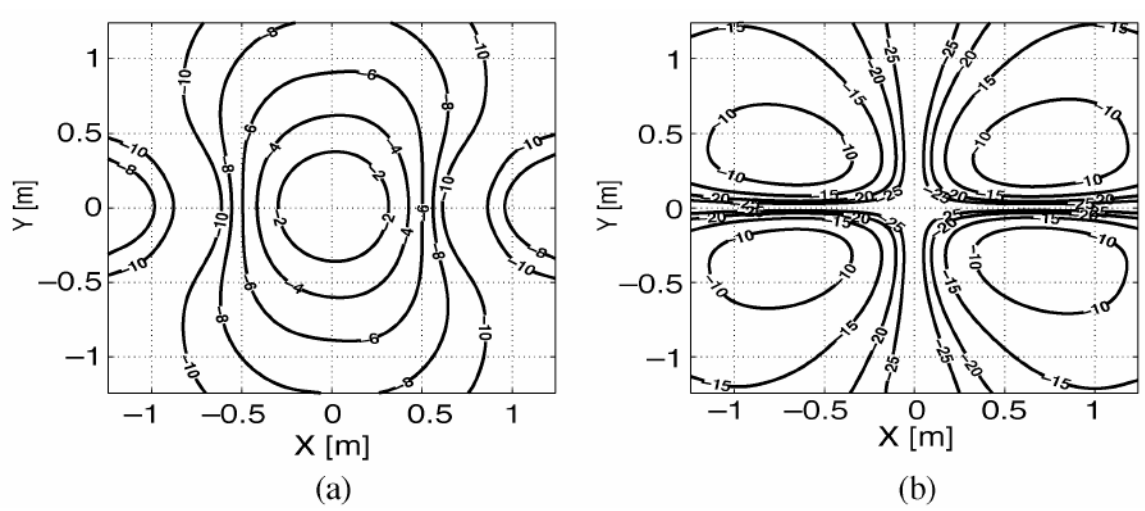

Figure 8. Simulated radiation field distribution in dB, plotted over a horizontal plane near the HFB antenna aperture. (a) co-polarized (b) cross-polarized.

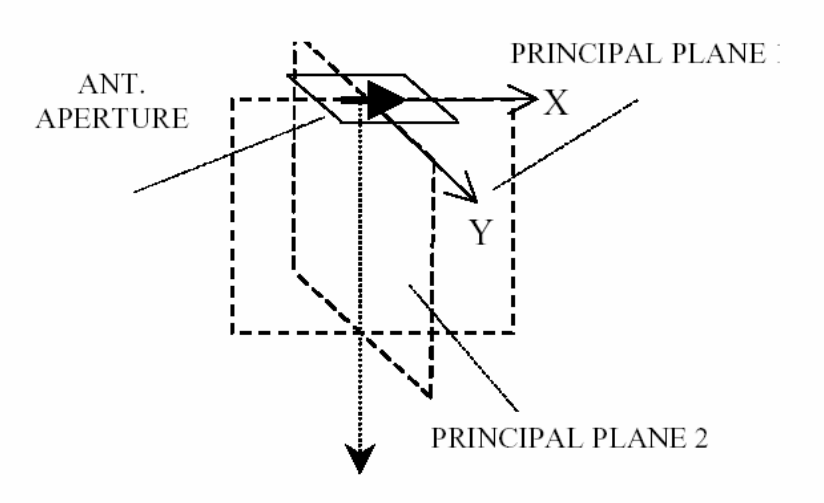

Figure 9. Principal planes of the radiating fields.

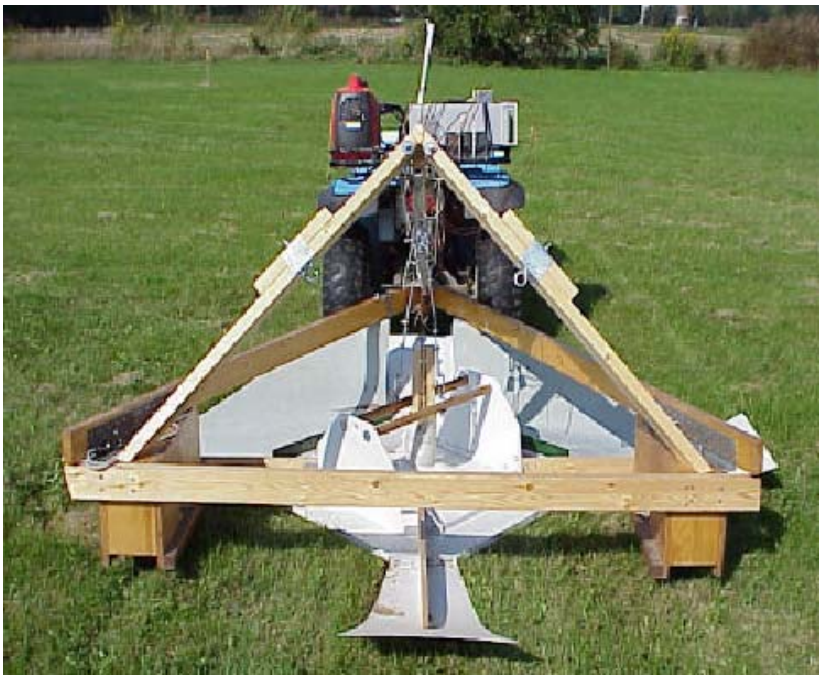

Figure 10. UXO GPR configuration used at BP, JPG, and Ft Ord sites, showing antenna arms aligned with and perpendicular to the travel direction.

2.2.3 Heading and Positioning

Since the target orientation was estimated with respect to the antenna orientation, a digital compass was attached to the mounting structure of the antenna. This compass provides the antenna's orientation. The compass was recalibrated at each test site. At the beginning of each linear scan, the compass readout is recorded in the header of the data file. The feature extraction routing then incorporated this information to generate target orientation with respect to the magnetic north (or true north). The positioning system of spatial increments in antenna location in each linear scan is not critical as far as GPR features are concerned. After some initial position relative to the apparent target location was ascertained, marks on the front wheel of the towing vehicle were aligned in succession with a reference on the vehicle frame, as shown in Figure 11. The vehicle stopped moving at each position while the radar was collecting data. The total scan for each radar pass covered approximately 120 inches in 3-inch increments, in times listed in the Cost Section below.

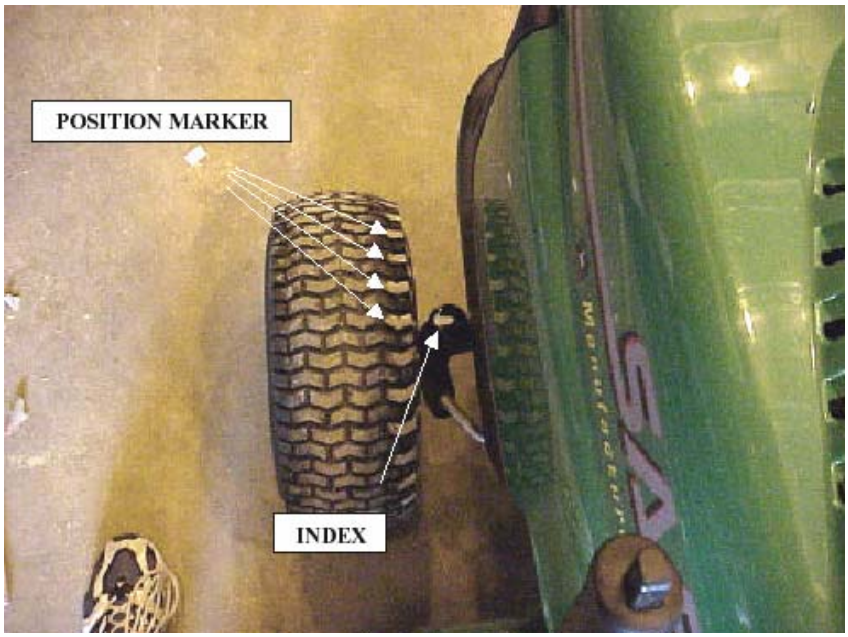

Figure 11. Marks on the front wheel for incremental positioning during each radar pass.

3 Demonstration Design

3.1 Performance Objectives

The overall objectives of the demonstration series were

- To assess the UXO discrimination capabilities of the UWB full-polarimetric GPR in cued surveying;
- To quantify that discrimination capability as a function of environmental conditions, UXO and clutter types, and processing approaches;
- Where possible to compare the GPR's discrimination with other, baseline technologies; and
- To estimate cost and cost savings from applying GPR discrimination in UXO remediation.

These overall demonstration objectives might be translated into primary and secondary "performance objectives":

- Primary: Achieve quantified discrimination capability that is better than arbitrary or random classification of anomalies that have been identified by other means, e.g. Mag, EMI surveys, or other records;
- Secondary: Achieve quantified discrimination capability that is better than that of established or baseline UXO discrimination technologies.

Showing some discrimination capability means producing a more successful UXO/non-UXO classification or consequent dig/no-dig judgment than random or arbitrary classification of anomalies. Discrimination performance is quantified here in terms of probability of detection (Pd) and probability of false alarm (Pfa); and in turn the relation between Pd and Pfa is examined in terms of the [misnomer] Receiver Operating Characteristic or ROC curve. Pd means here the percentage of items in the UXO class that were encountered that were successfully identified as members of that class. Pfa means here the percentage of items in the non-UXO class that were encountered that were identified by the processing as belonging to the UXO class.

A note of explanation on the construction and meaning here of ROC curves in terms of Pd and Pfa. Suppose one decided arbitrarily to classify all recorded signal anomalies as corresponding to a UXO. That would indeed produce a very high Pd, ~ 100%. At the same time, it would also

produce an extremely high Pfa of ~ 100%. At the other extreme, one could consider that *no* signal anomalies corresponded to UXO. This would produce a null Pfa, but also produce a zero Pd. Midway between these possible approaches, one could flip a coin over each anomaly to determine UXO/non-UXO classification, and presumably would arrive at a random 50/50 sorting. Half the time a declaration would be a correct detection and half the time a false alarm. These three points fall on a "line of no discrimination" (LOND) that contains other combinations of equal Pd and Pfa, all of which correspond to some imaginable scenario in which processing performs arbitrary or random classification (Figure 12). Thus the primary and most basic performance criterion is to produce a ROC curve that lies above the LOND. The more steeply a ROC curve rises on the left, the more successful the system that produced it. In practice, one can produce ROC curves from data by beginning with some very restrictive criteria by which essentially nothing is classed as UXO (the 0/0% point). Criteria are then loosened progressively, producing more detections but also picking up more false alarms. In this sense one proceeds up the ROC curve from the lower left (hopefully) to the upper right. Note that a ROC curve may start out promisingly but then hit an upper limit at less than 100% Pd, crossing below the LOND when the detection tops out at some maximum achievable Pd (ROC4 in the figure). Worse, random influences or pathological bias can produce even worse Pd/Pfa ratios than arbitrary or random classification, never rising above the LOND (ROC5).

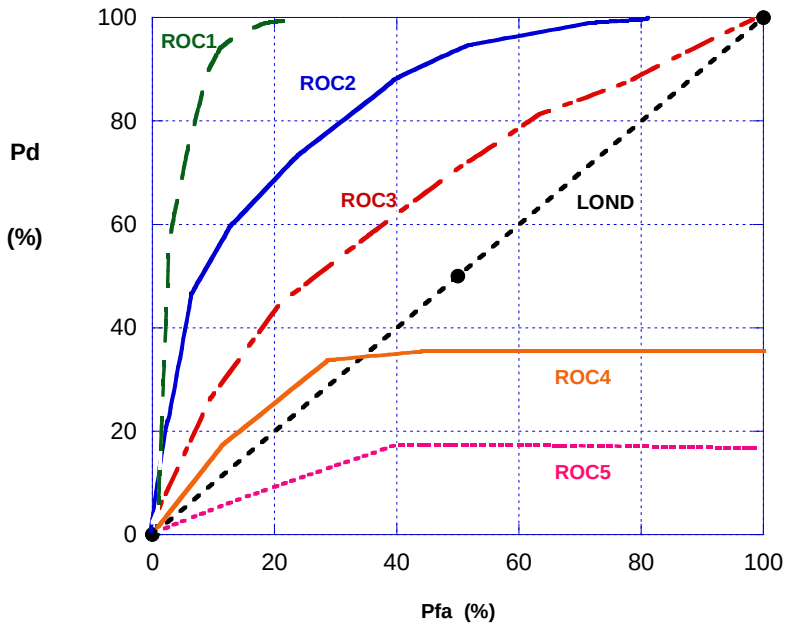

Figure 12. Hypothetical example ROC curves. The black circle markers indicate arbitrary or random Pd/Pfa classifications of 0/0%, 50/50%, and 100/100%. LOND = line of no discrimination.

3.2 Survey, Processing, and Interpretation Methods

This section describes the algorithms developed for processing the GPR data and for extracting target features including linearity, depth, length, and orientation. First, consider briefly how GPR signals originate and how they can be displayed. Figure 13 shows two schematic views of the same horizontal sensing pass by a GPR antenna. The top picture shows a spatial diagram of the antenna locations, the target, and the round trip signal paths. The bottom picture shows what the data display would look like for this same situation, as typically rendered in terms of antenna position and signal travel time ("delay"). When the antenna is located directly over the target, the signal path to and from the target is minimal; hence the travel time is a minimum. For antenna positions offset to the side of the target location, signal path lengths and travel times are both longer. In the (travel) time vs. antenna position plot (bottom), the reflection from the target thus appears as a hyperbola. Figure 14 shows some actual data in the usual signal travel time vs antenna position format. The target causes the dark arc clearly visible in the center of the figure.

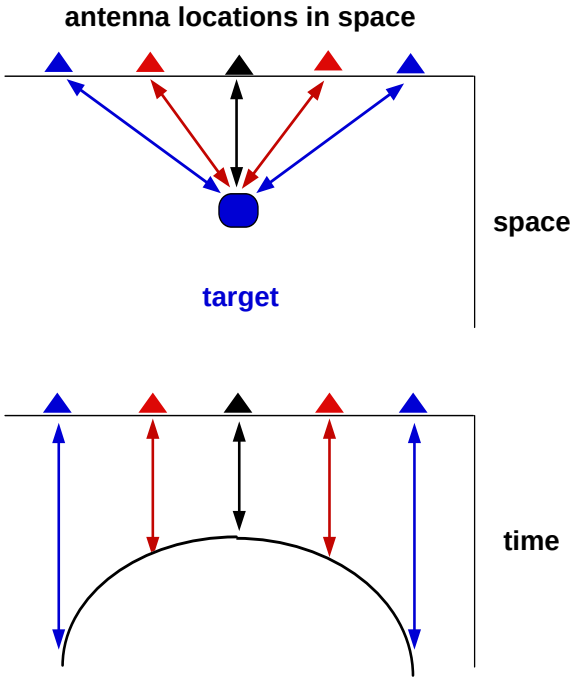

Figure 13. Top: Spatial view, in which the horizontal axis is spatial location of the antenna and the vertical axis shows depth in space. Bottom: Data for same, with antenna position again on horizontal axis but signal travel time ("delay") on the vertical axis.

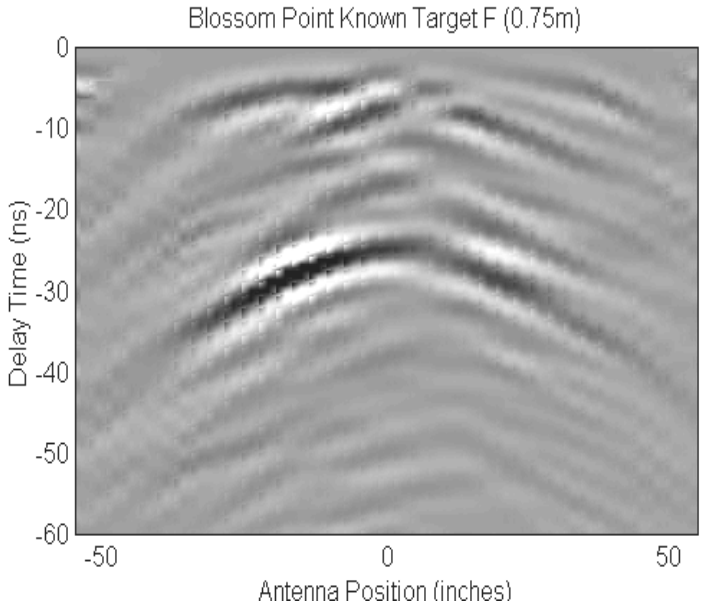

Figure 14. Recorded GPR response, displayed in terms of signal travel time (vertical) vs antenna position (horizontal), for a horizontal steel cylinder buried 75 cm deep at BP.

3.2.1 Measurement Approach

The measurement approach was finalized after the second demo. For each target locale, a minimum of two passes was performed in two or three stages, in orientations parallel and transverse to the ETO. Prior to the GPR measurements, a conventional Schonstedt magnetometer was used to survey manually the local area near the flagged "hot spot," to determine the maximum magnetic response position and to check for indications of a magnetic dipole (sign change in magnetometer reading or double-peak output in magnitude-only unit). A magnetic dipole response pattern indicates an elongated ferrous object that is not aligned with the earth's field. If a magnetic dipole was detected, the initial radar pass was then directed along the estimated orientation of the dipole, since that provided an approximate indication of the ETO. If no dipole was detected, an arbitrary orientation was chosen for the initial pass. The radar data collected from the first passes was processed overnight and on site to determine an ETO of any target that showed linearity (high ELF). If the orientation estimated from radar data was close to that from the magnetometer, then the

second pass was oriented transverse to the orientation of the first pass. If the ETO from GPR processing was significantly different from the apparent magnetic dipole orientation, the second and third pass would be directed parallel and transverse to the new orientation found from GPR data.

If GPR data collected from the first pass showed a maximum GPR response offset from the center of the GPR scan, i.e. flagged position, the second pass would be centered at the position where maximum GPR response was observed in the first pass. Figure 15 shows an example of all the passes conducted in Area 1 at JPG-V site. Note that the offset of each pass is not shown. In the JPG-V test, the orientations of 41 out of 72 UXO-like items were either approximately parallel or perpendicular to the scan directions predicted from the magnetic dipole, used to guide the first pass. This certainly significantly reduced the number of passes required, compared to the number that would have resulted from a randomly picked first orientation. Use of magnetic dipole orientation estimated from a more sophisticated mapping system would be more accurate and efficient than the manual Schonstedt-waving approach, possibly further improving the ultimate GPR performance.

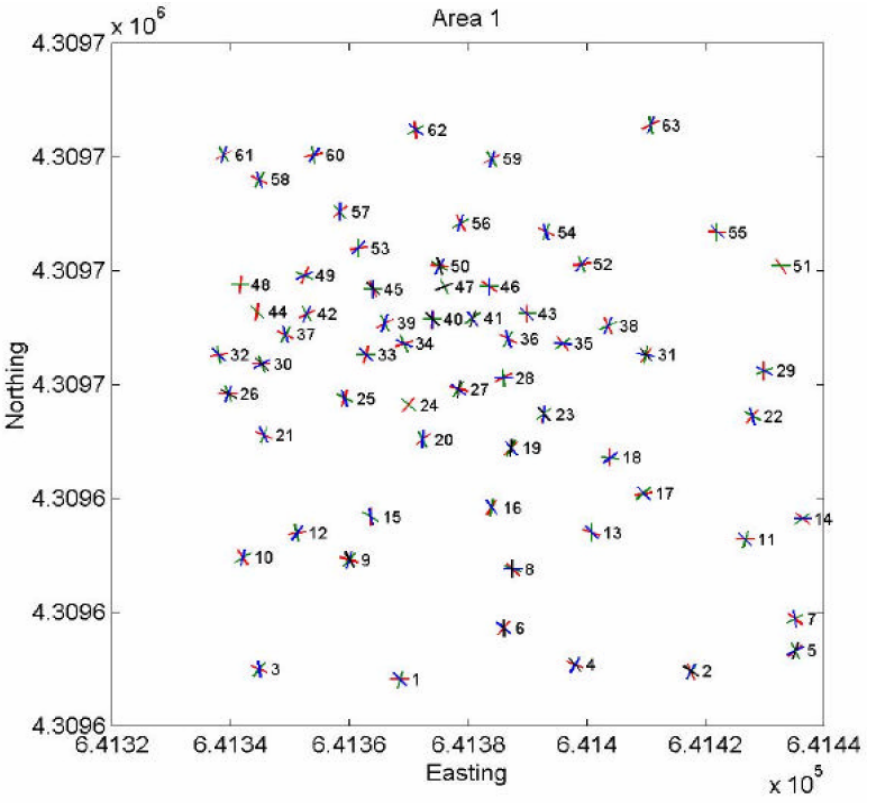

Figure 15. GPR passes for targets in Area 1 at JPG-V. (Red – Pass 1; Green- Pass 2; Blue- Pass 3; Black- Pass 4)

3.2.2 Pre-processing of GPR Data

The purpose of pre-processing the GPR data is to improve the signal-to-noise ratio (SNR) and signal-to-clutter ratio (SCR), so that the accuracy and stability of feature extraction are improved. Typical GPR data contain system and environmental noise that limits the ultimate sensitivity of the system. However, because the clutter level is usually much higher than noise level, it is the SCR that almost invariably determines the detection sensitivity in GPR measurements. A detailed treatment of this is provided in the report on the BP demo [19]. GPR signal clutter can come from ringing within the antenna itself or from reflection from the contact between the antenna and ground surface. Subsurface inhomogeneities due to variations in water content, soil composition, and natural features such as voids, roots, and rocks also produce signal clutter. Each type of clutter has its distinguishing features, which may or may not be similar to the signal content from a UXO. Most natural clutter does not have strong electromagnetic resonance. It also lacks linearity, except for (in these demos) some ditches or animal tunnels. Figure 16 shows an example of a high clutter level caused by a network of badger tunnels. The data were obtained at Ft Ord where the medium is dry sand, which would otherwise be favorable to GPR. These tunnels have openings to the surface with diameters ranging from about two to six inches or more. While it cannot be seen in the figure, which shows only signal magnitude, the elongated geometry of the tunnels tended to produce reflections that were more or less linearly polarized. This tended to confuse the algorithms designed to detect the linear polarization from late-time UXO signals.

In most GPR applications, the major clutter source is the antenna. However, for UXO classification, it is essential to have little or no ringing or polarization distortion from the antenna. This must be addressed in antenna design because these problems are very difficult to remove or calibrate out using processing procedures. In the absence of distorting environmental features, the antenna system used in these demos showed outstandingly good suppression of ringing and polarization quality. Thus any troublesome resonance and polarization distortions generally resulted from environmental features.

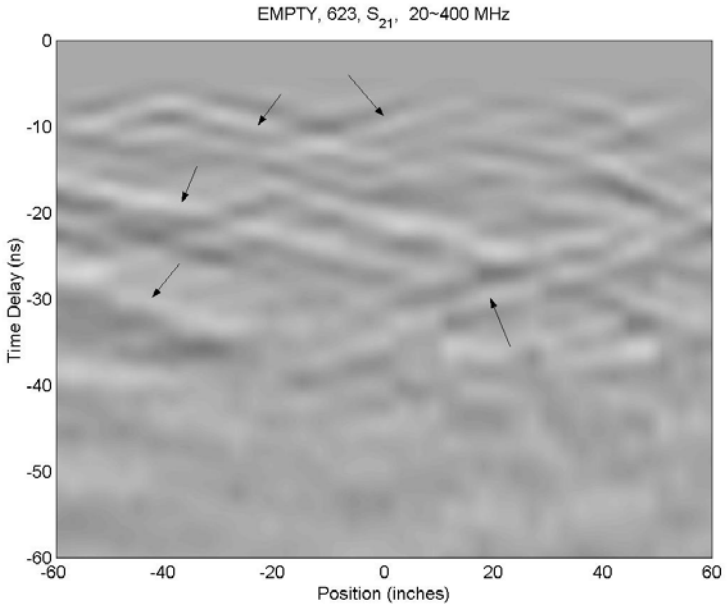

Figure 16. Example of clutter caused by underground badger tunnel networks in an empty site at Ft Ord.

3.2.2.1 Ensemble Background Subtraction

In the raw co-polarized responses, S_{11} and S_{22}, strong antenna clutter is present due to the reflection at the antenna feed point. For the HFB antenna, this reflection level is approximately –20 dB over the majority of the frequencies (Figure 6). For a broadband antenna, this value is considered excellent. It is very difficult to achieve a reflection level lower than –30 dB for the kind of bandwidth and frequency content considered here. However, for the specialized purposes here, this level is still intolerable. Because of soil losses and geometrical spreading of the radar beam, this level is much higher than signal strengths from most buried targets of interest. Because the HFB is specially designed to produce this reflection independent of the content of any particular measurements, such antenna clutter can usually be reduced by 30 ~ 40 dB via background subtraction. A common practice is to calculate the average waveform from all the waveforms collected in one scan and then to subtract this average waveform from the data. The underlying assumption is that the background is omnipresent and possibly smooth and will emerge in the averaging, relative to any discrete target. All the data presented in this document have had the background subtracted.

3.2.2.2 Data Calibration

A system calibration was also performed to remove any distortion related to the RF system and cables leading to the antenna. This was done by measuring standard loads such as a short or a matched load placed at the end of the cables. A field antenna calibration procedure was also performed. The purpose of these two calibrations is to obtain true target responses as if the incident field had a flat spectrum. Antenna calibration requires that the spectrum of the antenna transfer function be determined during a transmission measurement. Ideally, this requires an infinite plane that is a perfect reflector at the depth of the object of interest. In practice, the target depth varies and a perfect reflector at depth is clearly not available. Therefore an alternative method measured the backscattered responses of a very long conducting wire cable laid on ground surface beneath the antenna, such that the ends of the wire extended very far beyond the edges of the antenna. The wire was oriented at 45^{o} with respect to the antenna arms such that the S_{11}, S_{21}, and S_{22} responses should be similar if antenna arms 1 and 2 have similar characteristics. The background data in the absence of the wire were subtracted to obtain only the wire response multiplied by the antenna's transfer function.

The solution for the scattered fields from an infinitely long, thin PEC cylinder in free space or any homogeneous medium can be calculated exactly. However, this is probably unnecessary. Since such a thin, long conducting wire has a very smooth response spectrum, any large variation in the spectrum can be identified as coming from the antenna. Also, the transfer functions for S_{11}, S_{21}, and S_{22} should be similar because antennas 1 and 2 have the same characteristics. The long wire calibration procedure also automatically includes the effect of soil near the surface and was repeated when soil conditions changed significantly. Thus the procedure succeeds in accounting for the soil when it is coupled to the antenna.

Figure 17 plots the magnitude of the spectrum of the antenna transfer functions measured at JPG-V for dry and wet soil conditions. The 30 MHz peak is associated with antenna ringing. Figure 18 compares in a space-time plot the data before and after applying the antenna calibration. The target located near the center of the scan was a 81 mm mortar buried at the depth of 0.35 m with a 45^{o} inclination. The uncalibrated data show less scattering detail due to the presence of 30 MHz ringing. The subsurface layers are also more visible after the calibration.

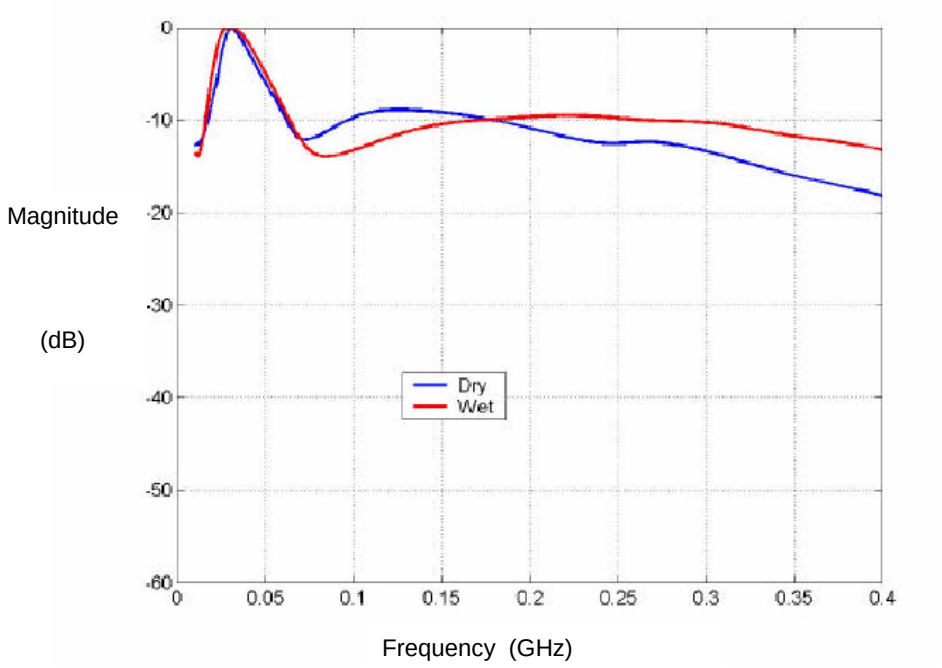

Figure 17. Antenna transfer functions measured at JPG-V using a long, thin conducting wire on the ground surface, under dry and wet conditions.

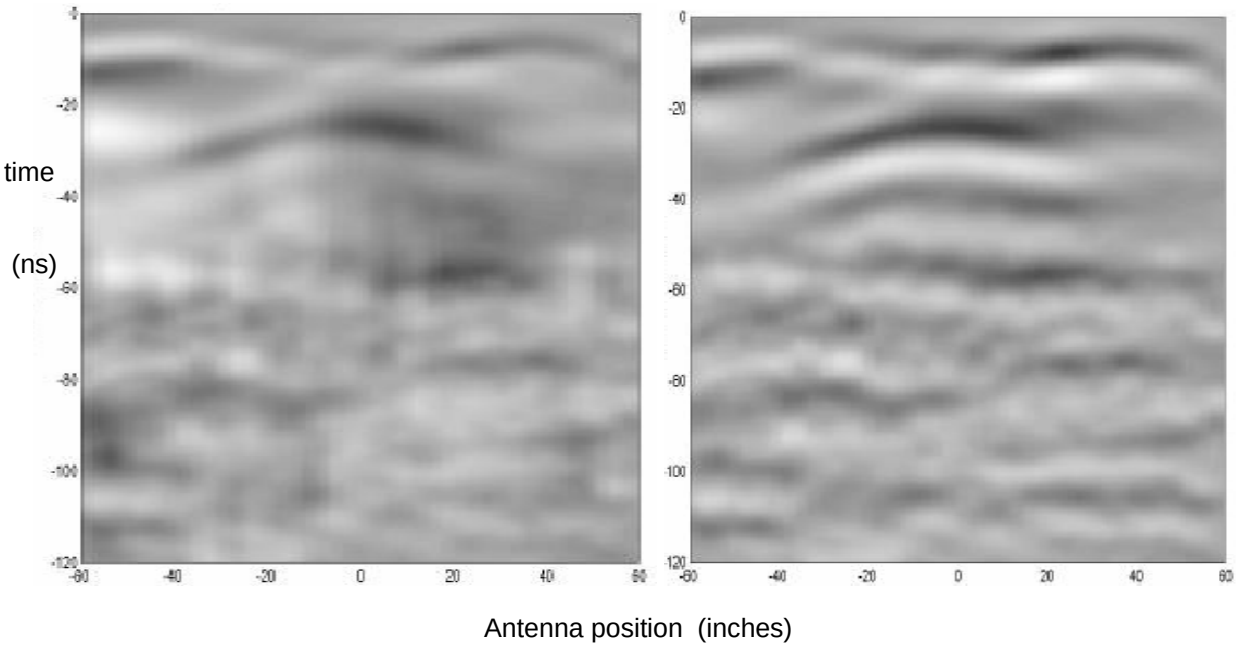

Figure 18. Comparison of GPR data before (left) and after field calibration (right). The target is an 81 mm mortar buried at 0.35 m depth, visible on the left at about 30 ns delay.

3.2.2.3 Adaptive 2-D Spatial Smoothing

During the Tyndall test, the target response was based on a single time waveform, collected at a single position. There was only very limited processing that could be done to enhance the target response. An improved method of selecting the onset of the crucial late-time response associated with the target was made possible in later demos by collecting multiple-position data. In such data, a target response typically appears as a hyperbolic arc, as explained in connection with Figure 13. Late time resonance appears in the (time) region below that arc. A new special-purpose algorithm was implemented that performs data smoothing along the hyperbolic arcs, greatly improving the signal-to-clutter ratio. First, the operator selects a desired hyperbolic band by manually choosing a few apparent points on the arc, i.e. along the feature designated by the dashed line in Figure 19. The software then automatically traces out the arc, as illustrated in the figure. This arc is extended over all the scan positions by extrapolation to the right and to the left. A smoothing window is then applied to the pixels along the arc. A similar smoothing process is repeated as the arc is shifted up and down, one pixel distance at a time (vertical arrows in Figure 19). The figure shows a comparison of GPR data before and after this spatial smoothing process. Notice that, before the smoothing, there are also other arcs with different intensities and curvatures resulting from surface and subsurface clutter sources. The presence of these undesirable arcs interferes with the target responses, causing errors and instability in feature extraction. After application of the spatial smoothing, the interferences are reduced, especially in the important late time-region. The data shown here correspond to a vertical UXO-like item. The vertical orientation of the target explains the weaker response near the center positions when the antenna was directly above the target, with stronger response from the side, especially towards the right end of the scan (Antenna position > 0).

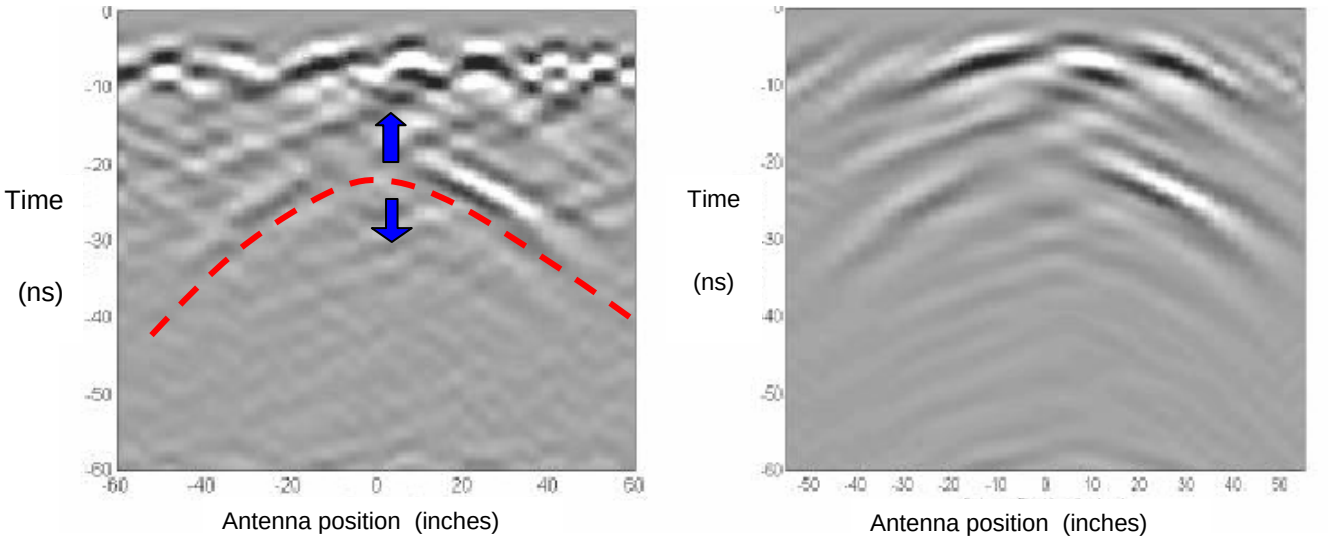

Figure 19. Comparison of GPR data before (left) and after (right) adaptive data smoothing, for BP known target G.

3.2.3 Feature Extraction

3.2.3.1 Electromagnetic Complex Natural Resonance (CNR) Feature Extraction

When a UXO is illuminated with broadband electromagnetic fields in the GPR frequency band, the incident fields stimulate currents on the conducting surface in characteristic ways. These currents flow along the UXO's curved surface and generate secondary radiation that is then received by the radar receiver. The currents flowing circumferentially around the object generate significant radiation only when the circumferential length is comparable to one wavelength in the surrounding medium, or greater, as in the case of a small loop antenna. When the currents flowing axially along the UXO reach the ends, strong diffraction occurs, releasing some energy into the medium while the rest flows back towards the other end. In colloquial language, the induced currents "bounce" back and forth between the ends, with losses radiating into the environment during each trip and reversal. This process continues until all the induced energy is used up in diffraction or absorption by the ambient medium. When a broadband radar records these secondary radiations, the responses appear as a damped sinusoidal signal in the time domain and a resonant

spectrum in frequency domain, with polarization predominantly oriented parallel to the UXO axis. More complete analysis and examples appear in the literature, e.g. [12, 25].

Resonant frequencies will be those for which the electromagnetic wavelength in the surrounding medium is an integral multiple of the length of the path back and forth that the currents travel. While curvature of a UXO surface increases this distance slightly, the path length followed by the axially oriented currents is approximately the length of the UXO. Therefore, the *estimated target length* (ETL) is defined as a half of the wavelength corresponding to the lowest resonant mode. In practice in the field, the resonant pole is calculated directly from the waveform in the late-time (resonant) region using the modified Prony method [29]. Accurate resonant frequencies can usually be obtained using this method when the signal/(clutter + noise) is higher than 10 dB. From the resonant frequency and the dielectric properties of the soil measured at each site with a probe, one obtains the estimated target length (ETL).

3.2.3.2 Late-Time Polarization Feature Extraction

The dominant scattered field from a typical UXO with elongated body is polarized parallel to the UXO axis. If the incident electric field is polarized in another direction, only the vector component that is parallel to the UXO axis will generate strong scattering, particularly as the signal fades, and only that component will excite strong resonance (lowest mode). Within the range of practical measurement, only the natural resonance along the axial direction of a typical UXO can be apprehended. Typically, the transverse resonance fades too quickly and is also therefore likely to be entangled in any near-surface (early time) clutter. Ideally, the late-time response should have a highly linear polarization, like that of an ideal thin conducting wire. It is also possible to determine an early-time linearity factor (early time ELF), measuring the extent to which the early time (initial reflection) signal shows directional dominance. Experiments were performed to see whether this could assist in strengthening the classification reliability. While including the early-time ELF did provide some slight benefit, on the whole, whenever the early time ELF indicated target linearity, the more reliable late time ELF also did. Therefore inclusion of the early time ELF is a matter of judgment, depending on its case by case clarity relative to late time ELF. Ordinarily it is not necessary to include it.

To obtain late time resonance information, the measured frequency-domain data were first transformed into the time-domain. A late-time region was then selected, based on observation of the damped resonance, as illustrated in Figure 20 for a buried rebar. The antenna arm #1 was approximately parallel to the rebar and resulted in a stronger S_{11} response. In a semi-log plot one sees a linear decline of the peaks in this late time region, indicating a single dominant mode in exponential decay.

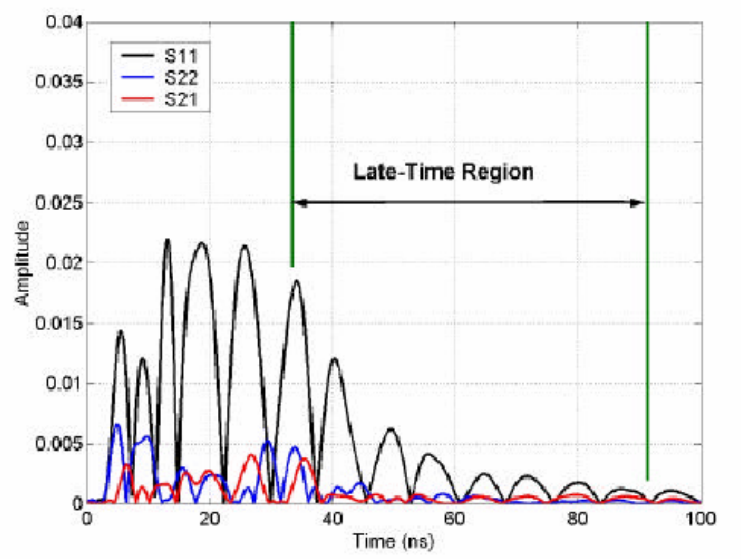

Figure 20. Measured response of a rebar buried at Tyndall site.

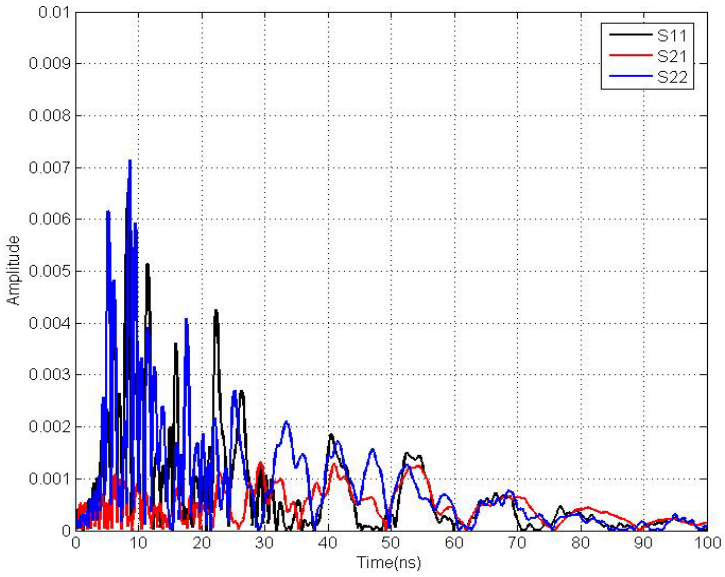

Figure 21. Response from a horizontal MK-82 (500 lb bomb) rotated 45^{o} between the antenna arms.

For more complex targets and configurations, one typically obtains more complex data patterns, but for resonant targets the same underlying features may still be apprehended. Figure 21 shows data from a horizontal MK-82 (500 lb, length 1.2 m, depth 1 m, maximum diameter 350 mm). It is oriented azimuthally at about a 45^{o} angle between antenna arms #1 and #2. This is why all three channels S_{11}, S_{21}, and S_{22} show similar responses. Before analysis, this pattern would be rotated so that one of the components would be clearly dominant, as per Figure 20. Even prior to such clarification and other routine smoothing, note the distinct late-time resonance after 40 ns (clearest in red curve for the cross polarized return). While both figures show expected lack of monotonic decay in the early time portion of the record, the picture is considerably more complicated for the larger target (Figure 21). In the latter case there is a greater disparity between the relatively low frequency late time resonance and the much higher frequency responses associated with other mechanisms, such as end diffractions, strong direct reflections from separate scattering centers on the large, non-uniform UXO, interference between these reflections, etc. Be this as it may, it is easy to recognize a steady period of roughly 14 ns in late time, which routine processing easily extracts. Also, it is relatively easy for an analyst to select the late time section of the signal by eye, as one can in these figures, based on the appearance of monotonic, approximately single mode decay. This was the ("human in the loop") system used in the analyses for this project. For the purposes of the analyses, one has considerable latitude in selecting the onset of late time without affecting results. Further, determining the approximate limits of late time can easily be automated, based on simple spectral analyses of different windows on the signal.

Initially, the S_{11}, S_{12}, S_{21} and S_{22} values at each sampled time step in the late-time region are combined into a full scattering matrix.

$$[S] = \begin{bmatrix} S_{11} & S_{12} \\ S_{21} & S_{22} \end{bmatrix}.$$

Two eigenvalues, $\lambda_{//}$ and $\lambda_{\perp}$, were then obtained from this scattering matrix, where $\lambda_{//}$ and $\lambda_{\perp}$ correspond to the parallel and transverse components of re-radiated resonant field intensity, in target coordinates. For a UXO-like target, these correspond to the field components parallel and transverse to the target axis, as projected onto the plane of the antenna (ground surface). The *estimated linearity factor* (ELF) is defined as

$$\text{ELF} \equiv \text{average}\left\{\left|\frac{\lambda_{//}(t)-\lambda_{\perp}(t)}{\lambda_{//}(t)+\lambda_{\perp}(t)}\right|\right\}, \quad t \in \text{late}-\text{time region}.$$

As discussed earlier, $\lambda_{\perp}$ would be negligible for such a target, ideally producing an ELF close unity. Notice that, for a rotationally symmetric target like a sphere or for another compact target, ELF ~ 0, because $\lambda_{//} = \lambda_{\perp}$. Of course, real data always contains a certain amount of random noise and undesired response, i.e. clutter. As calculated above, the ELF was sensitive to the noise and the choice of late-time region because the SNR deceases as a function of time during the fading of the resonance. In later generations of the processing, the scattering matrix was formed using the signal magnitude readily available in the coefficients of the Prony method during the extraction of resonant features [29]. This improved the performance in noisy data.

Solving for the eigenvalues of the scattering matrix also provides eigenvectors, corresponding to the parallel and transverse vectors of the UXO response, in antenna coordinates. The orientation of the dominant eigenvector provides the ETO. A "resonant-frequency ELF" (FELF) was also determined by obtaining the eigenvalues from magnitudes of the signal filtered by a narrow bandpass centered at the resonant frequency, estimated by Prony's method on the late-time data. Of course, signals from a real target in a field situation will not show response only in the direction of the dominant late-time eigenvector. As an additional measure of whether or not the target showed a dominant direction of response, as an elongated UXO should, the *angular density* (DEN) of responses was determined. The DEN was calculated as the sum of response magnitudes for polarizations $\pm 20^{o}$ on either side of the dominant direction (ETO), divided by the total (integrated) magnitude of response over all directions. Basically, it is a measure of how tightly clustered about the ETO the responses are.

3.2.3.3 Depth Information Extraction

The target depth was also estimated from the time delay of the earliest reflection, i.e. of the peak of the various hyperbolic arcs shown above. Depending on the UXO orientation, multiple echoes may be received from different parts of the UXO. In such cases the shallowest point was chosen to correspond to the "depth." Both length and depth estimation must be done in conjunction with a proper estimation of soil electrical properties, which were measured using an OSU soil

probe. The good quality of the depth estimations shown in the individual demo reports, when targets produced unequivocal reflections, attests to the accuracy of the probe data. This was usually done at the beginning of each day of survey, requiring only about a half an hour, and could be done less frequently if environmental conditions do not change.

3.2.4 Data Processing Summary

The data processing and feature extraction procedure adopted is summarized in the following block diagram (Figure 22).

Step (1): After the software plots signal magnitudes in both time vs. antenna position and frequency vs. position on the display, the operator selects a modified time range or frequency band, if desired.

Step (2): The truncated step-frequency data are transformed into time domain using inverse Fast Fourier transformation (IFFT) for each position X_n. Next the operator inspects the time vs. position GPR plots of S_{11}, S_{21} and S_{22} channels to pick the channel that shows the best SCR, i.e. clearest target responses. This channel will be used for determining the spatial filter in the next step. If none of the channels shows recognizable target responses, go back to Step (1) and try a different time range/ frequency band. Typically, a three-band approach, i.e. low band, middle band, and high band, should be sufficient. If the target responses are still invisible, then declare no target. If the SCR is good and the target responses are clear, there is no need to change the frequency range. Otherwise, enter the desired start and stop frequencies. If the target responses contain frequency content that is either very high or very low, adjust the frequency range to enhance the SCR.

Step (3): Select more than five points along a hyperbolic response pattern (broken or not broken) in the space-time plot, assumed to correspond to the target, for adaptive spatial smoothing. The GPR data of all three channels are replotted after the spatial smoothing. The points do not need to be selected in any order, but the waveform corresponding to the position of the first point will be used as an example waveform for determining the duration of the late-time region in the next step.

Step (4): Select the start and stop time positions from the example waveform to define the late-time region, for obtaining the late-time spectrum by transforming the waveform in the late-time region into frequency domain using fast Fourier transformation. The difference between the start- and stop-time positions also determines the length of the late-time region that will be used for feature extraction.

Step (5): A late-time spectrum obtained from the previous step is plotted. The operator now selects the center frequency (frequency peak) and the half-width of the bandpass filter.

Step (6): Apply the bandpass filter determined from the previous step to the background subtracted data (all channels) as used in Step (1).

Step (7): Transform the filtered data into time domain. Now the resonant signal should appear enhanced.

Step (8): Repeat Step (2) to apply the spatial smoothing to reduce interference from other scattering sources.

Step (9): This step selects the target region to be focused on for feature extraction and further investigation. This is done by selecting two diagonal points of a rectangular region that boxes the majority of the target related responses.

Step (10): This step determines the onset of the late-time region for every position. This is done by first manually selecting a few points on the strongest signal arc in the replotted time vs. position data. The software then automatically traces out maximum magnitude pixels along the arc. Each such pixel becomes the onset time of the late-time region for a given antenna position associated with that pixel. Recall that the duration of each late-time region is the same as was determined in Step (3). Note that the late-time regions for all three channels will be the same.

Step (11): For each antenna position within the target region selected in Step (8), Prony's method is applied to the response in the late-time region to extract the resonant frequency, damping factor and initial resonant amplitude. The resonant amplitude is given by the magnitude of the Prony's coefficient associated with each resonant mode.

Step (12): The resonant amplitudes obtained from S_{11}, S_{21}, and S_{22} channels are then used to form a scattering matrix, $\begin{bmatrix} S_{11} & S_{12} \\ S_{21} & S_{22} \end{bmatrix}$, from which the eigenvalues and eigenvectors are obtained. Polarization signatures are then calculated from the eigenvalues and eigenvectors, as discussed above.

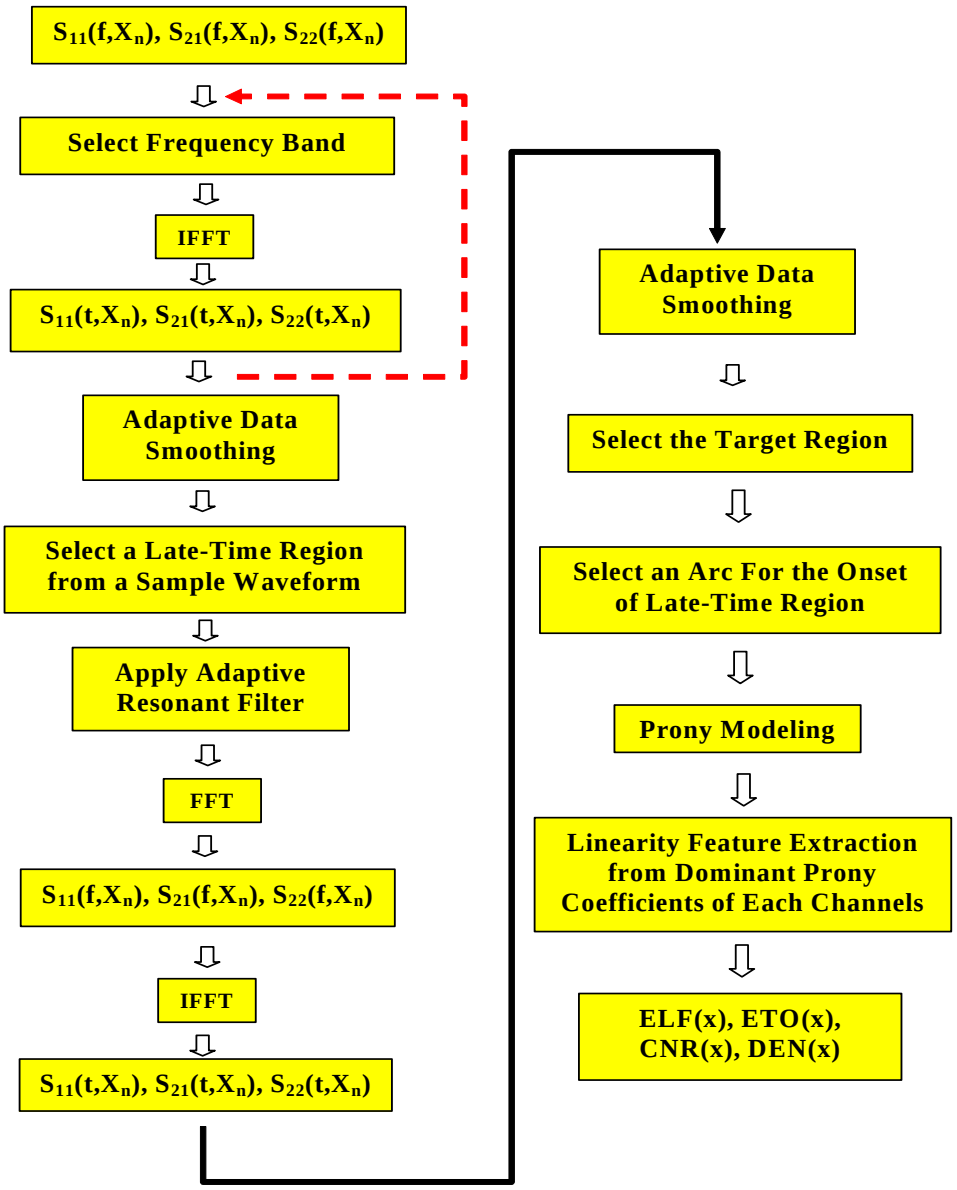

Figure 22. Full polarimetric, UWB GPR data processing and feature extraction procedures for UXO classification.

Figure 23 and Figure 24 below demonstrate how properly selected filters can improve the isolation of the target response in Step (2) above. The target is a 57 mm Projectile (12 cm in length) buried at 15 cm depth with an inclination of 15 degrees from the horizontal. The surrounding soil at JPG (Area 1) was quite wet, with dielectric constant and electrical

conductivity ranging respectively from about (20, 0.01 S/m) in near surface layers to about (30, 0.035 S/m) at greatest depths investigated, approaching 1 m. The original processing scheme relied on the visibility of the target “arcs” in the time-position plots generated from the whole band. The response from a small object tends to have weak scattering magnitude that concentrates in the high frequency region. Such a response then suffers from poor SCR in the time vs position plot based on the full band.

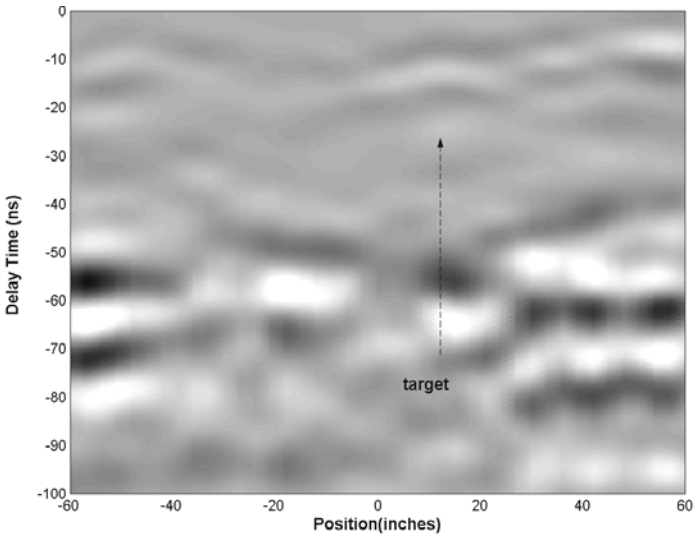

Figure 23. Typical time-position data obtained using the whole frequency band (10~410 MHz), for the case of a relatively small, high-frequency target.

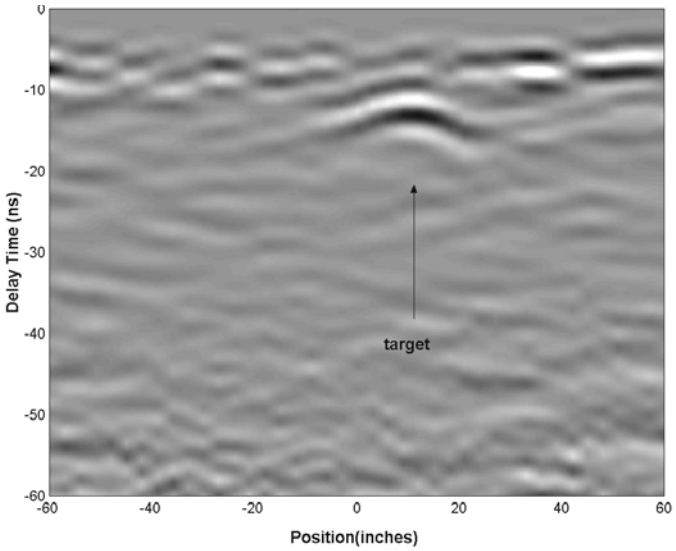

Figure 24. Time-position data in Figure 23 after application of a bandpass filter (150~410 MHz), for the same target.

3.3 UXO CLASSIFICATION RULES

A set of classification rules was developed to discriminate UXO-like items (usually L/D ratio greater than three) from other metallic objects. These rules are organized in a classification tree, illustrated in Figure 25. This classification tree was finalized for the JPG-V and Ft Ord tests. The rules were based predominantly on late-time polarization features (ELF and ETO) as a function of antenna position and scan orientation. Several rules involve qualitative spatial pattern recognition. All characteristics in the qualitative descriptions that are sought "by eye" can be shown to have a solid physical basis, based on rigorous numerical model simulations [30]. Further, recognition of the essential features has been automated during work following this project. The appendix to this report shows a "first cut" at such an expert system, using neural nets and fuzzy logic. As shown in Figure 43, performance of the automated system is as good as that of our team "expert" (Dr. C.C. Chen).

The whole UXO classification procedure starts with inspection of the spatial distribution of ELF values. This distribution has five categories (A-E) as illustrated at the top layer of the tree. Since data have been collected from different passes, it is easiest to start with the pass that has strongest target responses or has the best SCR. Then other passes can be used as a secondary confirmation later at lower layers of the tree. Each rule is discussed briefly in the list below. The classification criteria were found to be very effective if all GPR scans passed through the target, i.e. directly over its position. Classification error occurs when only some or none of the scans passes through the target position. Ways of alleviating this problem are discussed in the concluding section of this report.

Rule A: If the target has a high SCR and the ELF is low over one antenna width, this indicates that the target is not UXO-like due to low linearity.

Rule B: If the ELF values are high (> 0.6) near the target region, the object could be a UXO-like object, a vertical plate, or a vertically oriented bent metal object such as a horseshoe. Proceed to **Rule F**.

Rule C: If two elevated ELF regions next to the target center are observed (double peaks), the object could be a vertical UXO or shallow clutter that couples to the arms of antenna #1 strongly. Proceed to **Rule G**.

Rule D: If there is a region with high ELF values and it is offset to one side of target response (single peak), it is probably a moderately inclined UXO-like object or a horizontal UXO-like object with a position offset along the scan direction. In this case, the ETO near the high ELF region should remain unchanged regardless of the scan direction.

Rule E: If the response is weak and the ELF values vary erratically between 0 and 1, this is either an empty site or a deep target with poor SCR.

Rule F: In this rule, the time vs. position GPR data collected from a pass transverse to the ETO are examined. The dashed line in the block diagram indicates the scan direction. In this pass, a horizontal UXO-like object should have strong S_{22} response but very weak S_{11} response at all positions. If a strong scattering magnitude is observed in the S_{11} data at offset positions such that the scattering pattern appears as broken hyperbolic arcs, the object is not classed as UXO-like. It could be a thick vertical plate, vertical horseshoe, vertical bent wire, …, etc. The high ELF center observed in **Rule B** is caused by scattering from the top edge. Stronger S_{11} response at offset positions in the transverse pass is caused by scattering from the rest of the body when observed from its side. If the S_{11} scattering pattern does not show broken arcs, proceed to **Rule H**.

Rule G: In this rule, the time vs. position GPR data from S_{11} and S_{22} channels are examined simultaneously. A vertical UXO-like object would have a weak scattering magnitude when measured directly above due to relatively small cross-sectional area compared to the wavelength. The scattering magnitude increases as the incident angle moves away from its axis. This would produce broken hyperbolic arcs in the S_{11} data. The magnitude of the S_{22} data should remain weak away from the target center, because the electric field polarization is transverse to the UXO axis. Therefore, if a strong scattering magnitude is observed near the target center with complete arcs in both S_{11} and S_{22} data regardless of the scan direction, this indicates a non-UXO item: The high ELF region observed in **Rule C** is caused by coupling to the arms of antenna #1. In this case the ETO would also be the same as the scan direction in all passes.

Rule H: In this rule, the ETOs obtained from all passes are examined simultaneously. The dashed lines indicate the scan directions. A horizontal UXO-like object should register a similar ETO regardless of scan direction. When the ETOs are significantly different (>20 degrees) from pass to pass, the object is not likely to be a horizontal UXO.

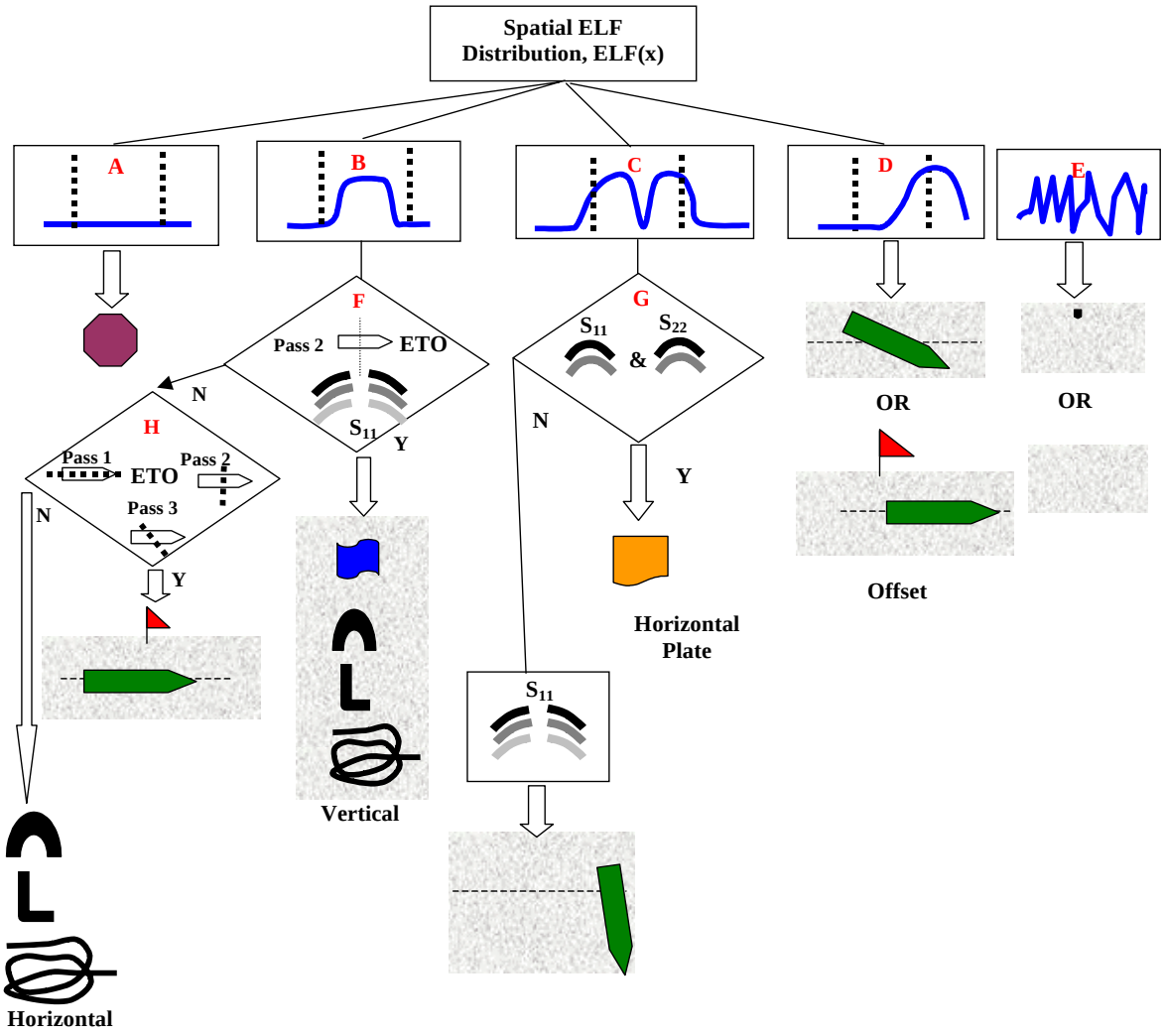

Figure 25. Target classification rule structure based on GPR signatures.

4 Classification Performance

The GPR UXO classification performance based on the above rules and parameters is summarized briefly here. The results presented focus on the blind tests performed at the most recent JPG-V and Ft Ord sites, where the final classification rules were adopted and the manual magnetometer survey accompanied the GPR. Detailed analysis of the classification performance and causes of errors for all blind tests are available in each individual ESTCP report [17, 19-21].

4.1 Baseline Performance

Figure 26 shows the UXO classification ROC curves from blind JPG-V and Ft Ord measurements based on the “TRUE-UXO” criterion. This means that even a piece of metal with geometry similar to a UXO was considered to be in the "non-UXO" class in the ground truth. The curves shown were obtained based on the following six judgment thresholds:

(1) UXO with HIGH confidence
(2) UXO with MEDIUM confidence
(3) UXO with LOW confidence
(4) CLUTTER with LOW confidence
(5) CLUTTER with MEDIUM confidence
(6) CLUTTER with HIGH confidence

The confidence levels were established based on the following qualitative observations:

- **HIGH** - good SCR, clear scattering patterns, clear ETO
- **MEDIUM** - medium SCR, discernible scattering patterns, at least identifiable ETO
- **LOW** - low SCR, ambiguous/insufficient/unfamiliar scattering patterns, unstable/ambiguous ETO

Application of the second threshold, for example, classifies any item as a UXO that the processing system has classified as a UXO and that also merits the medium or high confidence level. All other items are classified as clutter. While one can say that the processing shows some definite discrimination capability, producing lines above the LOND, the performance is not

inspiring. On the other hand, if the UXO-like criterion is adopted, the ROC curves in Figure 27 result, where “LD2” and “LD3” indicate whether the “L/D>2” or “L/D>3” criterion was adopted for target sorting in the ground truth. Over 50% of UXO-like items were correctly classified with 90% of clutter items rejected based on the top judgment threshold (1): UXO with high confidence. Unfortunately, the classification rate rises only slowly thereafter, as the thresholds decrease.

It is notable that similar classification performances were obtained from both test sites despite the very different environmental, UXO, and clutter characteristics. While the Ft Ord site contains mainly dry sand, the massive tunnel networks created by small animals resulted in high clutter levels. Figure 28 and Figure 29 give an idea of the size and number of tunnels at the Ft Ord site. Thus it is comprehensible that the classification performance was similar to that at JPG, where the soil conditions are well known to produce low signal-to-clutter ratios in radar applications.

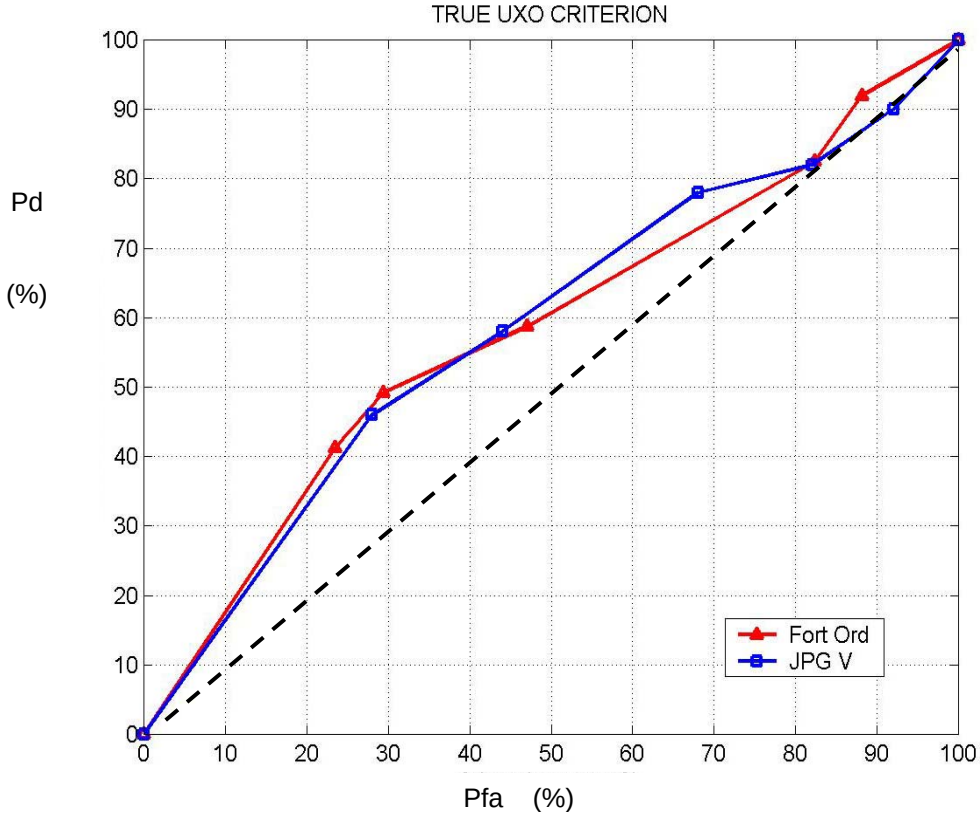

Figure 26. Classification ROC curves based on TRUE UXO criterion with dashed "line of no discrimination"

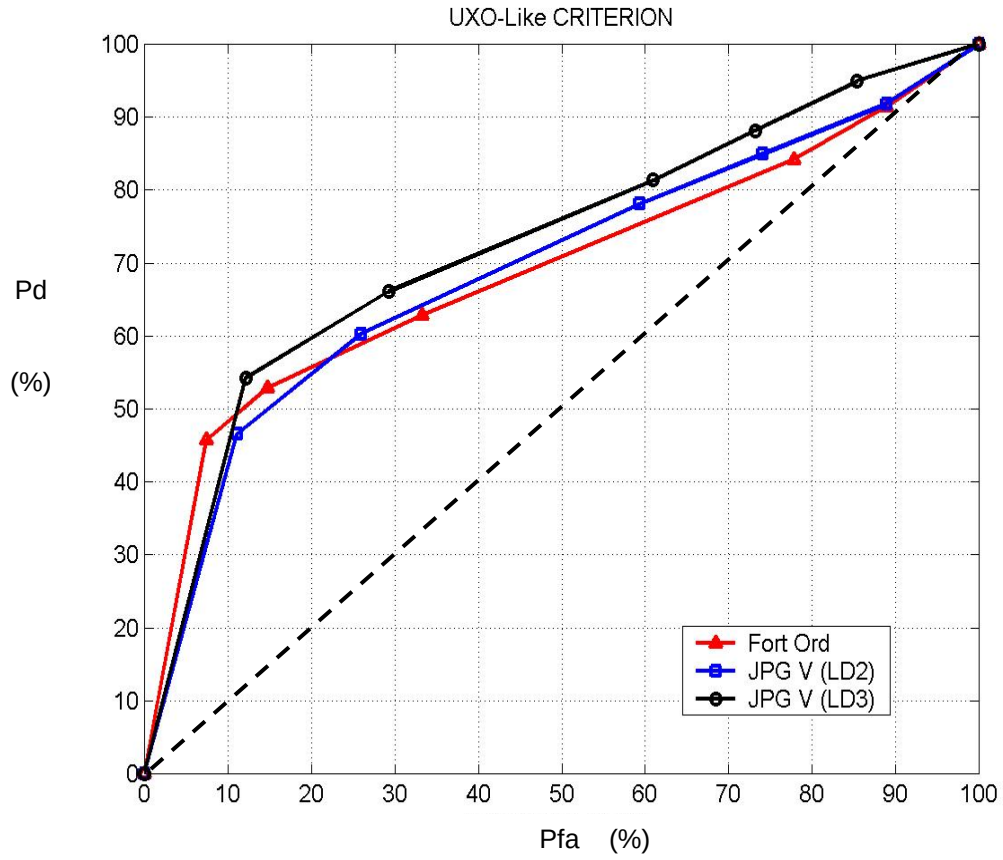

Figure 27. Classification ROC curves based on the UXO-LIKE criterion.

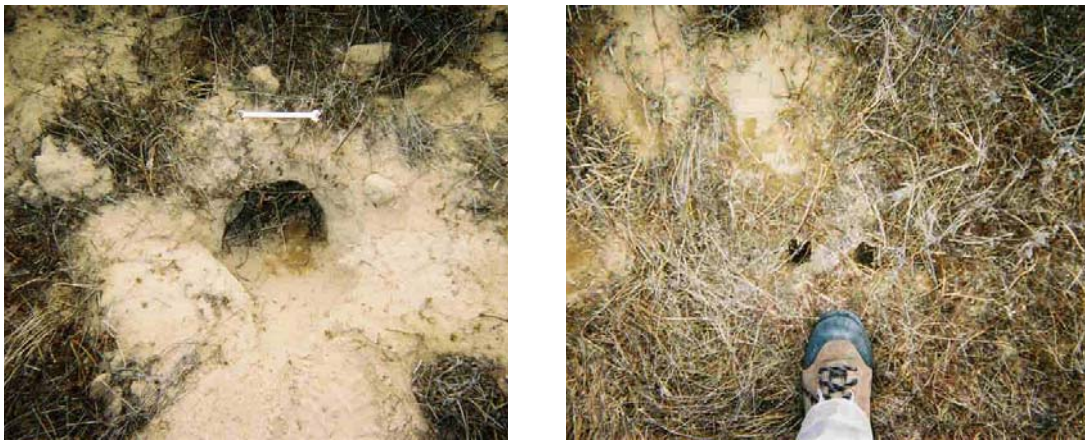

Figure 28. Example 6-inch and 1.5-inch holes in Ft Ord site.

Figure 29. Field view of the Ft Ord site, showing the density of the holes and covered openings (bare spots).

4.2 Performance Improvement

The measurements at Ft Ord contain an unusual number of UXO and UXO-like items with good resonance and linearity but ETO's that vary significantly between passes in different orientations. This caused them to be declared non-UXO items during the classification. Thus in cases where the first GPR pass had a significant offset from the target, a large error in ETO and position resulted, which affected the rest of the scans. Then the ETO's obtained from all the passes together represented target orientations observed from different oblique directions, which muddles the processing. However, the majority of these missed UXO items did indeed show magnetic dipole patterns during the manual magnetometer survey, as noted in our field logs. This prompted investigation of the inclusion of magnetic dipole indications in the classification processing. Table 1 shows the rule adopted for upgrading the classification based on the apparent presence of a magnetic dipole, regardless of its strength. Figure 30 compares the ROC curves before and after inclusion of the magnetic dipole criterion. A significant improvement in the correct classification rate is achieved, reaching about a 90% detection rate with a 50% false alarm rate. It is worth noting that the Mag data alone provide essentially no discrimination information. The Schonstedt operators ranked their perceptions that a dipole was or was not present as weak, medium, or strong. Using their classifications as sorting thresholds and counting all items with

evident dipoles as UXO's produces the ROC curves in Figure 31. Interestingly, although the Mag data are essentially without discrimination value alone, they help the GPR performance significantly and the combination is better than each alone.

Table 1. Rule for class upgrade when magnetic dipole is present (1 = UXO).

Original GPR ID	GPR Confidence	ELF Values	Upgraded ID	Upgraded Confidence
1	H	0.7~1.0	1	H
1	M	0.7~1.0	1	H
1	L	0.5~0.7	1	M
0	L	0.7~1.0	1	M
0	L	0.5~0.7	1	M
0	LMH	0.0~0.5	1	L

Given that external or prior information estimating target depths could improve performance, additional means were sought to improve results by attacking the flattening of the ROC curves in the upper portions, where ideally they should reach 100% Pd before encountering 100% Pfa. In examining the classification performance for the BP demo, note that many of the missed targets were relatively deep in the very lossy soil. Thus the signals from the target were quite faint, and the processing focused erroneously on stronger reflections from near-surface soil disturbances. In a sense, the discrimination algorithm operated correctly in that it reported that these signals did not correspond to UXO's. However, this resulted in a reduced Pd. Therefore the proposition was tested that this kind of problem could be alleviated by inclusion of depth estimates from some other sensing mode, i.e. Mag/EMI. Figure 32 shows "ROC points" for JPG, in all cases obtained with the same GPR decision criteria in the processing but with estimated depths used to cue the windowing of the GPR data for analysis. The points labeled EMI correspond to data that were furnished from other JPG-V classification tests using EMI equipment. Round 1 shows results obtained from GPR data alone. In Round 2, the GPR processing also referred to the estimated depth information. In Round 3, the GPR processing again referred to depth information, but used accurate i.e. ground truth values. While the EMI-estimated depths did not affect results very significantly, raising the detection rates only slightly, the ground truth depths moved the results into a lower false alarm range without appreciably lowering the detection rates. This indicates that the GPR performance can be improved

significantly by depth indications from other sources, provided that the information is high enough quality.

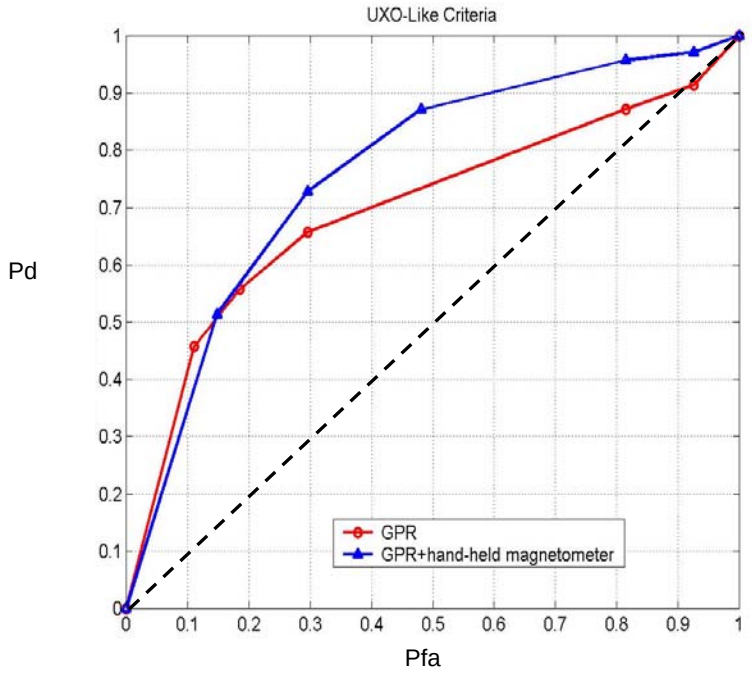

Figure 30. ROC curves for Ft Ord, showing performance obtained from GPR alone, and improvement from inclusion of Mag dipole presence as a factor.

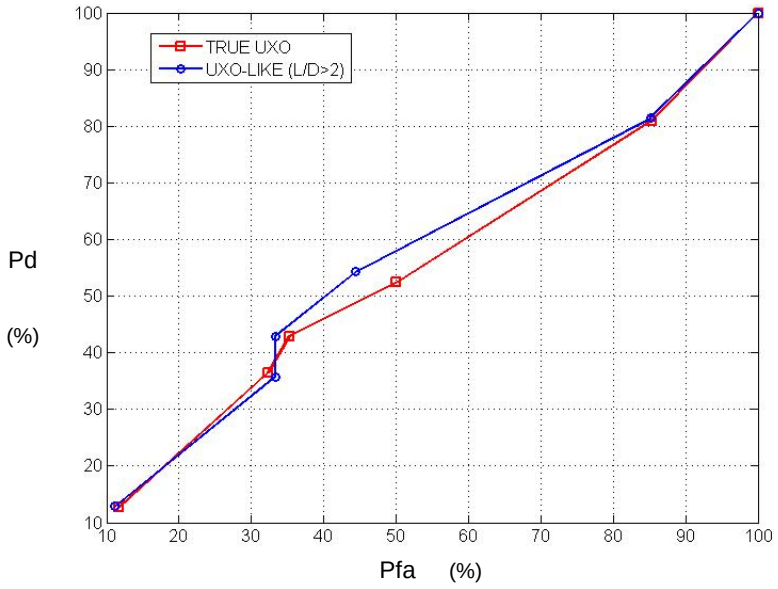

Figure 31. ROC curves for the Ft Ord data derived from the Mag data alone.

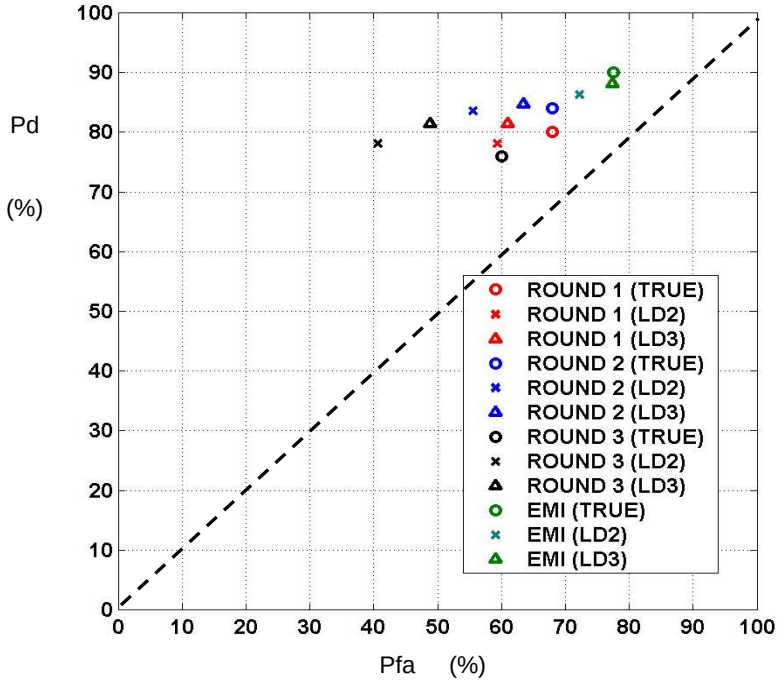

Figure 32. "ROC points" from the GPR classification for JPG, all based on same decision criteria except for Round 1 = classification based on GPR only; Round 2 = GPR processing + depth estimations from EMI; Round 3 = GPR processing + ground truth depth information.

Other target features that can be useful for improving UXO classification are produced in the course of the processing. Figure 33 plots the absolute error of the estimated length and depth for UXO-like items that were correctly classified. The correctly classified items were used because incorrectly classified items often constituted cases with poor SCR, poor CNR (needed for length estimation), or other data incoherence, so that no length or depth estimation would reasonably be credited to those cases. Most of the length error is less than 10 cm and most of the depth error is less than 20 cm. Note that these results were obtained only from blind GPR processing results. The length values tend to be over-estimated due to the additional propagation distance of the induced currents on the curved body and over the fat ends of some UXO's. The depths also tend to be over-estimated possibly due to the bandpass filtering. This widens the pulse width and results in longer delay of the pulse peak relative to the predetermined time position of the ground surface, which is obtained from the data using the whole frequency band. This could be improved upon by selecting the time position of the surface reflection after the bandpass filtering.

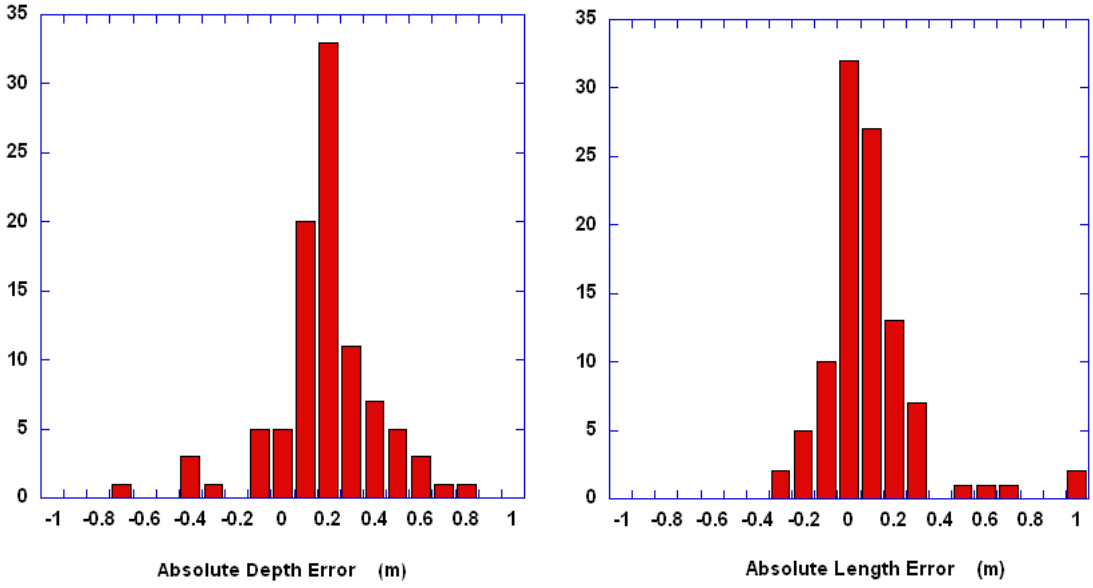

Figure 33. Absolute depth estimation error (left) and length estimation error (right) for correctly classified UXO-like items. Data were compiled from JPG-V and Ft Ord blind-test results based on GPR alone.

As mentioned above, most other UXO discrimination systems attempt to infer much the same things as the system here, in the sense that parameters are evaluated to infer the general shape of the unseen object. By contrast, others seek signatures of specific targets, based on information that certain types of ordnance may be found at a particular site ("fingerprinting" approach). In a step towards the second approach, improved classification performance is produced in some cases from the Tyndall site when estimated target length (ETL) is included as a discriminant. At Tyndall there were large enough numbers of particular target types with sufficiently contrasting sizes so that one can construct ROC curves for individual UXO types. Figure 34 shows ROC curves for the 105 mm projectiles buried at Tyndall, obtained when the usual decision criteria were applied together with a judgment as to whether the estimated target length coincided with that for the target sought. Thus the classification system asked the questions: 1) Is this item UXO-like? and 2) Is its length within some specified tolerance of the particular UXO sought?

This is a particularly challenging approach because the ETL is determined from the resonant frequency that is extracted from the data for each target. Because the resonant peaks are

not sharp, there is considerable uncertainty in the lengths obtained. Therefore one must allow a substantial tolerance about the known UXO length when searching for a particular UXO type. Because UXO's other than the one sought are regarded as clutter in this test, the procedure is liable to drive up apparent false alarm rates. Despite all this, when the ETL is used as an additional classification parameter the processing performance is good, reaching a 100% Pd at a 40% Pfa (Figure 34). Also, it is worth noting that these results were obtained in the earliest demo, when only signals from a single observation point were processed. One may speculate that if the more complete surveying practiced in later demos had been applied, enhanced performance might have been obtained at smaller length error tolerances.

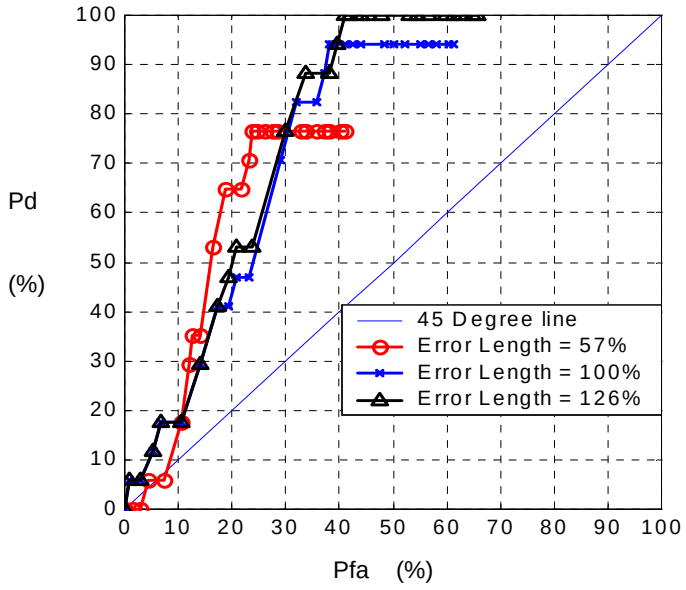

Figure 34. ROC curve for 105 mm projectile based on usual decision criteria plus estimated target length, for different ETL error tolerances.

Figure 35 shows ROC curves obtained in this manner for other targets as well as for the 105 mm's. While the curves necessarily proceed in gross steps when only a few of some ordnance types were present, clearly the trend is towards good performance, with 100% detection at Pfa's between about 35% and 45%. Note that the very coarse curves really consist essentially of ROC points at the left edges of each step. With that recognition guiding one's eye, it is clear (and interesting) that essentially all ordnance types subjected to this kind of processing produced very similar, near linear ROC curves.

Figure 35 also indirectly illustrates the roles of different length error tolerances (LET) for different members of this target population when they all appear together in the way that they did at this site. The LET required for the 60 mm, 105 mm, 500 lb bomb and 8-inch shell ROC curves to reach 100% Pd were 150%, 125%, 67%, and 50%, respectively. The true lengths of these UXOs are 23 cm, 43 cm, 120 cm, and 100 cm, respectively. A LET equal to or greater than 100% indicates that all ETL's are accepted between zero and (1+LET)*(target length). Thus, when the processing searches for the 60 mm UXO, it classifies as a detection all items rated as UXO-like with ETL's between zero and about 58 cm. Thus virtually all of the 8 inch shells and 500 lb bombs will be excluded, and only some of the 105 mm's will contaminate the results by producing false alarms. In searching for the 8 inch shells, the processing will accept UXO-like targets with ETL's between 50 cm and 150 cm. This excluded most if not all of the 60 mm and 105 mm UXO's; and because there is only a small number of 500 lb bombs, the "false alarms" they produce will not materially affect the Pfa.

Of course, in real application one would not want to count detections of UXO's other than the particular one queried as false alarms, but would be content to place them on the dig list. Otherwise put, the best situation for applying the ETL in processing is one in which essentially all UXO's have lengths that are significantly different from all objects that are true clutter. Overlapping ETL intervals for the different UXO's would not be a problem, i.e. would not contribute to apparent false alarms as they do in Figure 35, because any UXO classification would place the target (appropriately) on the dig list. While ideally one would like to exclude metallic clutter items from the dig list when they are the same size as possible UXO's, at present (and in the near future) this is not realistic. Site managers and cleanup crews are bound to dig items that appear to be about the same size as possible UXO's or that appear to be even a significant fraction thereof. Thus the GPR discrimination system here that uses the ETL's seems well designed to meet applicable standards for inclusion and exclusion from dig lists: It will be most successful when the clutter and UXO's are significantly different sizes; and when they are not, all must be dug in any case.

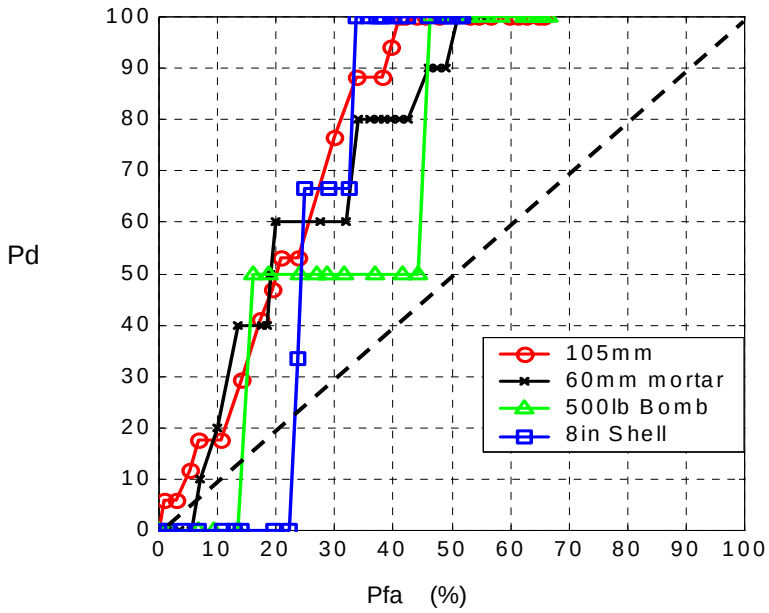

Figure 35. ROC curves for the Tyndall site for different ordnance types, obtained when LET's are 150% for the 60 mm, 125% for the 105 mm, 67% for the 500 lb bomb, and 50% for the 8 inch shell.

4.3 Analysis of Performance

The baseline performance in the last two, focal demos is shown most succinctly in the ROC curves of Figure 26 and Figure 27. When asked to identify true UXOs in the target set, the system produced results consistently above the line of no discrimination, but not greatly. The system clearly does much better when asked to do what it was designed to do - detect the presence of objects with proportions like those of UXOs (UXO-like criterion). Particularly for the purposes of comparison to other sensing systems, the UXO-like criterion seems most appropriate. This is partly because ascertaining UXO-likeness in signal parameter patterns is what essentially all other system in fact do. Both other systems and that treated here will do better when clutter is very different in form from a UXO, and will do worse when it is not. This makes it particularly difficult to compare tests that involved differing target sets. Favoring this criterion also follows the guidance of field personnel from the Huntsville Center who have stated repeatedly that, if a surveyor indicates that an object is the size and shape of a UXO that could be present, they will dig it up regardless of what else the processing indicates. This has also been cited to us as a legal requirement (Dr. Anne Andrews, personal communication).

An effort was made to seek sites with very different environmental conditions to see the dependency on soil type and state. However, despite the very considerable physical and target set differences between these last two sites, classification performance was quite similar. Unfortunately, this probably does not reflect some consistent character or capability in the surveying and processing. Rather, countervailing influences more or less "cancelled out" in the Ft Ord test, where dry sandy soil was very favorable to GPR but signal clutter from animal burrows and the clustering of targets was not. Because post-processing analyses indicate that the performance at Ft Ord was clutter limited, one can speculate that better performance would be seen under similar soil conditions and target set but without the subsurface clutter sources. Be all this as it may, the level of performance observed under a diversity of conditions does support the view that one is likely to achieve roughly comparable performance at other sites.

Causes of limitations on performance can be viewed through causes of false alarms, on one hand, and reasons for missed UXO's (failed detections) on the other.

Causes of False Alarms:

(1) Ground scattering from formations that had linear features such as trenches, directional depressions, or animal tunnels.

(2) Small vertical plate-like scrap.

(3) Scrap with thin extended parts (curved or non-curved).

Causes of Missed UXO-like Items:

(1) Co-polarized channels for targets of small sizes and depths were contaminated by the scattering from subsurface layers and inhomogeneous medium.

(2) Processing focus on incorrect depth, i.e. late-time identification

(3) Weak or absent target responses.

(4) Target position offset, in turn possibly due to linear features as in (1) above.

(5) Multiple target interference.

Major directions for future development in processing/classification algorithms are identified as follows.

Incorporating information in the GPR processing from manual (untrained) magnetometry improved both the GPR surveying and the processing. It expedited surveying by often indicating preferred directions and also improved data quality when there was an offset between the flag position and the target's geometric center. In some cases at Ft Ord, proximate multiple targets and/or linear geophysical features made target orientation determination ambiguous. Magnetic dipole indications estimated crudely from the manual survey ahead of the GPR rig were included cooperatively as a factor in the classification decisions based on GPR processing. That is, detection of a magnetic dipole, regardless of its clarity, was regarded as a "vote" for UXO-like character, affecting the confidence level applied to UXO/non-UXO GPR classification. Addition of this information effected a desirable lift in the otherwise resistant portion of the Ft Ord ROC curve into the high Pd region (Figure 30). In particular, this produced a Pd of about 90% with about a 50% Pfa. Particularly because the Mag information was so crude, this suggests that exploitation of more sophisticated Mag/EMI data might improve GPR performance rates beyond the best case that appears in that figure.

Experiments exploiting estimated target depths at JPG-V were tried as a result of lessons learned during the BP demo. Such additional depth information improved the classification performance, provided that it was accurate. The specific level of accuracy required in depth estimates to achieve a given GPR classification performance improvement has not yet been established. Depending on the particular ground truth sorting criterion used, use of depth guidance to enhance the GPR processing led to Pfa reductions from values greater than about 60% to something above 40%, without appreciable decrease in detection.

4.4 Performance Comparisons

It is difficult to compare the GPR discrimination performance here with that of other systems because 1) there are few other discrimination systems; 2) others generally considered different situations, operating with other technologies, objectives, criteria, and/or analytical frameworks; and 3) results were often reported in terms such that they are not entirely

comparable to the ROC curves here, e.g. using false alarm count as opposed to Pfa, or producing Pd/Pfa ratios only at isolated points. These differences notwithstanding, a few highly approximate comparisons follow for the sake of the perspective they may offer.

EMI is usually regarded as the most promising UXO discrimination tool. EMI discrimination processing to date has usually inferred principal magnetic polarizability values ("β" values) of an unseen target, and from those has judged whether the object is UXO-like or not. A matched filter approach based on these β values produces ROC points in ESTCP project UX-9918 [4]. For JPG Area 1 the raw Pd was 67% with a Pfa of 80%; however this result below the LOND was largely due to undetectability of small 20 mm UXO's. When the 20 mm's are discarded, the Pd is about 88% vs a Pfa of 80%, which is above but near the LOND. In a similar pattern, for JPG area 3 the cited project shows a ROC point slightly below the LOND when the 20 mm's are included, and a ROC point of Pd 94% vs Pfa 83% when the 20 mm's are excluded. These are comparable to the performance shown here under various options. However, the comparison is not terribly illuminating in that these points are only in the high Pfa/ high Pd region where essentially all ROC curves converge, necessarily, on the upper corner of the ROC plot. The best performance here, in Figure 30, is clearly superior to those in the cited project; however, it is unclear how performance in the other project might have improved if they had used the UXO-like criterion with the target set they treated. Basically, the closeness of their best ROC points to the LOND is probably a consequence of 1) the aim of achieving a high Pd, pushing the results into the high Pd/ high Pfa corner of the plot; and 2) the fact that, like essentially all other discriminating processors, they have used a classification system based on UXO-likeness in extracted parameters but scored detections based only on the TRUE UXO criterion.

In a Mag and EMI sensor fusion project (ESTCP-9812), ROC curves in terms equivalent to Pd and Pfa are shown [5]. Figure 14 from that reference is reproduced here as Figure 36, with a dashed LOND added. ROC curves for three methods are shown for the "L Range Demonstration." One, based on "Mag size," is deemed comparable to the discrimination that the MTADS system [31] could produce for this site, based on magnetometry alone but with reference to a calculated "magnetic dipole size." Curves from two other methods are also plotted, including results in connection with the sensor fusion system that was applied. The baseline (red) curve deemed representative of MTADS Mag treatment alone is of roughly the same quality as the baseline case here, using the TRUE UXO criterion (Figure 26). The main differences are slightly stronger performance in the approach here at the lower Pfa's and worse performance at the higher

Pfa's. The baseline performance curves here using the UXO-like criterion with depth feedback (Figure 27) are much stronger than any of the cases in Figure 36 in the lower Pfa range, but are again weaker in the upper Pfa region. The improved ROC curves shown above for Ft Ord, based on the UXO-like criterion with inclusion of Mag dipole presence as a factor (Figure 30), are stronger than any of the curves in Figure 36, over the entire Pfa range. Of course, one cannot say how much the curves in Figure 36 would change if the investigators had also used the UXO-like criterion

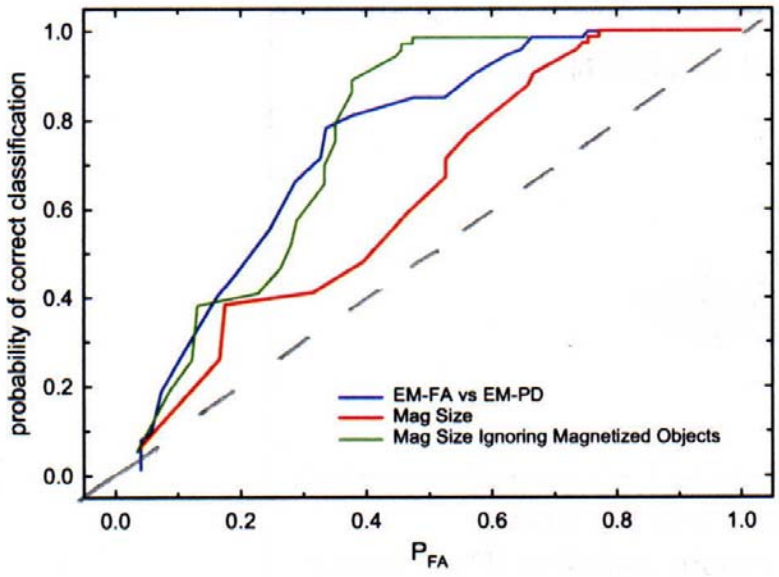

.

Figure 36. From ESTCP-9812 final technical report: Red line to represent MTADS discrimination using Mag data alone; Green line: enhanced results obtainable from MTADS Mag data, including mag dipole orientation information; Blue line: Results including information from "three β" EMI data.

The particular target set and mix at a site can change performance quality dramatically. In particular, performance can be improved greatly if relatively distinct classes of ordnance and clutter are present. In the example from the Tyndall demo, the 105 mm projectiles formed a distinct enough portion of the target population so that including even crude estimates of target length helped greatly in distinguishing these items as UXO's (Figure 34, Figure 35). The ROC curves in those figures generally rise as steeply or more steeply than those in Figure 36. In another study [5], processing is optimized for treatment of three relatively distinct, geometrically simple, hefty ordnance types (105 mm, 155 mm, 8 in rockets), relative to frag, frag clusters, and a smaller amount of ordnance scrap. For this specialized circumstance and optimized processing, extremely steep (i.e. good) ROC curves are produced. The recommendations below discuss the

desirability of tuning sensor and processing choices for a best fit, on a case by case basis, perhaps even on a target by target basis.

5 Cost Assessment

5.1 Cost of the Demonstrations

The following two tables provide information on the costs of the demos, first in terms of labor and human activity (Table 2) and then in terms of equipment costs (Table 3). In the former, "target" as in "number of targets" simply indicates a surveyed location, whether a UXO, non-UXO, or any target at all was present. In terms of throughput, on average about 24 min per target was required for the actual GPR scans, with very little variation across the sites. While more data were collected in the later surveys, efficiency was also greater. The newer UWB polarimetric GPR system (Section 10) can cover ground at a slow walking speed. If one considers a "slow walk" to be ~ 20ft/min, and assumes 5 to 10 ft long grid lines at 1 ft spacing, that implies approximately 1 to 5 min/target actual survey time with the new GPR, not counting transition time between target locales. Because the newer units are small, light, and inexpensive, a number of them could be operating in parallel at any particular site.

Table 2. Labor and activity costs of the demos.

	JPG	Tyndall	Ft Ord	BP	Hour/unit
No. of targets	100	152	97	87	
No. of GPR scans	243	365	242	209	0.1667
No. of Mag scans	100	0	97	0	0.0333
Soil property measurements /day	1	1	1	1	0.5
Target data processing sequences	243	365	242	209	0.0833
Equipment setups /day	1	1	1	1	0.5
Work hrs per Day	8	8	8	8	
Labor hours for:					
GPR scans	**41**	**61**	**40**	**35**	
Mag scans	**3**	**0**	**3**	**0**	
Soil property measurement	**3**	**4**	**3**	**3**	
Data processing	**20**	**30**	**20**	**17**	
Equipments setting	**3**	**4**	**3**	**3**	
Total Labor Hours @ Each Demo.	**70**	**99**	**70**	**57**	
Labor Hrs/ Target	**0.70**	**0.65**	**0.72**	**0.66**	
Overall Average Labor Hrs / Target	**0.68**				

Table 3. Equipment costs of the demos

Network analyzer	$11,512	1	$11,512
Generator	$500	1	$500
Notebook computer	$5,000	1	$5,000
Antenna	$15,000	1	$15,000
Tractor	$1,500	1	$1,500
Frame	$1,000	1	$1,000
Switching box	$500	2	$1,000
etc	$2,000		$2,000
Total Equipment Cost			**$37,512**

5.2 Cost Comparisons and Savings

It is difficult to make meaningful cost comparisons between the GPR system here and other discrimination technologies. This is because 1) it is difficult to identify a "baseline" discrimination (as opposed to detection) technology; 2) the GPR technology and consequent application techniques have developed rapidly during the course of the demos and thereafter during this report's preparation; and 3) other e.g. emerging discrimination systems used different analytical renderings to treat cases that were different from those here, sometimes quantifying results in other terms. Be this as it may, one can say that the initial capital cost for the GPR equipment as it existed at the time of the ultimate demos was not great, as survey equipment goes. While the newer equipment might cost only about $5 to $10k, compared to the $37k expended in these demos, one might use $15k in estimates to account for maintenance, replacement, and upgrades. In any case, the primary cost did and will reside in man hours in the field and in processing. As noted above, using the costs in these demos as a guide indicates a labor cost of between ~ $50/target and ~ $100/target, depending on the level of training and professional qualifications of the personnel. There is no reason that systematic implementation could not be carried out ultimately with less highly trained personnel than even the least skilled who were used here. This, together with the faster, handier GPR systems, could drive the cost well below $50/target.

Estimating potential savings from this GPR technology can be done only very approximately. Consider an overall average, rule of thumb cost per dig to be ~ $200 (Roger Young, Huntsville Center, personal communication). Many sources attest to the fact that at most actual UXO cleanup sites, many, many more non-UXO items are dug up for each UXO that is excavated. Of course, many of these were not approached as potential UXO while being excavated, but were recognized as clutter and presumably removed without the care and attendant cost devoted to a potential UXO. Regarding only the "serious" digs, then, consider situations in which results such as those in Figure 34 and Figure 35 might be expected. The very high number of digs executed in real cleanup is driven by the determination to achieve near 100% detection. The aforementioned figures show ~ 100% Pd at around 40% Pfa. Optimistically then, under the assumed conditions, about 60% of the false alarms in serious digs could be avoided by using the demonstrated GPR technology. Even given the requirement that the situations warrant reference to these particular ROC curves (favorable i.e. dry, relatively homogeneous soil, distinct target types...), this is optimistic primarily because it assumes that at a real site the density of metallic clutter would not degrade performance below what appears in the figures. All in all, 60% savings might be regarded as an upper bound on potential savings. The lower bound is zero: Under unfavorable conditions (lossy, heterogeneous soil; a large spectrum of target types with overlapping characteristics; clutter with shapes much like UXO...), GPR use would gain one nothing and should not be applied.

6 Discussion, Evaluation, and Recommendations

The UWB, full polarimetric GPR and associated processing system indeed succeeded in demonstrating some discrimination capability on the basis of which, as above, one can estimate advantages or savings that might be achieved by applying it. At the same time, we do not in general recommend the application of our system in most circumstances at this time. This is because, in the majority of (but not all) circumstances and under the most common processing criteria (i.e. Figure 26 and Figure 27 as opposed to Figure 34 and Figure 35), the persistently missed detections limit performance stubbornly in the upper portions of the ROC curves. A desirable level of detection awaits development of an expeditious but optimally effective combination of GPR with Mag or EMI, in the very least along the lines suggested by the fledgling approach applied in the Ft Ord demo. Further, the newer, much handier, faster,

and cheaper GPR that has been developed under SERDP auspices should reduce substantially the main limitations of the GPR system that was demonstrated. While one cannot always forego application in anticipation of the next generation of improvement, in this instance we feel that the deficiencies in the old system and the capabilities of the emerging system warrant waiting.

The complexity of the UXO classification problem requires quite involved processing algorithms to suppress noise and clutter, enhance target response, extract useful features, and improve both stability and sensitivity. Many effective algorithms have been developed leading up to and during these demonstrations, a good example being application of well-chosen bandpass filters to bring out target response (Figure 23 and Figure 24). However, even with the improvements made in the emerging GPR system, further developments are necessary for a desirable level of performance in future implementations. In terms of specific recommendations, for most effective implementation it is necessary to:

(1) **Develop more effective algorithms to suppress surface and subsurface clutter**. As discussed earlier, scattering from surface and subsurface layers contaminates radar data and distorts the resonance and polarization features, thus leading to false alarms and missed UXO's. The much higher clutter level in the co-polarized channels compared to the cross-polarized channel is related to planar form of the ground surface and near surface layers. Some surface clutter reduction algorithms have been developed in the past [29] dealing with simpler surface scattering. More developments are much needed to improve these techniques to handle more general ground conditions, including perhaps linear environmental features.

(2) **Automate data processing and feature extraction procedures.** The current processing algorithm requires experts or trained personnel to perform this function properly. It is necessary to increase the degree of automation in order to make the system more widely available for field use. This can in fact be done. Note Figure 43 in Appendix B, showing virtually identical performance by the first generation automated neural network/fuzzy logic classification system and by the team expert.

(3) **Optimize and automate classification rules.** The current classification rules for the ultimate demos were established using the various features learned from canonical UXO-like and non-UXO items encountered during the previous demos, as well as in prior backyard and lab tests. In the final demo, proximate multiple targets and/or linear geophysical features made target orientation determination ambiguous. Experiments suggested that, to some degree, performance could be enhanced by reducing the weight of parameters in the processing most affected by low confidence parameters (e.g. ETO) and focusing more closely on features that survived the interference (resonance). Broadening the cases covered by the classification rules and then also automating their application would facilitate implementation under more realistic site conditions than typically appears on test plots.

(4) **Develop smaller, lighter, faster radars to achieve greater ground coverage in a target's locale**, e.g. 2-D grids instead of a few lines. As of this writing, a faster, smaller, lighter system has been developed in SERDP project work (UX 1282). See Section 10 below. Horizontal grids of measurement over easily designated templates will allow [quasi-] 3-D as opposed to the current 2-D views, resolving many ambiguities that have limited discrimination performance heretofore. Other GPR's along the lines of that discussed in Section 10 should also be constructed as needed, to optimize for particular sites and conditions. All this should enhance interpretation of the GPR data as long as we:

(5) **Develop processing for 3-D data obtained from grids.** This processing would in fact be considerably more onerous than for the current 2-D views, such as are displayed in many figures above, i.e. the antenna position - signal travel time plots that typify GPR data presentation. However, it can be done, can be optimized so it is sufficiently fast, and is well worth doing. A good deal of physical and intellectual maneuvering described above centers around the need to get an appropriate view of the target, without being (oblivious to an) offset from the actual target position. This would be dealt with effectively by 3-D data.

For identification of more general future directions, note that two relatively robust features of the radar records in the face of multi-target scenes are 1) resonance, 2) target position/depth location under dry conditions. These suggest a route for exploiting GPR to help address the difficult multi-target (highly contaminated site) problem, as pursued in a current

SERDP project [27]. EMI processing has been enhanced significantly when it was cued with estimated target depths from Mag surveying [28]. Similarly here, target depth information enhanced the GPR performance. However, there are settings in which GPR would provide better information on 3-D target position than EMI or Mag, e.g. a target at large depths in dry sand, or a target beneath diffuse, small, near-surface metallic clutter. When not defeated by lossy soil or overwhelming clutter, GPR is more precise than magnetometry. While EMI range is usually limited by the attenuation due to dipole type magnetic field geometry, GPR can usually see considerably deep in dry soil. Perhaps most important, the locations of distinct targets nearby one another can often be discerned by GPR when they could not be by EMI/Mag, and GPR data could be used beneficially to constrain the inversion of EMI data [27].

The results of these demos argue for multi-sensor surveying. The most immediate motivation for this is evident when one considers that the greatest failure in the GPR classifications constituted missed UXO's. Experience in these demos suggests that this might be avoided by inclusion of Mag or EMI data, both for inference of magnetic dipole type behavior and for estimation of target position. In this regard, note that the ROC curve in Figure 27 for the UXO-like criterion begins very well, rising quickly to about a 50% detection rate at about a 10% false alarm rate. However, further loosening of threshold criteria fails to pick up many of the remaining UXO-like objects very quickly, relative to the rate of increase in false alarms. Inclusion of magnetic dipole indications in the processing improved GPR performance significantly, under what were otherwise adverse circumstances. Many future improvements could be achieved with cooperative processing of GPR and EMI/mag data. This is best done at the "feature level," as cooperative or collaborative processing, as distinct from complete joint inversion. The former has much more relaxed requirements in terms of co-registration of data and algorithmic complexity. Improved EMI/Mag data processing that provides more accurate azimuthal orientation, position, or depth could improve the accuracy of GPR during the survey and processing so that no target is left behind. Additional EMI/Mag information such as linearity and mass estimation could be incorporated into the classification rules. Similarly, the length, depth, and orientation estimated from GPR could also be utilized during the EMI/Mag processing, modeling, or data fitting, as has been done profitably in [27].

Ideally, one would like to be able to discriminate true UXO even from elongated fragments with lengths comparable to some UXO. Extracting more information on target geometry with GPR could be substantially enhanced by the capability to determine the 3-D

scattering pattern, for separating an elongated, plate-like fragment from a cylinder-like UXO. The developing GPR systems mentioned above may be capable of this and might also be used in bi-static mode (separate transmitter and receiver locations) to maximize scattering information. In addition, recent progress in interpreting broadband electromagnetic induction (EMI) responses of metal objects suggests that target aspect ratios might sometimes be estimated from EMI data [33, 34]. Combined with length information from GPR, this would allow inference of general target dimensions. For complex objects, however, this kind of aspect ratio estimation via EMI will break down. At the same time, emerging signature, forward modeling, classification, and inversion approaches offer the possibility of much more sophisticated classing of unseen metal objects [36-40]. While "the jury is still out" on the ultimate utility and practicality of these new approaches, there is little doubt that ancillary or "prior" target information from GPR could relieve the associated data processing and inversion challenges, e.g. ill-conditioning. For example, early results suggest that the new systems can often infer detailed spectral signatures and locations for each of two nearby objects, when their signals overlap spatially and each contributes significantly. However, the EMI processing must have some initial guidance to the effect that, in fact, more than one object might be present, when this is not at all obvious from the EMI data. Also, some constraint on the possible positions of the objects facilitates the EMI processing enormously.

In closing, we offer three general ideas for optimizing GPR implementation, with or without EMI/Mag collaboration:

1. **Smart site selection**: This pertains both to the soil characteristics of the site and also the nature of the UXO contamination. The Tyndall demo site did in fact contain some environmental challenges, including a shallow water table and other layering. However, overall the dielectric heterogeneity and lossiness of the sand were limited, providing a relatively clear GPR view. Further, the targets present fell into sufficiently contrasting length classes so that inclusion of ETL with the other classification criteria produced steeply rising ROC curves for particular ordnance types. At other sites with limited ordnance diversity and favorable (dry, relatively homogeneous) soil characteristics, similar classification advances might be achieved.

2. **Smart data acceptance/rejection for individual targets**: While casting the discussions above in terms of ROC curves makes sense for many aspects of performance quantification and interpretation, it diverts attention from other ways of proceeding. In particular, to produce ROC curves one necessarily considers all cases encountered, not "cherry picking" the most appealing ones. One also progressively loosens target acceptance criteria as far as one dares, to strive for a 100% Pd as the termination of the ROC curve. However, the best role of GPR may sometimes not be to supplement Mag/EMI, regardless of the strength of the GPR results in each case. Rather, it would make more sense to involve GPR where its likelihood of good performance is strong, in the very least to reduce pervasive false alarms even where probability of detection by other means is high. The GPR data would simply not be used when clarity and confidence are low. While that would not help in the discarded cases, it would likely improve discrimination performance in the others, resulting in substantial savings.

3. **Smart interpretative precedence** (who helps whom, case by case): Some of the feedback obtained in the course of this project indicated that the GPR performance was being viewed and judged on the assumption that it would be used strictly as a "confirmatory" technology, fine tuning or building on results from e.g. Mag/EMI. While that fits in some ways with the cued interrogation orientation of the project, there is no reason that GPR ought to play that particular role exclusively. For example, under some circumstances GPR can produce superior estimates of target location. This could then support EMI processing to address other things that, under the particular circumstances at hand, GPR could not. Conversely, under other circumstances Mag data might provide superior estimations of target location and depth, which would allow GPR to zero in on the correct locale and perform discrimination at a level that Mag/EMI cannot. There is no reason *a priori* that one technology should be regarded across the board as only appropriate for supporting the other.

7 References

Publications supported wholly or in part by this ESTCP project are printed in bold blue.

1. Navy Tri-Service Environmental Quality Research Development, Test and Evaluation Strategic Plan, October 1994, p. Cleanup-21.

2. U.S. Army Environmental Center. *FY02 Army Environmental Requirements and Technology Assessments (AERTA).* SFIM-AEC-PC-CR-2002040, Final Report, October 2002.

3. Defense Science Board. 1998, *Task Force Report on Unexploded Ordnance (UXO) Clearance, Active Range UXO Clearance, and Explosive Ordnance Disposal (EOD)Programs*. Task Force Report to the Office of the Under Secretary of Defense (Acquisition and Technology), April 1998.

4. ESTCP Project UX-9918, *Matched Filter Processor for Detection and Discrimination of Unexploded Ordnance*, Final Technical Report and also Cost and Performance Report, see www.estcp.org.

5. ESTCP Project UX-9812, *Electromagnetic Induction and Magnetic Sensor Fusion for Enhanced UXO Target Classification*, Final Technical Report and also Cost and Performance Report, see www.estcp.org.

6. SERDP Project #1282, Second Year Interim Technical Progress Report.

7. D.L. Moffatt and R.J. Puskar, A Subsurface Electromagnetic Pulse Radar, Geophysics, vol. 41, no. 3, pp. 506-518, June 1976.

8. G.A. Burrell, J.H. Richmond, L. Peters, Jr., and H.B. Tran, A scattering model for detection of tunnels using video pulse radar systems, in *Acoustic, Electromagnetic and Elastic Wave Scattering- Focus of the T-Matrix Approach*, Pergamon Press, 1980.

9. L. Peters Jr. and J.D. Youn, Application of subsurface transient radar, in *Time Domain Measurement in Electromagnetic*s, E.K. Miller (ed.), New York, Van Nostrand Reinhold, 1986, pp. 297-351.

10. L. Peters Jr., J.J. Daniels, and J.D. Young, Ground penetrating radar as a subsurface environmental sensing tool, Proc. IEEE, Vol. 82, No.2, pp. 1802-1822, 1994.

11. L. C. Chan, D. L. Moffatt, and L. Peters, Jr., A characterization of sub-surface radar targets, Proc. IEEE, Vol. 67, no. 7, pp. 991-1001, July 1979.

12. Chi-Chih Chen and L. Peters Jr., Buried unexploded ordnance identification via complex natural resonances, IEEE Tran. Ant. & Propagat., vol. AP-42, pp. 1645-1654, Nov. 1997.

13. J.I. Halman, K.A. Shubert, and G.T. Ruck, SAR processing of ground-penetrating radar data for buried UXO detection: Results from a surface-based system, IEEE Tran. Ant. & Propagat, vol. AP-46, pp. 1023-1027, Jul. 1998.

14. J.D. Young, *Summary Report on the Yuma Tests of SOCS*, Ohio State University ElectroScience Laboratory Technical Report 734724-2, Sep. 1998.

15. Chi-Chih Chen, A New Ground Penetrating Radar Antenna Design - The Horn-Fed Bowtie (HFB), Antenna Measurement Techniques Association (AMTA) Symp, Oct. 1997.

16. J.I Halman, Chi-Chih Chen, K.A. Subert, L. Peters, Jr., *Jefferson Proving Ground Survey Data Analysis Report (JPG IV)*, Battelle Technical Report, Oct. 1998.

17. **K. O'Neill, *Data Processing Results for UXO Classification using UWB Full-Polarization GPR System*, Mar 2001, ESTCP report. See also OSU/ESL Technical Report 737990-2, M. Higgins and Chi-Chih Chen: *Dual Broadband Fully Polarized Radar Discrimination of UXO's; Preliminary Data Processing Results for Phase I Tyndall UXO Characterization GPR Measurement*, July 2000.**

18. **Chi-Chih Chen, M. Higgins, K. O'Neill and R. Detsch, Tyndall AFB measurement results of UXO characterization using full-polarimetric ultra-wide bandwidth (UWB) GPR, UXO Forum, Anaheim, May 2000.**

19. **K. O'Neill, *GPR Classification Results for the Blossom Point Site*, Mar 2002, ESTCP Report. See also M.B. Higgins and C.-C. Chen, *GPR UXO Classification Results of The Blossom Point Site*, OSU/ESL Technical Report 737990-6, May 2001.**

20. **K. O'Neill, *GPR UXO Classification Results for Jefferson Proving Ground V*, June 2002, ESTCP Report and also CRREL Contractor Report.**

21. **K. O'Neill, *Fort Ord Site UXO Classification Demonstration Using Fully Polarimetric GPR*, July 2002, ESTCP Report. See also C.-C. Chen, *Fort Ord Site UXO Classification Demonstration Using Fully Polarimetric GPR*, OSU/ESL Technical Report 737990-9, Aug 2002.**

22. **Chi-Chih Chen, M.B. Higgins, K. O'Neill and R. Detsch, UWB fully-polarimetric GPR classification of subsurface unexploded ordnance, *IEEE Tran. Geosci. & Remote Sens.*, Vol. 39, No. 6, pp. 1221-1230, June 2001.**

23. H.H. Nelson, J.R. McDonald, and R. Robertson, *Design and Construction of the NRL Baseline Ordnance Classification Test Site at Blossom Point*, Naval Research Laboratory Report NRL/MR/6110—00-8437, March 20, 2000.

24. K.-H. Lee, Chi-Chih Chen, R. Lee, and K.A. O'Neill, A numerical study of the effects of realistic GPR antennas on the scattering characteristics from unexploded ordnances, Proc. IGARSS 200*2*, Toronto, June 2002.

25. K. O'Neill, Discrimination of UXO in soil using broadband polarimetric GPR backscatter, IEEE Trans. Geosci. & Remote Sens., vol 39, No. 2, 356-367, 2001.

26. K. O'Neill, S.A. Haider, S. Geimer, and K.D. Paulsen, Effects of the ground surface on polarimetric features of broadband radar scattering from subsurface metallic objects, IEEE-Trans. Geosci. Remote Sensing, Vol 39, No. 7, 1556-1565, 2001.

27. K. O'Neill, *UXO Discrimination in Cases with Overlapping Signatures*, SERDP Project UX-1282, First Year Report, Mar 2003; Second Year Report, Mar 2004; Third Year Report, Mar 2005.

28. L.R. Pasion, S.D. Billiings, and D.W. Oldenburg, Joint and cooperative inversion of magnetics and electromagnetic data for the characterization of UXO discrimination problems, Symp. Appl. Geophysics to Eng & Enviro. Probl. (SAGEEP), San Antonio, Texas, U.S.A., Feb 6-10, 2003.

29. M.D.A. Rahman and K.-B. Yu, Total least squares approach for frequency estimation using linear prediction, IEEE Trans. Acoust., Speech & Signal Proc., vol. ASSP-35, 1440–1454, Oct. 1987.

30. **K.-H. Lee, N. Venkatarayalu, Chi-Chih Chen, F. Teixeria, and R. Lee, *Application of Fully Polarimetric GPR for Buried UXO Classification*, Ohio State University ElectroScience Laboratory Technical Report 741119-Final, Dec. 2001.**

31. ESTCP MTADS Reports, e.g. Project 9526, www.estcp.org.

32. J.D. Young, K.A. Shubert and D.L. Moffatt, Synthetic radar imaginery, IEEE Tran. Ant. & Propagat, vol. AP-24, May 1976.

33. F. Shubitidze, K, O'Neill, K. Sun, and I. Shamatava, Application of broadband EMI responses to infer buried object's aspect ratio, Proc. IGARSS'02, Toronto, June 24-28, 2002, Vol III, pp. 1542-45.

34. K. Sun, K.O'Neill, I. Shamatava, and F. Shubitidze, Application of prolate spheroid solutions in simulation of EMI scattering with realistic sensors and objects, Proc. Applied Computational Electromagnetics Symp, Monterey, CA, 2003, pp. 531-537.

35. J.L. Salvati, Chi-Chih Chen and J.T. Johnson, Theoretical study of a surface clutter reduction algorithm, Proc. IGARSS, July 1998.

36. X. Chen, K. O'Neill, B.E. Barrowes, T.M. Grzegorczyk, and Jin Au Kong, Application of a spheroidal mode approach with differential evolution in inversion of magneto-quasistatic data for UXO discrimination, Inverse Problems, Vol. 20, No. 6, p. 27-40, 2004.

37. K. Sun, K. O'Neill, F. Shubitidze, I. Shamatava, and K. D. Paulsen, Fundamental mode approach to forward problem solutions in EMI scattering - Inferring fundamental solutions from training data, Proc. Applied Computational Electromagnetics Symp, April 2004.

38. F. Shubitidze, K. O'Neill, I. Shamatava, K. Sun, and K.D. Paulsen, A new numerical procedure for efficient and accurate representation of low frequency EM responses for a heterogeneous object, Proc. Applied Computational Electromagnetics Symp, April 2004.

39. K. Sun, K. O'Neill, F. Shubitidze, I. Shamatava, and K.D. Paulsen, Fast data-derived fundamental spheroidal excitation models with application to UXO identification, SPIE Defense & Security Symp., 12-16 April 2004, Orlando, FL.

40. F. Shubitidze, K. O'Neill, I. Shamatava, K. Sun, and K.D. Paulsen, Use of standardized source sets for enhanced EMI classification of buried heterogeneous objects, SPIE Defense & Security Symp., 12-16 April 2004, Orlando, FL.

Additional publications, supported wholly or in part by this ESTCP project:

K.R. Rao, Chi-Chih Chen, R. Lee, and K. O'Neill, A comparison of broad-bandwidth radar scattering characteristics of buried UXO and non-UXO objects, UXO Forum, Anaheim, May 2-4, 2000.

Chi-Chih Chen, M. Higgins, K. O'Neill, and R. Detsch (2000). UWB Full-Polarimetric Horn-Fed Bow-Tie (HFB) GPR Antenna for Buried Unexploded Ordnance (UXO) Discrimination, Int'l Geosci. & Remote Sensing Symp (IGARSS) 2000, Honolulu, July 2000, Vol. 4, 1430-1432.

M.B. Higgins, Chi-Chih Chen, and K. O'Neill, Improvement of UXO classification based on fully polarimetric GPR data, Proc. UXO Forum, New Orleans, April 10-12, 2001.

Chi-Chih Chen, M. Higgins, and K. O'Neill, Improved subsurface UXO discrimination with full-polarimetric, ultra-wideband, ground based radar, using space and frequency dependent signal features, Workshop on Remote Sensing by low-frequency radars, 20-21 September 2001, Naples (Italy).

Chi-Chih Chen and K. O'Neill, Performance limitations of the current UWB fully polarimetric GPR in UXO classification, 9th Int'l Ground Penetrating Radar Conf, Santa Barbara, CA, April 29 - May 2, 2002.

Chi-Chih Chen and K. O'Neill, UWB fully polarimetric GPR database from Tyndall, Blossom Point, Jefferson Proving Ground, and Fort Ord UXO Sites, 9th Int'l Ground Penetrating Radar Conf, Santa Barbara, CA, April 29 - May 2, 2002.

Chi-Chih Chen, M.B. Higgins and K. O'Neill, Advanced classification of buried UXO using a broadband, fully polarimetric ground penetrating radar, Proc. IGARSS'02, Vol III, 1569-71, Toronto, June 24-28, 2002.

8 Appendix A. Points of Contact

ESTCP

Dr. Jeffrey Marqusee	ESTCP Director	(703) 696-2120 Jeffrey.Marqusee@osd.mil
Dr. Anne Andrews	ESTCP UXO Program Manager	(703) 696-3826 Anne.Andrews@osd.mil

ERDC-CRREL

Dr. Kevin O'Neill	Principal Investigator	(603) 646-4312 Kevin.O'Neill@erdc.usace.army.mil

OSU-ESL

Dr. Chi-Chih Chen	Co-principal Investigator	(614) 292-3403 chen.118@osu.edu

9 Appendix B: Automation of GPR Classification Processing

9.1.1 Feature Extraction

Partial or complete automation of feature extraction and classification procedures can be achieved via neural network methods. For instance, the neural network can be trained to recognize the spatial variation patterns of the ELF and ETO from the parallel and transverse passes. It can also be trained to recognize the scattering pattern in the time-position plot or magnitude relationship between the different channels. These are some of the features required to execute the classification rules. An example of applying neural network techniques to automatically detect the presence of target response in the presence of clutter is shown in Figure 37 and Figure 38. As one can see, the target responses (arcs) are correctly detected by a neural network algorithm without any involvement of the operator. Figure 39 and Figure 40 give another example of applying neural networks to automatically detect scattering features associated with drainage pipes. There are two pipe systems at the site. They are slightly offset from each other and have slightly different depths. The network was trained to detect specific temporal and spatial patterns using a training set. These capabilities can be used to isolate the signal features we require to execute the more complex classification processing, considered next.

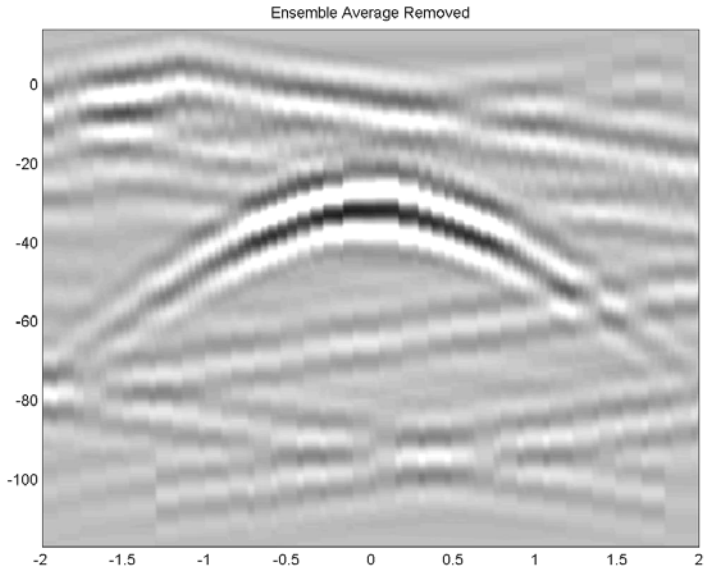

Figure 37. Simulated GPR data containing surface clutter.

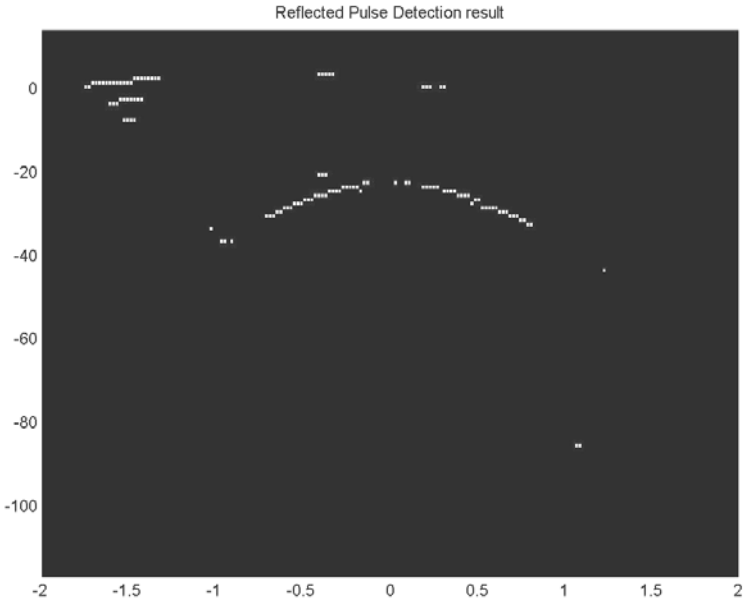

Figure 38. Output from neural network trained to detect target arcs.

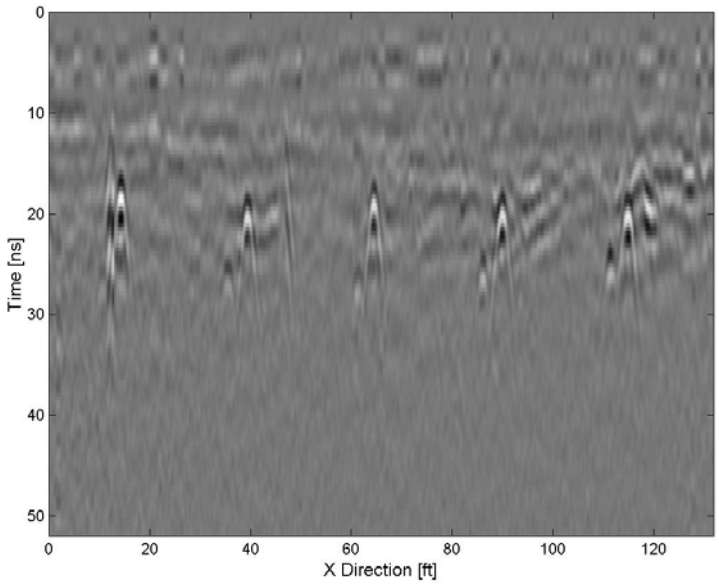

Figure 39. GPR measurements showing buried drainage pipes in farmland.

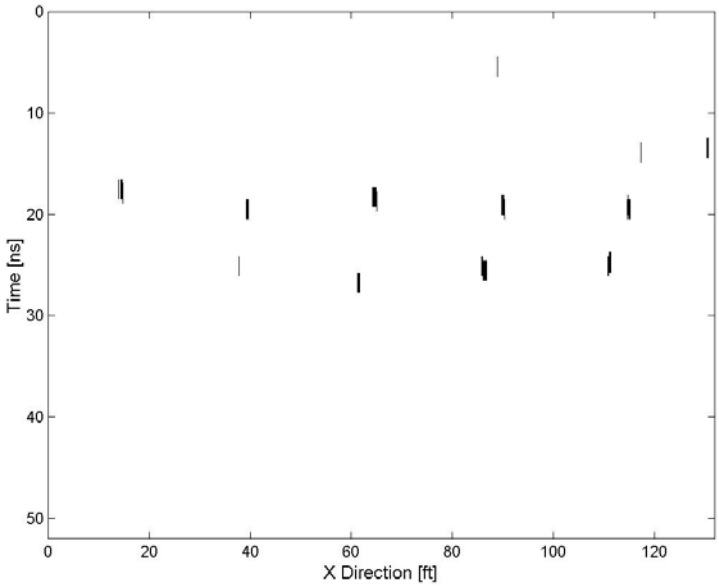

Figure 40. Neural network detection of the drainage pipes from time vs position GPR data.

9.1.2 Classification

A pilot version of an automatic classification algorithm has been developed using an artificial neural network (ANN) and fuzzy logic to perform the GPR data processing that was done by human operators to produce the results in this project. This is an expert system based on the current OSU UXO-like features and classification criteria. The algorithm reads the extracted features and performs UXO classification automatically. The ANN classifies the object into (A) non-elongated object; (B) possibly elongated with small inclination; and (C) elongated with large inclination. The fuzzy logic rules are then applied to perform further classification of UXO-like or non-UXO according to the classification tree. The ultimate results are shown in Figure 43, in which the ANN/ fuzzy logic system performed as well as the team expert.

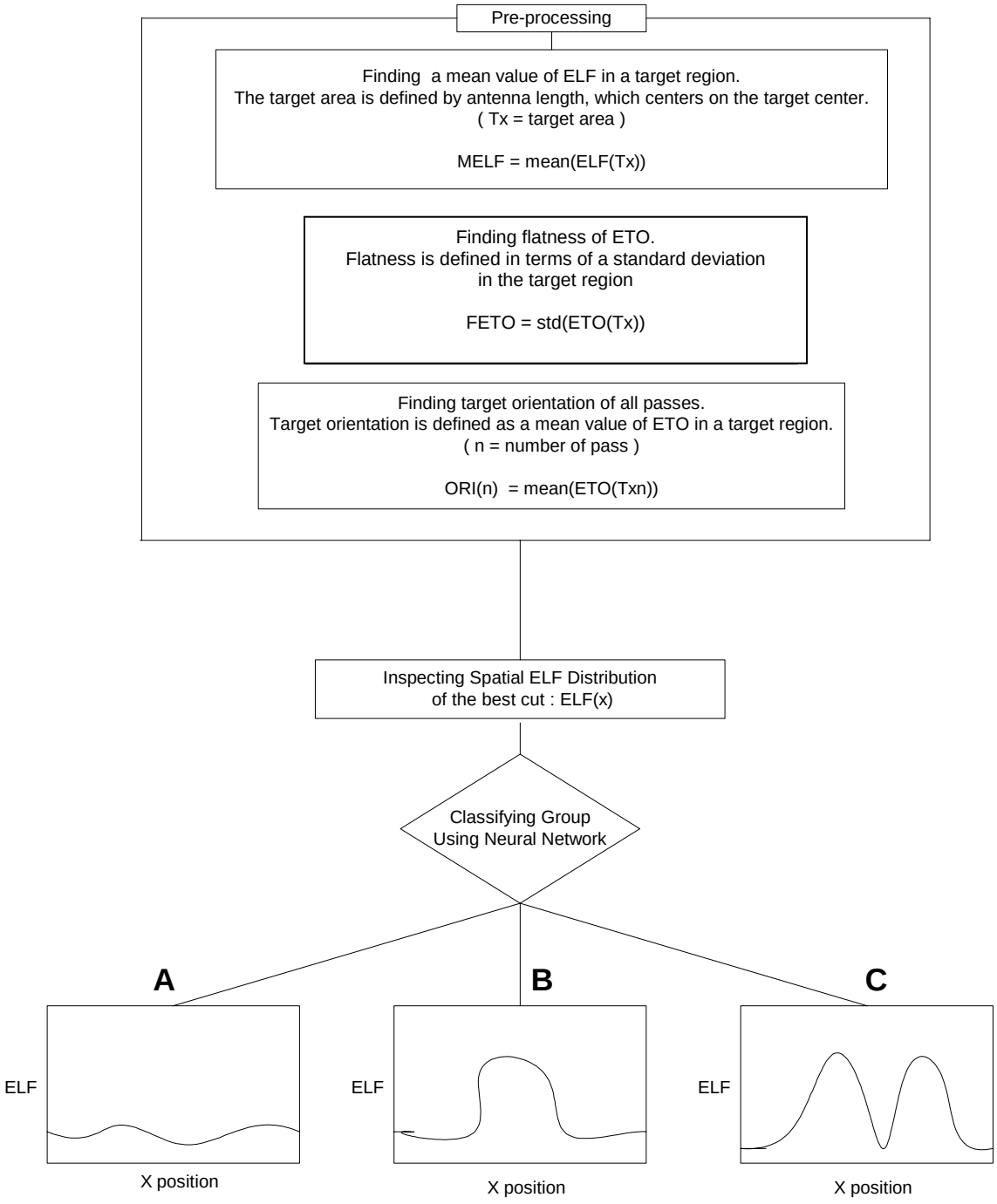

Figure 41. Top of ANN/ fuzzy logic classification tree.

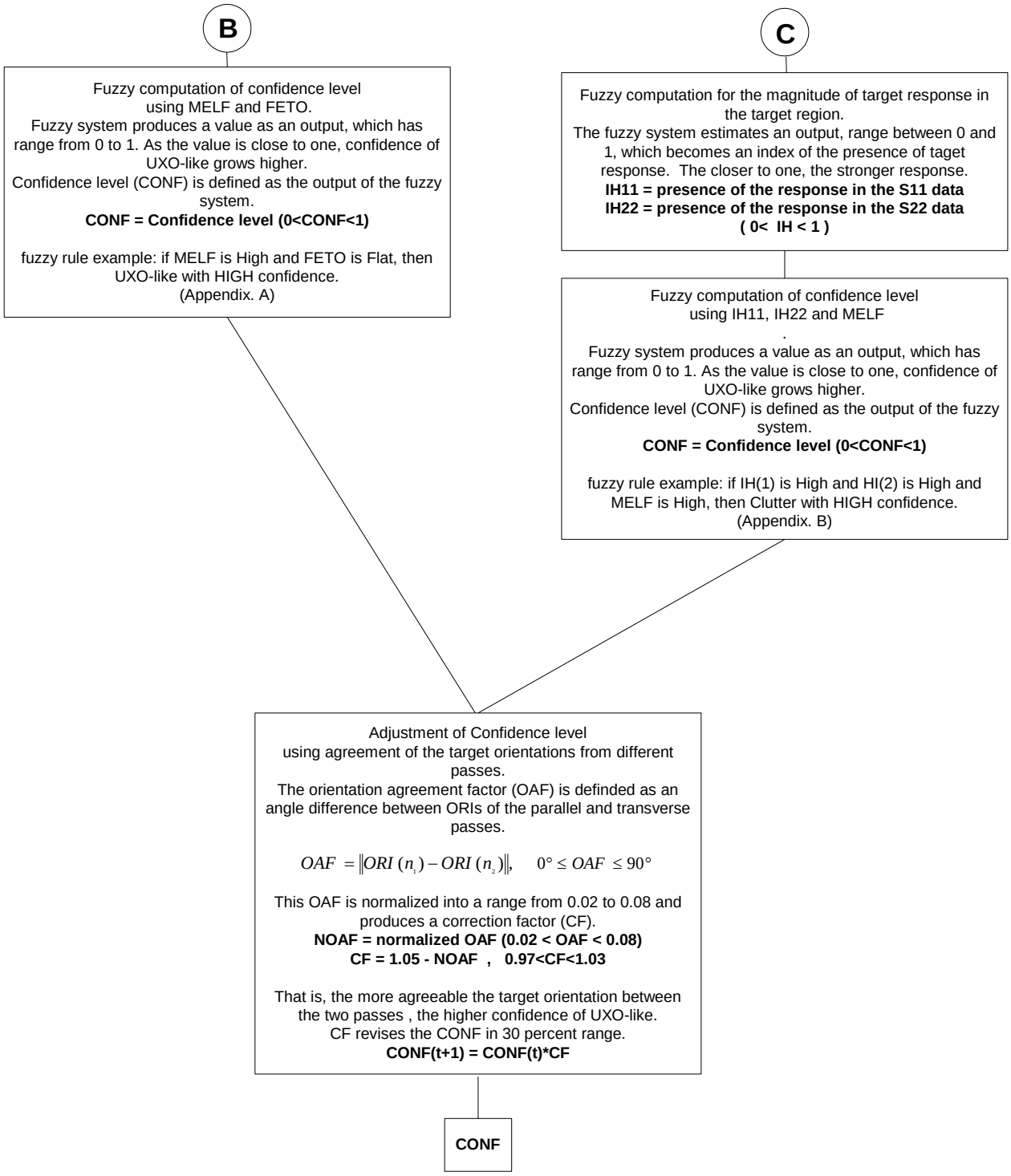

Figure 42. Bottom of ANN/ fuzzy logic classification tree.

A. Fuzzy system for Group B

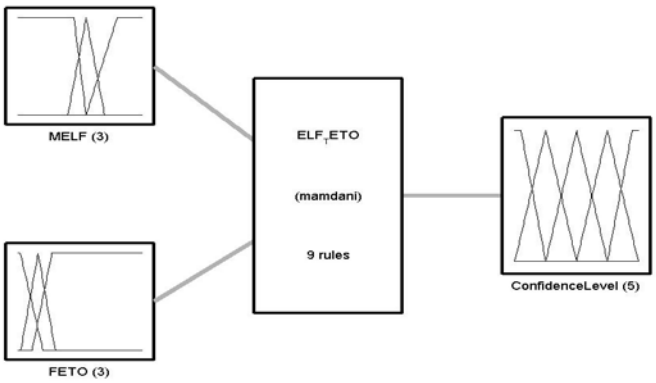

(a) Block diagram of fuzzy system for Group B.

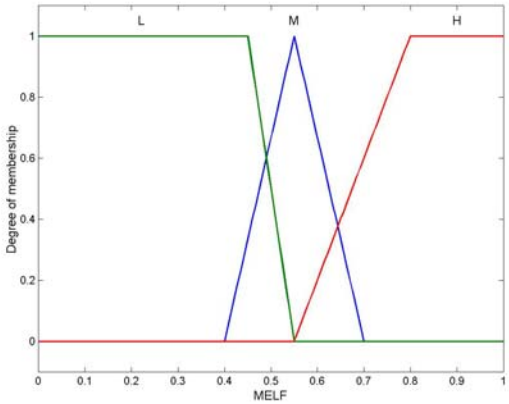

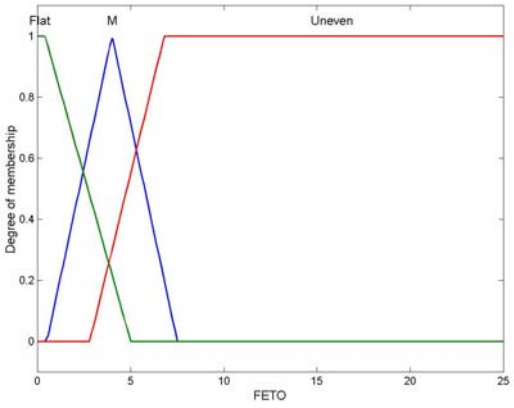

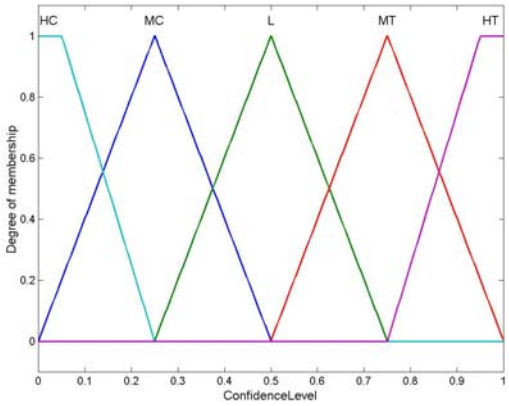

(b) Fuzzy membership functions for output variables.

FETO	**MELF**
F = Flat	H = High
M =Medium	M = Middle
U= Uneven	L = Low

Confidence Level

HT = High confidence Target

MT = Medium confidence Target

L = Low confidence

MC = Medium confidence Clutter

FETO **MELF**	**F**	**M**	**U**
H	HT	HT	L
M	MT	L	MC
L	MC	HC	HC

(c) The fuzzy rule base for Confidence Level

B. Fuzzy system for Group C

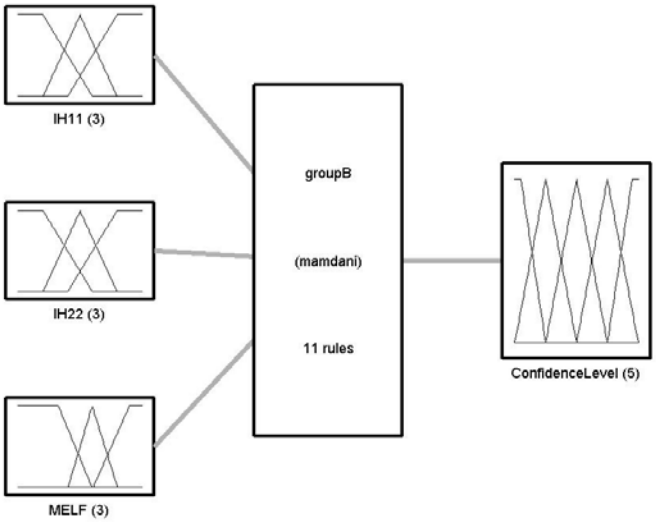

(a) Block diagram of fuzzy system for Group B.

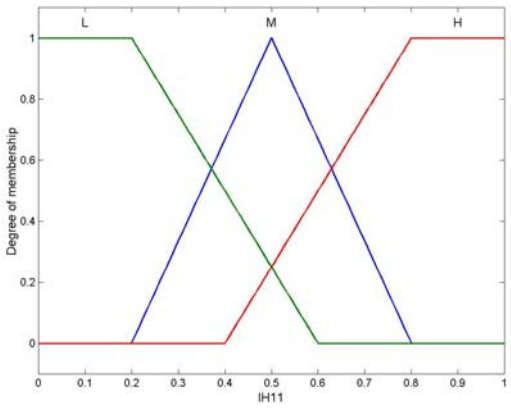

(b) Fuzzy membership functions for IH11

Fuzzy membership function for HI22 is the same as that of HI11.
Fuzzy membership functions for MELF and Confidence Level are the same as that in fuzzy system for Group B.

IH11	IH22	MELF	Confidence Level
H	L	H	HT
H	M	H	MT
H	H	H	HC
H	H	M	MC
H	H	L	MC
L	L	H	L
L	L	M	L
L	L	L	MC
M	L	H	HT
M	H	H	MT
M	L	M	MT

(c) The fuzzy rule base for Confidence Level.

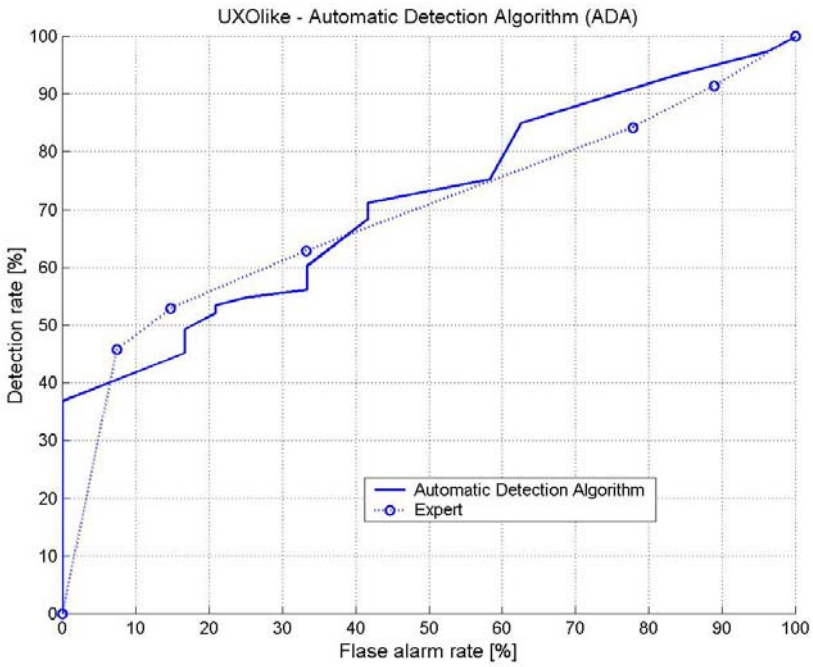

Figure 43. Classification ROC curve based on UXO-like criteria (Ft Ord).

10 APPENDIX C: The New GPR System

The large antenna footprint of the GPR used in these demos presented an important limitation in spatial resolution and in separating clustered objects. This was because of significant antenna scattering from large antenna arms that were designed to couple more low frequency energy into the ground. Such scattering subsequently interacts with intended subsurface objects and complicates scattering pattern signatures. Developing a new antenna with reduced footprint and reduced antenna scattering, i.e. radar cross section (RCS) was needed to further enhance discrimination capability of clustered objects. Experience during the demos also showed that more GPR passes provide vitally enhanced spatial information. More passes or even a 2-D grid data will require much longer survey time using the existing prototype system. Therefore, developing a faster radar system was undertaken in a SERDP project (UX 1282). With the improvements listed below, the new system can be operated at roughly a slow walking speed, compared to the older 3 sec per shot stop-and-go system. This will allow one to take grids of radar data, i.e. repeated parallel transects, to cover an area over a target, in contrast to surveys along a couple of lines as practiced in the past.

To date we have (1) designed, fabricated, and tested a new, faster GPR system that incorporates the advanced digital down converter (DDC) and direct digital frequency synthesis (DDS) technology suitable for UXO detection/classification tasks; (2) designed, fabricated and tested a new low-RCS GPR antenna suitable for UXO detection/classification tasks. Figure 44 shows the block diagram of the new GPR system suitable for UXO application or any other GPR applications. It contains four major parts: (1) RF front-end components such as filters, amplifiers, couplers, switches, and attenuators, (2) fast direct digital frequency synthesizers (DDS), (3) dual-channel digital down converter (DDC), and (4) new low-RCS, dielectric-loaded quad-ridge horn antenna. Each will be described briefly below.

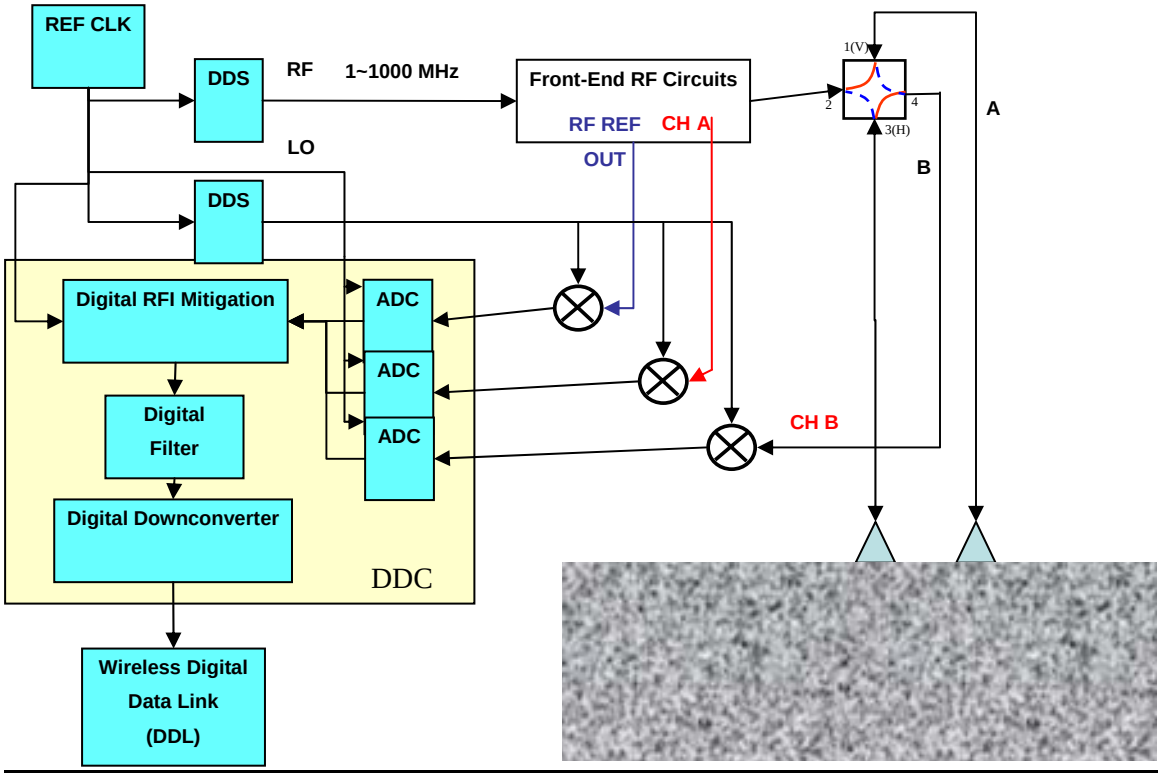

Figure 44. New OSU/ESL GPR System Block Diagram.

10.1 RF Front End

The transmitting side of a conventional RF front-end circuitry is responsible for up converting the IF (< 5MHz) signal to the actual RF frequency (10~1000 MHz) to be radiated out by mixing the IF signal with a local reference signal (LO). For GPR application below 1 GHz, the RF signal can be directly synthesized using DDS. RF amplifiers are also used to generate the desired radiation power level. For fully polarimetric measurements, RF switches are also required.

The receiving side of RF front-end circuitry is responsible for down converting the RF signal to IF frequency such that its frequency is low enough for sampling. Again this frequency down conversion is achieved by mixing the received RF signal with a local reference (LO) signal.

During the frequency sweeping, both IF and LO sweep simultaneously and maintain a fixed frequency difference, i.e. the IF frequency. The phase of both RF and LO signals are locked together with respect to a stable reference clock at 10 MHz. Figure 45 shows the radar hardware where the RF front-end components as well as DDS and DDC parts are all indicated.

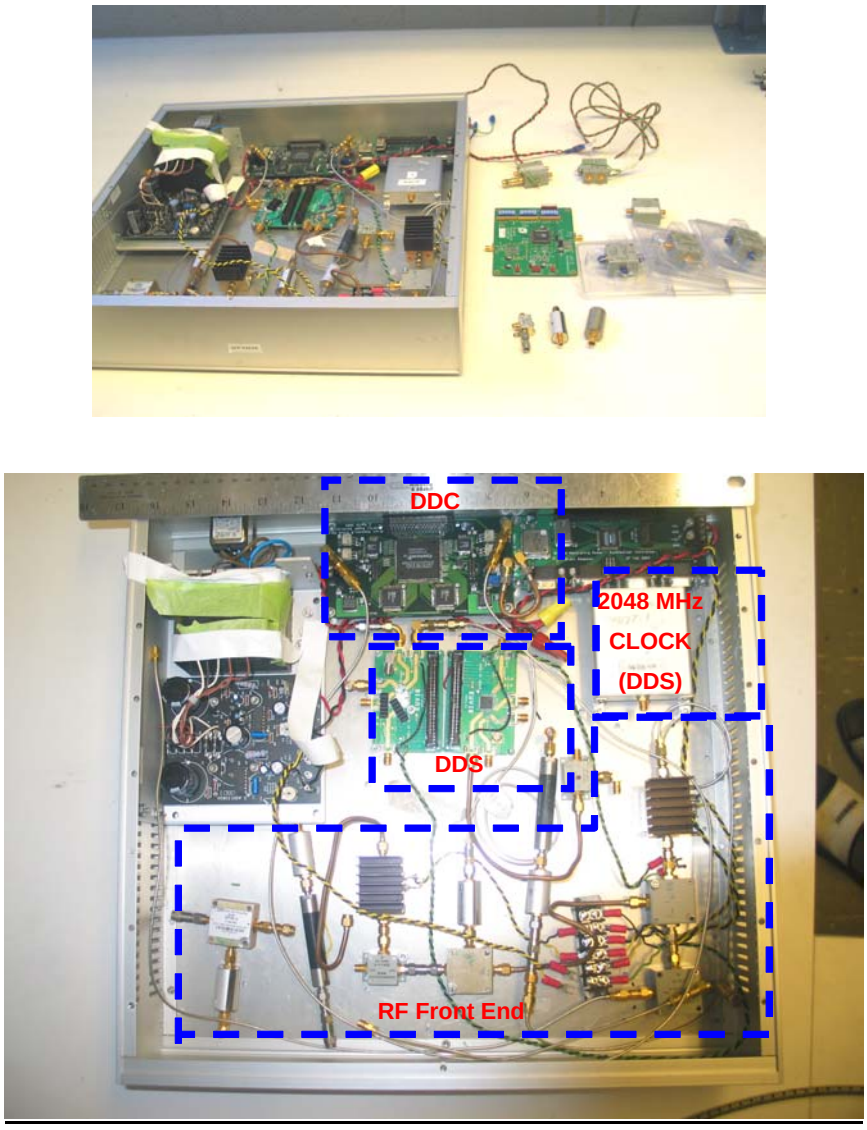

Figure 45. Hardware of the new dual-channel GPR radar.

10.2 Digital Down Converter (DDC)

Traditional coherent receivers for radar systems use the familiar I/Q demodulator architecture seen in Figure 46. Before the advent of fast and affordable DSP technology, this operation had to be done in the analog domain. This method presents a whole host of issues that must be taken into consideration in order to get a reliable measurement. One of these issues is that the phase difference between I and Q channels is not exactly ninety degrees for an analog device. As a result, the vector diagram becomes distorted, producing an unwanted image component in the frequency domain.

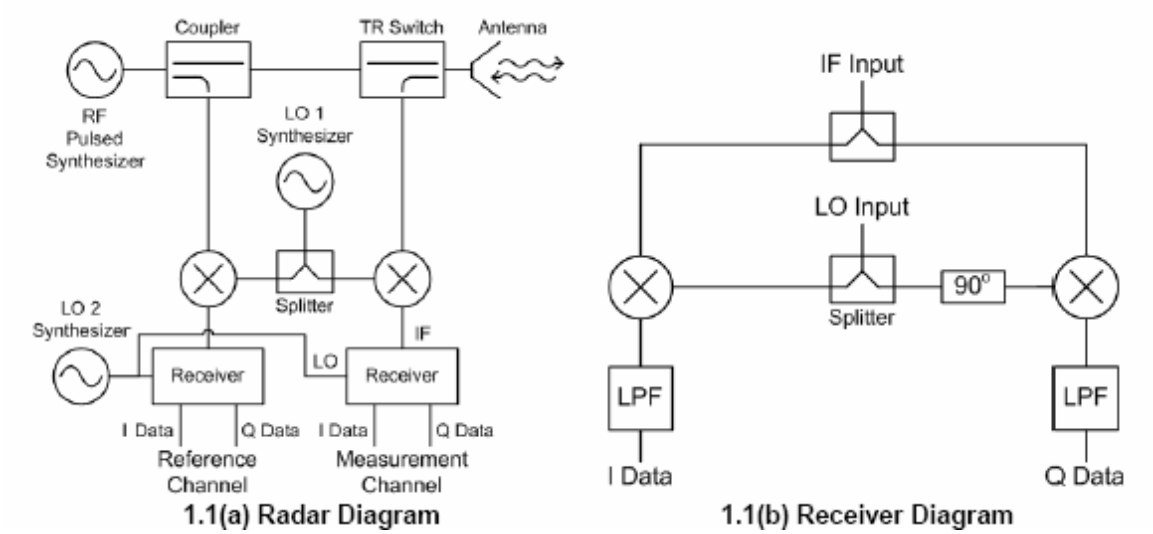

Figure 46. Conventional Analog Radar Receiver Architecture.

The recent advance in integrated circuits due to the demand of wireless industry has led to a new generation of RF receiver designs that not only eliminate the previous I/Q imbalance issue but also provide many desirable capabilities that are suitable for GPR application. Some of these features include compact dimension, lower power consumption, real-time interference mitigation, and simultaneous multiple channel reception. Figure 47 shows the simple architecture of a *Digital Down Converter* (DDC). The input RF signal (10~1000 MHz) is first down converted to the IF frequency (5 MHz) by a conventional mixing method. At this point, all the magnitude and phase information is preserved in the IF signal. The IF signal is then digitized using a fast analog to digital converter (ADC). The digitized data are then fed into a DSP (or FPGA) chip inside which I/Q demodulation, integrated, and filtering are performed in real time. The resultant

data have no phase distortion and have much greater sensitivity compared to their conventional analog counterpart.

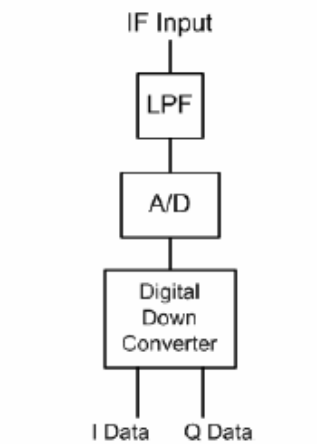

Figure 47. OSU/ESL Digital Down Converter (DDC) Radar Receiver Architecture.

A physically arranged block diagram of the digital receiver is shown in Figure 48. The picture of the actual board is shown in Figure 49. The data are sent back to computer via a fast digital I/O (DIO) interface for storage, display, or further processing.

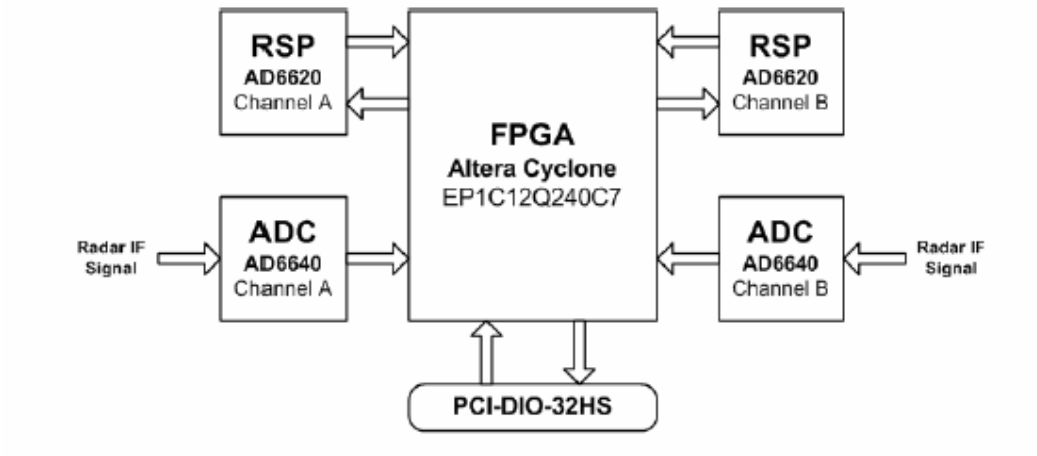

Figure 48. OSU/ESL Digital Receiver Block Diagram.

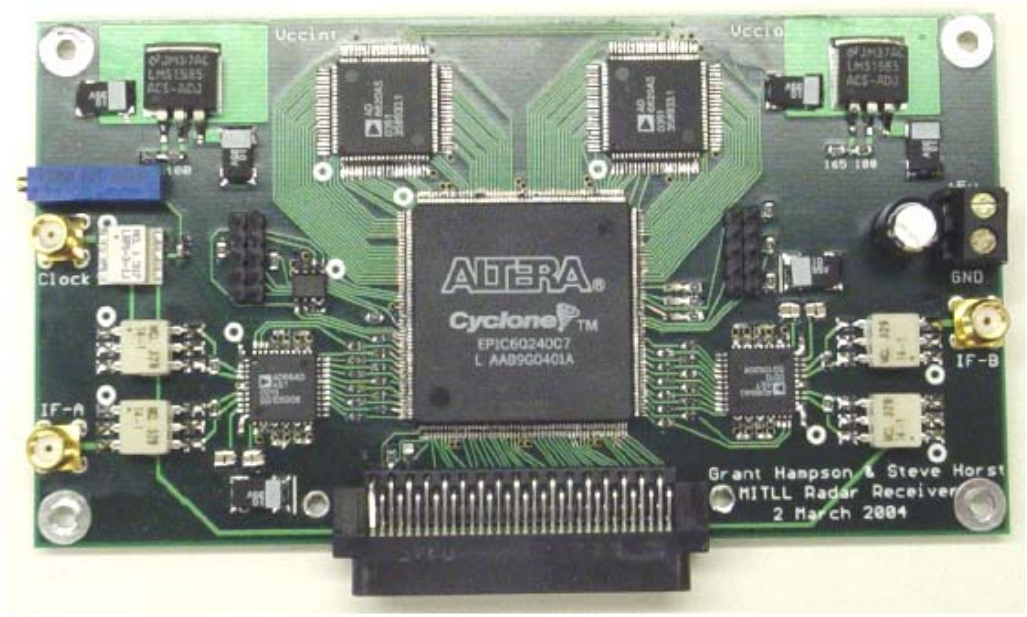

Figure 49. OSU/ESL Dual Channel Digital Receiver.

10.3 Direct Digital Synthesizer

For UXO application, the GPR needs to be able to cover a frequency range at least from 10 MHz to 800 MHz by sweeping the frequency at 10 ~ 20 MHz increments. The existing GPR utilizes a commercial network analyzer that is relatively slow in sweeping. For instance, it takes approximately 1 second to sweep 201 frequency points with 300 Hz bandwidth. This means three seconds for measuring fully polarimetric data at each location, with perhaps 40 positions along each survey line. A new frequency source design is adopted using a high-speed direct digital frequency synthesizer (DDS) chip by Euvis DS852 and DS853 (center of Figure 50). The new design reduces the collection time by a factor of three, i.e. 0.3 seconds for 201 frequency points.

The inputs of this DDS chip include 32-bit single-ended digital signals Vi0 ~ Vi31 for frequency control providing extremely fine frequency resolution, a reset signal RST for accumulator reset, a strobe signal STRP for strobe of frequency control input, and a pair of differential clock signals. All the input signals except the clock signals are connected to an on-board 50-pin IDC interface that can be controlled by a PC with a proper data interface. The clock

input pair allows the clock source to be presented in either single-ended or differential form, with SMA connectors. The outputs of the evaluation board consist of a pair of differential analog outputs OUTP/OUTN and an accumulator's carryout COUT.

Summary of Key Features

- 32-bit frequency tuning word
- One chip DAC with 10 bit linearity
- Clock rate up to 2 GHz
- Sine wave generation up to 1 GHz
- Complementary analog waveform outputs with 50 W back terminations
- Carry bit RF output from phase accumulator
- Worst SFDR > 50 dBc (DC to 1-GHz Bandwidth) at a 2 GHz clock rate
- TTL/CMOS digital pattern control input
- Reset (RST) pin to initiate phase 0 starting state
- High speed strobe LVPECL or LVDS compliant inputs (STRP/N) to change DDS output
- frequency from ~ 10 MHz up to ~ 800 MHz
- 4.2 W power consumption with a single -5.2V power supply
- 64-pin QFN package

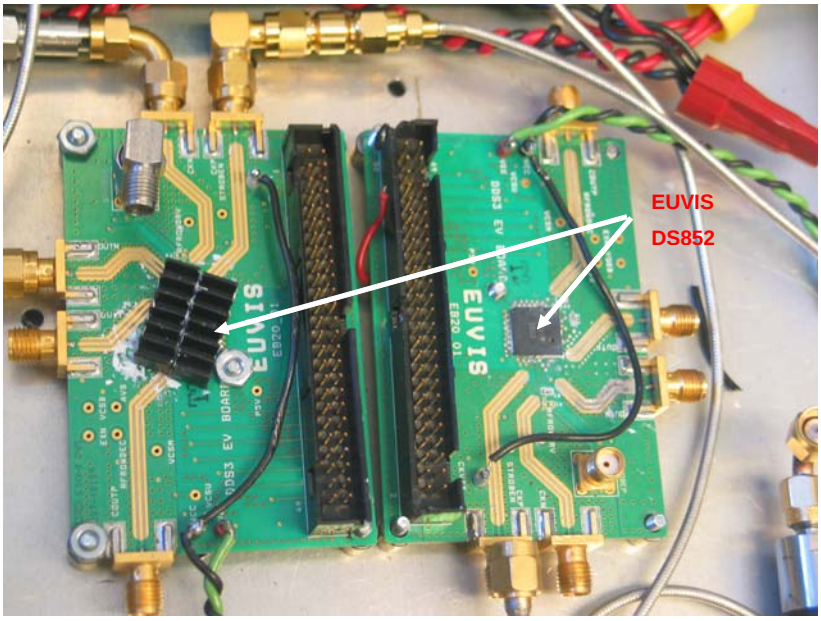

Figure 50. DDS board as frequency source for new OSU/ESL GPR.

10.4 Small Footprint, Low-RCS GPR Antenna Development

10.4.1 Quad-Ridge Horn Antenna with Dielectric Loading

A new fully polarimetric antenna that has a much smaller footprint and support structure was designed and fabricated. We have adopted a UWB quad-ridge horn design filled with low-loss dielectric material. This new antenna will be tested and compared with the existing HFB antenna and eventually replace the HFB antenna for future UXO measurement. Figure 51 shows the picture of the new antenna under construction before being filled with dielectric loading.

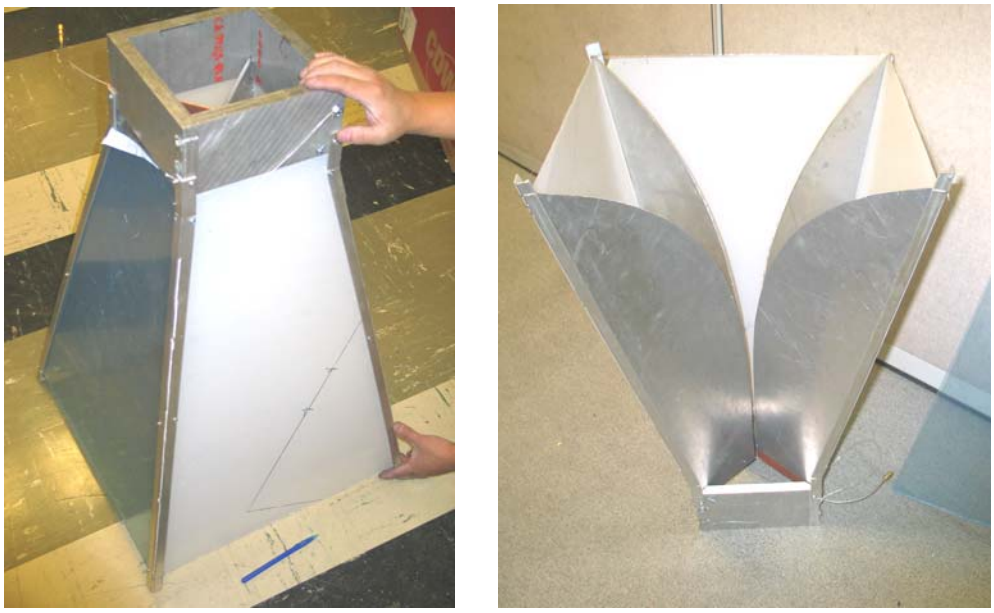

Figure 51. Quad-ridge horn antenna under construction without dielectric filler.

10.4.2 Dual-Linear Resistive-Loaded Dipoles on a High Dielectric Constant Layer

Another small UWB antenna being designed and fabricated is a dual-linear bowtie antenna on a high-dielectric layer as shown in Figure 52. The arms of the dipole elements are terminated with tapered resistive film to reduce antenna ringing. The antenna size is approximately 30 cm by 30 cm by 2.5 cm. The dielectric constant of the substrate is chosen to be 16. Figure 53 shows the predicted gain for 10 ohm/square resistive film in free space. The expected lower gain value results from resistive loading. Higher radar output power with a proper equalizer filter will compensate for this, such that lower frequencies get more gain without saturating higher frequency response. The important characteristics that we are after are the smooth gain curve (i.e. no antenna ringing) and non-diminishing gain level at 20 MHz (i.e. UWB). Figure 53 also demonstrates the low cross-polarization level, a desired feature for fully polarimetric measurements. Additional layer(s) could be added between the ground and the high dielectric layer to provide smoother dielectric transition when the ground has a dielectric constant quite different from 16. For instance, a layer of 9 and a layer of 4 can be added for dry sand environment.

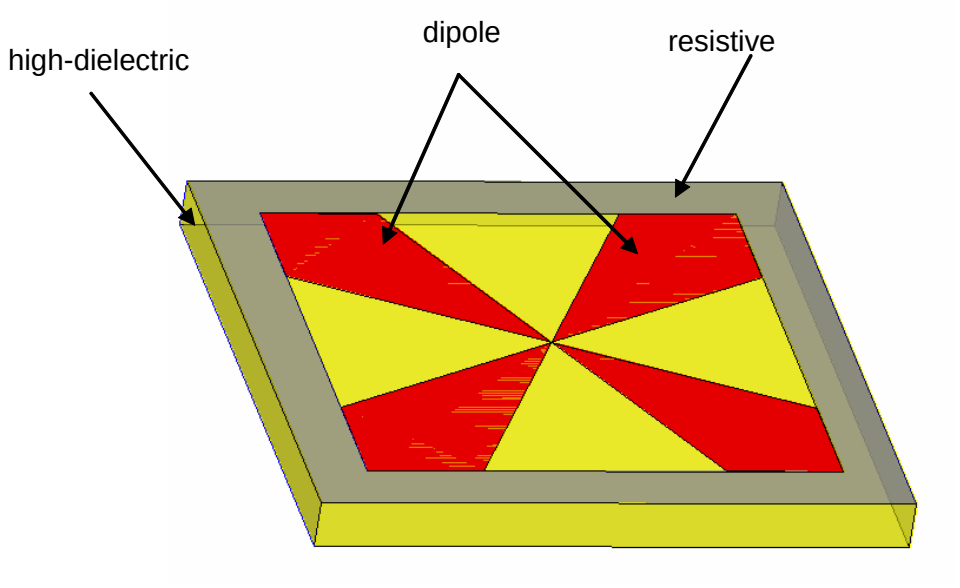

Figure 52. Small UWB GPR antenna with high dielectric loading being developed for fully polarimetric UXO classification.

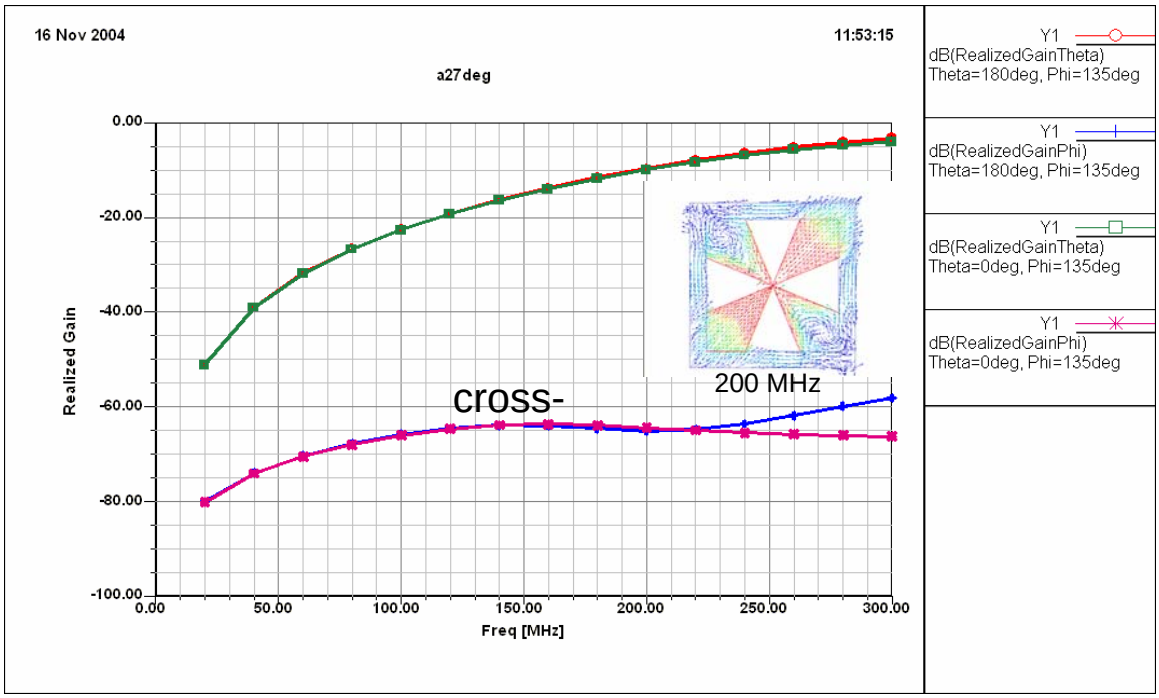

Figure 53. Calculated gain of the small UWB GPR antenna with high dielectric loading being developed for fully polarimetric UXO classification.